The Role of Axonal Prion Protein in Myelin Maintenance

Dissertation

zur

Erlangung der naturwissenschaftlichen Doktorwürde
(Dr. sc. nat.)

vorgelegt der

Mathematisch-naturwissenschaftlichen Fakultät

der

Universität Zürich

von

Alexander Friedrich Küffer

von

Ins BE

Promotionskommission

Prof. Dr. Adriano Aguzzi (Vorsitz und Leitung)
Dr. Michaela Thallmair
Prof. Dr. Martin Schwab

Zürich, 2019

Die vorliegende Arbeit wurde von der Mathematisch-naturwissenschaftlichen Fakultät der Universität Zürich auf Antrag von Prof. Dr. Adriano Aguzzi angenommen.

Contents

1 Abbreviations

aa	amino acid
ATP	adenosine-5'-triphosphate
BSA	bovine serum albumin
BSE	bovine spongiform encephalopathy
cAMP	cyclic adenosine monophosphate
CC1	positively charged charge cluster of PrP^C (aa 23-27)
CC2	positively charged charge cluster of PrP^C (aa 95-110)
CD	central domain (of PrP^C)
CDP	chronic demyelinating polyneuropathy
CJD	Creutzfeldt-Jakob disease
CMT	Charcot-Marie-Tooth disease
CNS	central nervous system
Dpl	protein doppel
Dhh	desert hedgehog
DNA	deoxyribonucleic acid
DRG	dorsal root ganglion
EGFP	enhanced green fluorescent protein
ELISA	enzyme-linked immunosorbent assay
EM	electron microscopy
Erk	extracellular-signal-regulated kinase
FFI	fatal familial insomnia
FT	flexible tail of referring to aa23-110 of the cellular PrP
GDNF	glia cell line-derived neurotrophic factor
GFP	green fluorescent protein
GPI	glycosyl-phosphatidyl-inositol
Gpr	G protein-coupled receptor
Gpr126	G protein-coupled receptor 126
GSS	Gerstmann-Sträussler-Scheinker syndrome
HC	hydrophobic core (of PrP^C)
i.v.	intravenous
kDa	kilo Dalton
LPS	lipopolysaccharide
MAG	myelin associated glycoprotein

MALDI-TOF/TOF	matrix-assisted laser desorption/ionization-tandem time-of-flight
MAP	mitogen-activated protein
MAPK	mitogen-activated protein kinase
MBP	myelin basic protein
MPZ	myelin protein zero (see also P0)
NCV	nerve conduction velocity
NGF	nerve growth factor
NSE	neuron specific enolase
OR	octarepeat region (of PrP^{C})
PBS	phosphate-buffered saline
PBST	phosphate-buffered saline (with) Tween-20
PCR	polymerase chain reaction
PIPLC	phosphatidylinositol-specific phospholipase C
PK	proteinase K
P0	myelin protein zero (see also MPZ)
PNS	peripheral nervous system
PRNP	gene encoding the human prion protein
Prnd	gene encoding the mouse doppel (doppelganger of the prion protein, Dpl)
Prnp	gene encoding the mouse prion protein
PrP^{C}	cellular isoform of the prion protein
PrP^{Sc}	pathological isoform of the prion protein
RNA	ribonucleic acid
RT	room temperature
s.d.	standard deviation
SDS-PAGE	sodium dodecyl sulphate polyacrylamide gel electrophoresis
s.e.m	standard error of the mean
Shh	sonic hedgehog
SOD	superoxide dismutase
TBST	tris-buffered saline (with) Tween-20
TSE	transmissible spongiform encephalopathy
wt	wildtype (mouse/ mice)

Parts of the Summary, Introduction, Results, Methods and Discussion sections are reproduced or adapted from our following publication:

"The prion protein is an agonistic ligand of the G protein-coupled receptor Adgrg6."
By Alexander Küffer, Asvin K K Lakkaraju, Amit Mogha, Sarah C Petersen, Kristina Airich, Cédric Doucerain, Rajlakshmi Marpakwar, Pamela Bakirci, Assunta Senatore, Arnaud Monnard, Carmen Schiavi, Mario Nuvolone, Bianka Grosshans, Simone Hornemann, Frederic Bassilana, Kelly R Monk and Adriano Aguzzi

published in Nature August 25th 2016, issue 536, page 464-468.

2 Summary

Ablation of the cellular prion protein PrP^C leads to a chronic demyelinating polyneuropathy (CDP) affecting Schwann cells. Neuron-restricted PrP^C expression prevents the disease (Bremer et al., 2010b), suggesting that it acts through an unidentified Schwann cell receptor. In my thesis I found that the cAMP concentration in PrP^C deficient sciatic nerves is reduced, suggesting the involvement of a G protein-coupled receptor GPCR. The amino-terminal "flexible tail" FT (residues 23-120 of PrP^C) triggered a concentration-dependent cAMP increase in primary Schwann cells, in the Schwann-cell line SW10, and in Hek293T cells overexpressing the GPCR Gpr126/Adgrg6. In contrast, naïve Hek293T cells and Hek293T cells expressing several other GPCRs did not react to the FT and ablation of Gpr126 from SW10 cells abolished the FT-induced cAMP response. The FT contains a polycationic cluster (KKRPKPG) similar to the GPRGKPG motif of the Gpr126 agonist, type-IV collagen Col 4 (Paavola et al., 2014). A KKRPKPG-containing PrP^C-derived peptide (FT_{23-50}) sufficed to induce a Gpr126-dependent cAMP response in cells and mice and improved myelination in hypomorphic Gpr126 zebrafish mutants. Substitution of the cationic residues with alanines abolished the biological activity of both FT_{23-50} and the respective Col4 peptide. I conclude that PrP^C promotes myelin homeostasis through FT-mediated Gpr126 agonism. Besides clarifying the physiological role of PrP^C, these observations may be relevant to the pathogenesis of demyelinating polyneuropathies, common debilitating diseases with limited therapeutic options.

3 Zusammenfassung

Die Ablation des zellulären Prionproteins PrP^C führt zu einer chronischen demyelinisierenden Polyneuropathie CDP. Auf Neuronen beschränkte PrP^C-Expression verhindert die Krankheit (Bremer et al., 2010b), was darauf hindeutet, dass PrP^C via einen bisher nicht identifizierten Schwann-Zellrezeptor zu Myelinisierung führt. Ich habe in meiner Dissertation herausgefunden, dass die cAMP-Konzentration in PrP^C-defizienten Ischiasnerven reduziert ist, was auf die Beteiligung eines G-Protein-gekoppelten Rezeptors (GPCR) schließen lässt. Der aminoterminale flexible Teil (FT, Reste 23-120) von PrP^C löste einen konzentrationsabhängigen cAMP-Anstieg in primären Schwann-Zellen, in der Schwann-Zelllinie SW10 und in Gpr126/Adgrg6 überexprimierenden Hek293T-Zellen aus. Im Gegensatz dazu reagierten naive Hek293T-Zellen und Hek293T-Zellen, die mehrere andere GPCRs exprimierten, nicht auf FT und die Ablation von Gpr126 aus SW10-Zellen hob die FT-induzierte cAMP-Antwort auf. FT enthält einen polykationischen Cluster (KKRPKPG), der dem GPRGKPG-Motiv des Gpr126-Agonisten Typ IV-Collagen Col4 ähnlich ist (Paavola et al., 2014). Ein KKRPKPG-haltiges, von PrP^C abgeleitetes Peptid (FT_{23-50}) reichte aus, um eine Gpr126-abhängige cAMP-Antwort in Zellen und Mäusen zu induzieren und verbesserte die Myelinisierung in hypomorphen Gpr126-Zebrafischmutanten. Die Substitution der kationischen Reste durch Alanine hob die biologische Aktivität sowohl von FT_{23-50} als auch des jeweiligen Col4-Peptids auf. Ich schließe daraus, dass PrP^C die Myelinhomöostase durch FT-vermittelten Gpr126-Agonismus fördert. Neben der Aufklärung der physiologischen Rolle von PrP^C können diese Beobachtungen auch für die Pathogenese von demyelinisierenden Polyneuropathien relevant sein.

4 Introduction

4.1 The cellular prion protein

4.1.1 PrP^C

The *PRNP* gene in humans and the *Prnp* gene in mice encode the cellular prion protein PrP^C, a 35kD glycosylphosphatidylinositol-anchored and membrane bound extracellular protein with 2 N-linked glycosylation sites. Its secondary structure is described as a carboxy-terminal globular domain (aa135-231) formed by three α-helices and two β-sheets. The amino-terminal domain aa 23-110 is called the "flexible tail" FT, because NMR-Spectroscopy analysis revealed no distinct secondary structure (Riek et al., 1996). The hydrophobic core HC (aa111-134) connects the globular domain and FT. FT contains two charge clusters CC1(23-27) and CC2(95-110) and the octapeptide repeat region OR.

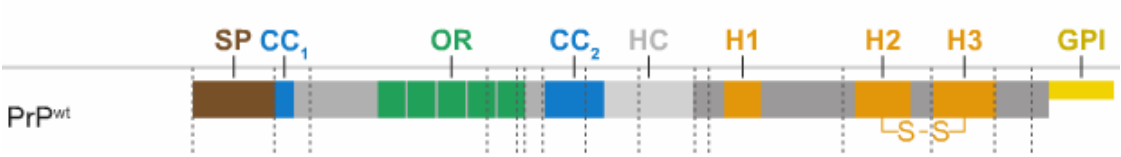

Figure 4.1. **The cellular prion protein.** Adapted from (Aguzzi et al., 2008), SP signaling peptide, CC1/CC2 charge clusters 1 and 2, OR octapeptide repeats, HC hydrophobic core, H1-3 α-helices, GPI glycosylphosphatidylinositol anchor.

4.1.2 PrP^C is GPI-anchored

After translation and transport to the cell surface, PrP^C is assigned to extracellular lipid rafts (Naslavsky et al., 1997). 70-80% of PrP^C has been reported to be released from the cell surface of N2a cells stably transfected with chicken *Prnp* after phosphatidylinositol-specific phospholipase C (PIPLC) treatment (Harris et al., 1993), indicating that PrP^C is anchored to the extracellular membrane by a GPI-anchor. Full length PrP is also physiologically shedded at the GPI-anchor, releasing the entire protein in a soluble form. Interestingly, membrane anchorage seems to be a prerequisite for α-cleavage, since PrP mutants lacking a GPI anchor are not proteolytically processed at the α-site.

4.1.3 Posttranslational proteolytic processing of PrP

PrP^C can undergo α-, β- and probably γ-cleavage events. The first description of PrP^C α-cleavage was published by Harris et al. (Harris et al., 1993) who studied posttranslational processing and trafficking in chicken PrP^C. They found that stably transfected A26 cells released a 11.5kD fragment into culture media. Immunoblotting with different antisera revealed a peptide starting at the very amino-terminus of PrP^C, just after the signal sequence at Lys^{25} (chicken numbering) up to a cleavage site around Phe^{116}. More than half of PrP^C was N-terminally truncated, indicating the importance of this event under physiological conditions. α-cleavage in mice occurs at around aa110/111 resulting in the membrane bound carboxy-terminal C1 fragment (aa111-231) and the soluble amino-terminal N1 fragment also called FT(aa23-110) (Chen et al., 1995; Mange et al., 2004). α-cleavage is an important process since it can prevent the C1 fragment from being misfolded into Prp^{Sc} (Westergard et al., 2011). Transgenic mice expressing mutant forms of PrP^C which did not undergo physiological α-cleavage, suffer from neurodegeneration and polyneuropathy suggesting that α-cleavage is crucial for physiological function

of PrP^C. ADAM family metalloproteinases have been reported to cleave PrP^C (Altmeppen et al., 2015). Different mutant forms of PrP^C with alterations around the α-cleavage site revealed a surprisingly limited sequence specificity for cleavage (Oliveira-Martins et al., 2010). β-cleavage is leading to the fragments N2 and C2. It is mainly a pathological process since C2 is protease resistant and detergent-insoluble. C2 fragment is abundant in CJD brains (Chen et al., 1995). γ-cleavage was recently discovered generating a C3 fragment of which the function is still unclear (Lewis et al., 2016).

4.2 Scrapie prion protein PrP^{Sc}

Scrapie prion protein PrP^{Sc} is the disease-associated isoform of PrP^C, which is post-translationally modified and comprises increased β-sheet content. PrP^{Sc} is insoluble in non-denaturating agents and shows partial protease resistance (Prusiner, 1982). PrP^{Sc} is differently cleaved by the so called β-cleavage event.

4.3 The aminoterminus of PrP^C in disease

When looking for polymorphisms and mutations in the *PRNP* gene, it is very obvious that a vast majority affects the carboxy-terminal part of the protein. Only a handful of polymorphisms and mutations are reported in the aminoterminus. This shows that mutations in the amino terminus of *PRNP* are hardly tolerated. A loss of function of the probably important amino terminus seems to have an evolutionary negative effect and has been selected out. A Pro to Leu point mutation at codon 102 with methionine homozygosity at codon 129 was reported in a 54 year old Japanese woman suffering from Gerstmann-Sträussler-Scheinker GSS like symptoms such as dementia, gait disturbance myoclonic and akinetic mutism (Iwasaki et al., 2014). A similar disease with a slower course occurred in a 57 year old Japanese woman and a P105L mutation in *PRNP* was diagnosed (Yamazaki et al., 1999). The missense P39L variant was the cause of a case of frontotemporal dementia FTD in a 67 year-old male with short term memory deficit, postural deficit and positive family history for dementia (Oldoni et al., 2016). And the same P39L mutation was reported in two further FTD cases in Italy (Bernardi et al., 2014). A Chinese group studied *PRNP* gene mutations in a huge population of 683 patients with either Alzheimer's disease or frontotemporal dementia FTD and detected a novel S17G missense mutation in a 70 year-old female patient suffering from Alzheimer's disease (Zhang et al., 2016). The mutation S17G affects the signaling peptide important for PrP trafficking and is not part of PrP itself. Individuals with 10 or more octapeptide repeats develop a transmissible familial Creutzfeldt-Jakob disease (Goldfarb et al., 1991). On the other hand, a two-octapeptide repeat deletion was found in a patient with rapidly progressing dementia (Beck et al., 2001). The number of octapeptide repeats is negatively proportional to patient age at disease onset.

4.4 Function of the prion protein

4.4.1 Generation of prion protein deficient mice

By the end of the 1980s the generation of knock out mice became feasible (Mansour et al., 1988) and already in 1992 the first *Prnp*$^{-/-}$ mouse has been created. PrP^{C} is expressed in most tissues and highly in CNS and peripheral nerves (Bendheim et al., 1992), therefore an obvious phenotype of a knock out mouse was expected. But the *Prnp*$^{-/-}$ mice were viable, fertile and showed a normal life expectancy. Therefore, they were considered as healthy throughout. Most surprisingly, *Prnp*$^{-/-}$ mice were even resistant to prion infection (Bueler et al., 1993; Sailer et al., 1994). The only identified function of the prion protein was causing vulnerability for prion's disease. Later on, when transcriptomics got available, the expression of PrP^{C} during CNS development was studied in more detail. Interestingly, the number of differentially expressed genes in the hippocampus of PrP^{C}-deficient mice compared to wild-type animals was low (Benvegnù et al., 2011). There was no obvious difference even in strictly co-isogenic ZH3 mice (Nuvolone et al., 2016), concluding that lack of PrP^{C} can be compensated during CNS development. However, a bigger difference occurs when PrP^{C} is deleted postnatally when compensation for gene loss is not easily done anymore (Chadi et al., 2010).

4.4.2 Doppel overexpression

In 1996, a phenotype with ataxia and loss of cerebellar Purkinje neurons was reported (Sakaguchi et al., 1996). The problem occurred in four *Prnp*$^{-/-}$ lines caused by a targeting vector design resulting in a larger deletion of *Prnp* exon 3 containing a splice acceptor site. This resulted in overexpression of the *Prnd* gene and its gene product the Doppel protein (Moore et al., 1999)and therefore the symptoms were not caused by *Prnp* ablation.

4.4.3 Genetic challenges with *Prnp* ablation

To create the very first *Prnp*$^{-/-}$ mouse strain ZH1, a mixed C57BL/6 J × 129/Sv(ev) background was used. The knockout alleles have been generated in Sv129 embryonic stem cells and resulting mice were backcrossed for more than 12 generations on a black 6 strain. Even after 12 generations of backcrossing, a tiny part of the chromosome flanking the *Prnp* locus originates from the Sv129 mouse strain. Some functions attributed to PrP^{C} were in reality caused by polymorphisms in a flanking gene and were not a function of PrP^{C} (Bueler et al., 1993). The best studied example is the role of PrP^{C} in phagocytosis. Macrophages of *Prnp*$^{-/-}$ mice were reported to present superior phagocytic activity leading to the hypothesis that PrP^{C} negatively regulates phagocytosis (de Almeida et al., 2005). Expression of PrP^{C} in macrophages is very low and therefore some doubt was raised against this finding. In our lab, we could show that polymorphisms in the *Prnp*-flanking gene SIRPα were responsible for alterations in phagocytosis of apoptotic cells (Nuvolone et al., 2013). In 2014 a new *Prnp*$^{-/-}$ mouse was created with TALEN nucleases in fertilized mouse oocytes (Nuvolone et al., 2016). The genetic background was kept strictly black six. These mice have been called Zurich 3 (ZH3) and they differ from wild-type mice only by deletion of 8 nucleotides resulting in disruption of the PrP reading frame. Consistently, all studies that do not use the ZH3 mouse or the Edinburgh Mouse should be repeated

with one of these mouse strains. Since the ZH3 mouse only existed from 2014 onwards, most of the studies about the function of PrP^{C} were performed in non-coisogenic mouse strains. All these studies should be interpreted with particular caution.

4.4.4 Deletion variants of the flexible tail FT(23-110)

To identify the domain causing the isoform switch from PrP^{C} to PrP^{Sc}, transgenic mice expressing truncated prion proteins have been generated. Surprisingly, expression of only part of PrP caused spontaneous neurodegenerative disease and co-expression of full length PrP could again rescue the neurotoxic phenotype. First deletion mutants of the flexible tail were published by Fischer who re-introduced full length PrP^{C} or PrP lacking the 26 and 46 very amino-terminal amino acids into *Prnp*$^{-/-}$ mice (Fischer et al., 1996). Mice were then infected with prions and all of them accumulated PrP^{Sc} and died from fatal neurodegeneration leading to the conclusion that the aminoterminus of PrP^{C} plays no role in conformational change from PrP^{C} to PrP^{Sc}. In 1997 Muramoto et al. deleted aa 23-88 which contains charge cluster 1. These mice were healthy and could be infected with PrP^{Sc} (Muramoto et al., 1997). Charge cluster 2 around aa100 might replace the function of CC1 in those mice. But deletions including CC2, PrPΔ23−88 Δ95−107 showed no phenotype either and propagated PrP^{Sc}. Shmerling created further deletions of aa 32-121 and aa 32-134. These mice unexpectedly developed ataxia and degeneration of the cerebellar granular layer 2-3 month after birth. The phenotype could be rescued by reintroduction of a wt *Prnp* gene. Shorter deletions aa 32–80, 32–93 or 32–106 did not lead to spontaneous neurodegeneration. Shmerling hypothesized that truncated PrP variants may compete with similar proteins for a common ligand (Shmerling et al., 1998).

4.4.5 Prion protein knockout animals

The cellular prion protein has been ablated in cattle (Richt et al., 2007) and goats (Yu et al., 2006) and there is one published report about a spontaneous mutation leading to naturally prion protein ablated Norwegian dairy goats. All these animals are healthy, but they have not been thoroughly examined and there is no interest of the companies involved to do so. At the beginning of my work with peripheral nerves, I asked a company generating prion protein knockout cows if I could get peripheral nerve tissue. Unfortunately, I have never received an answer to my request. The knockout cows were generated with the aim of raising cattle for the food market. Had w found a pathology in these animals, this would have put the company's business at risk.

4.4.6 *PRNP* deficiency in humans

In a large population analysis containing exome sequencing data of over 76000 individuals, three heterozygous loss-of function variants were identified (Minikel et al., 2016). A *PRNP*$^{-/-}$ human is not reported so far.

4.4.7 Sleep regulation

Mutations in the *PRNP* gene are responsible for the development of fatal familial insomnia FFI, so it is not surprising that a role of PrP^C in the regulation of circadian rhythm was suspected. Indeed ZH1 and Edinburgh *Prnp*$^{-/-}$ mice showed altered activity patterns in changing light/dark cycles and sleep was more fragmented compared to wild-type controls (Tobler et al., 1996). *Prnp*$^{-/-}$ mice have an increased slow wave activity (SWA) after severe sleep deprivation (Huber et al., 1999).

4.4.8 PrP^C and memory

Synaptic dysfunction or even synaptic loss is an early change in prion's disease (Jeffrey et al., 2000) Following prion infection by injecting the mouse scrapie strain 22L, pre-and postsynaptic degeneration were predominantly detected in the stratum radiatum of the hippocampus (Šišková et al., 2013). After synaptosomal fractionation, PrP^C was isolated from synaptic membranes and synaptic activity correlated with the amount of PrP^C in presynaptic neurons in cerebellar slices (Herms et al., 1999). ZH1 and Edbg mice showed weakened GABA receptor-mediated fast inhibition (Collinge et al., 1994) and impaired long-term potentiation (Manson et al., 1995). The neurophysiological phenotype with weakened inhibitory GABAergic synaptic transmission and impaired long-term potentiation could be rescued by introduction of human PrP^C in high copy numbers and seemed to be specific (Whittington et al., 1995). But shortly after, contradictory studies were published. According to them, *Prnp*$^{-/-}$ mice had no deficit in synaptic inhibition and did not show any difference in long-term potentiation (Lledo et al., 1996). The first report by Büeler et al. did not mention any significant differences in memory performance, although *Prnp*$^{-/-}$ mice were searching a bit longer for a submerged platform in the swim test, what was interpreted as superior spatial memory or reduced behavioral flexibility (Bueler et al., 1992). A later study showed impaired spatial learning with normal non-spatial learning and a reduction in long-term potentiation. These deficiencies were cell-type specific for neurons since reintroduction of PrP^C under the neuron-specific enolase promotor (NSE) fully rescued the condition (Criado et al., 2005). Memory disturbances were reported to be age dependent (Coitinho et al., 2003) with differences in 9-month old animals. On the other hand a 2-year longitudinal study revealed no deficiencies in spatial learning (Lipp et al., 1998).

4.4.9 Copper, zinc and lactate metabolism

In 1965, William Carlton treated mice with the copper chelator Cuprizone aiming to create a mouse model to study the known neurodegeneration triggered by copper deficiency. The common histological features of copper deficiency and scrapie disease with spongiform change and severe demyelination of cerebellum and brainstem were discussed again in 1971. Thanks to the phenocopy of the diseases, it was hoped to gain an insight into the underlying pathophysiology. Re-substitution of copper could not rescue the demyelinating effect of copper chelation and it remained unclear if cuprizone exerts a direct toxic effect on myelin. 20 years later, Brown described 5 to 6 copper binding sites in the octapeptide repeat domain PHGGGWGQ of PrP^C. Two different *Prnp*$^{-/-}$ mouse lines (ZHI and Edinburgh) showed reduced copper contents in membrane enriched brain extracts and in synaptosomal and endosomal

enriched fractions (Brown et al., 1997). Although copper contents are altered in *Prnp*$^{-/-}$ mice they do not show any of the severe symptoms of a disturbed copper homeostasis. Binding to the histidine residues of the octapeptide repeats was reported to be specific for Cu^{2+} (Stöckel et al., 1998) but the octapeptide repeat domain is also involved in zinc uptake (Watt et al., 2012). Maybe any divalent cation is able to interact with the OR. Copper causes a conformational change in the amino-terminus(Viles et al., 1999), therefore a functional change of PrP^C upon copper binding is feasible. Copper can induce PrP^C expression in primary hippocampal and cortical neurons (Varela-Nallar et al., 2006). A recent structural study reported an interaction of the copper bound octapeptide repeat domain with a charged c-terminal pocket in the globular domain which matches exactly the POM1 antibody recognition site(Evans et al., 2016). POM 1treatment is toxic in cerebellar slice cultures and the flexible tail is needed to transduce toxic signaling originating in the globular domain (Sonati et al., 2013). The authors propose an important role in the regulation of the flexible N-terminus of PrP^C. Copper seems not to play an important role in prion infection since mice lacking the effector site for copper binding, the octapeptide repeat domain, are still susceptible to scrapie. Interestingly, these mice still have a lower incubation time and histopathologic changes in the brain are absent while they are unchanged in the spinal cord (Flechsig et al., 2000). PrP^C is also reported to be involved in the regulation of lactate transport in astrocytes mediated by its interaction with GluR2-containing AMPA receptors.

4.4.10 PrP^C and metabotropic glutamate receptors

PrP^C interacts with two metabotropic glutamate receptors of group I, mGluR1 and mGluR5, which are G protein-coupled receptors. Both receptors are normally activated by Glutamate but PrP^C can bind to mGluR5 in a complex with Aβ-oligomers, leading to intracellular Fyn activation (Um et al., 2013). Aβ–PrP^C–mGluR5-complexes can lead to long-term depression in vivo (Hu et al., 2014) and loss of dendritic spines in neuronal cultures (Um and Strittmatter, 2013). Coworkers in our lab, Goniotaki et al. found a delayed onset of motor deficits and a prolonged survival in prion infected mice treated with the mGluR5 inhibitor MPEP, showing that mGluR1 and mGluR5 can form toxic complexes with PrP^C (Goniotaki et al., 2017). Again these functions of PrP^C occur under pathologic conditions and do not give a hint about the physiological function of PrP^C. Therefore the study of Beraldo has to be mentioned which reports a signaling pathway for neuritogenesis initiated by PrP^C and laminin complexes via metabotropic glutamate receptors of group I (Beraldo et al., 2010).

4.4.11 Oxidative stress and superoxide dismutase activity

Superoxide dismutase activity is diminished in brain und muscle of *Prnp*$^{-/-}$ mice (Klamt et al., 2001). Waggoner et al. could not confirm the finding for Cu-Zn superoxide dismutase and cytochrome C expression levels in brain extracts, as those were similar in *Prnp*$^{-/-}$ mice compared to controls (Waggoner et al., 2000). Furthermore, our own group could not find a contribution of PrP^C to total SOD activity (Hutter et al., 2003).

4.4.12 Mitochondria

Interestingly the mitochondria number in CA1 hippocampal neurons and in the myocardium of Edinburgh *Prnp*$^{-/-}$ mice is reduced (Miele et al., 2002) but a study measuring mitochondrial respiration in different regions of *Prnp*$^{-/-}$ brains revealed no change compared to controls (Lobão-Soares et al., 2005).

4.4.13 Phagocytosis and immune response

Macrophages of *Prnp*$^{-/-}$ mice were reported to present superior phagocytic activity culminating in the hypothesis that PrP^{C} negatively regulates phagocytosis (de Almeida et al., 2005). In fact, PrP^{C} expression in macrophages is very low and the finding was caused by a flanking gene bias (Nuvolone et al., 2013). *Prnp*$^{-/-}$ mice better tolerate infection with the bacterium Brucella abortus (Watarai et al., 2003). This data could not be reproduced in B. suis (Fontes et al., 2005). *Prnp*$^{-/-}$ mice are even refractory to infection with herpes simplex virus (Thackray and Bujdoso, 2002) a finding which seems more plausible since PrP^{C} overexpressing tga20 mice were easily infected by herpes simplex virus. An advantage against Brucella or Herpes simplex virus infection would have been an evolutionary advantage for *Prnp* null alleles which are very rare and were obviously not selected (Aguzzi and Hardt, 2003). But one has to admit that also prion's disease did not elicit selective pressure in favor of the *Prnp* null allel and therefore it's plausible that PrP^{C} indeed has an important function. Otherwise it's hard to argue why this protein is highly conserved in vertebrates. PrP^{C} on dendritic cells were reported to be crucial for T-cell stimulation in vitro and in vivo (Ballerini et al., 2006).

4.4.14 Neuronal excitability and seizures

CA1 hippocampal neurons from ZH1 *Prnp*$^{-/-}$ mice presented faster after-hyperpolarization currents and impaired long term potentiation (Collinge et al., 1994). Similar findings were described in Edinburgh *Prnp*$^{-/-}$ mice by Manson (Manson et al., 1995). Reintroduction of PrP^{C} could rescue the phenotype (Whittington et al., 1995). Other groups could not reproduce the findings (Herms et al., 1995; Lledo et al., 1996) but published contradictory data in a later study (Herms et al., 2001). ZH1 *Prnp*$^{-/-}$ mice are prone to seizures upon injection of kainic acid, a finding reproduced independently by two different groups (Rangel et al., 2007; Walz et al., 1999). Timm staining of the hippocampus showed more granules in the granular layer, the inner molecular layer of the dentate gyrus and the infrapyramidal region of CA3 (Colling et al., 1997).

4.4.15 Chronic demyelinating neuropathy in *Prnp*$^{-/-}$ mice

Our group reported an extensive chronic demyelinating polyneuropathy CDP in four independent *Prnp*$^{-/-}$ mouse strains at 60 weeks of age (Bremer et al., 2010a). The CDP was evident in all examined peripheral nerves, including sciatic and trigeminal nerves. Genetic reintroduction of PrP^{C} via crosses to the PrP overexpressing *tga20* mice, or introduction of one *Prnp* allele fully prevented the polyneuropathy. Electron microscopic analysis of 60 week old *Prnp*$^{-/-}$ mice showed characteristic ultrastructural signs of demyelination. Electrophysiological analyses performed on sciatic nerves revealed significantly reduced nerve conduction velocities in *Prnp*$^{-/-}$ mice. Our group further showed

that *Prnp*$^{-/-}$ mice expressing the *tg*NSE-Prp transgene which expresses PrP^C specifically in neurons (Radovanovic et al., 2005) did not suffer from polyneuropathy (Bremer et al., 2010a), leading us to the unexpected conclusion that neuronal expression of PrP^C is required for myelin sheath maintenance. The proteolytic α-cleavage event seems to be important to prevent peripheral neuropathy. PrP in tgC4 mice (Δ32-93) and $tgPrP_{\Delta CC}$ mice (Δ94-110) are α-cleaved and mice do not show peripheral neuropathy. On the other hand, tgE11 (Δ32-121) and tgF35 (Δ32-134) suffer from peripheral neuropathy and these deletion variants are not cleaved and the probable signaling domain aa 23-32 is retained at the cell surface. E11 and F35 mice do not have a normal life expectancy and they suffer from cerebellar degeneration indicating a deleterious effect if cleavage cannot happen. This is also the case in deletions of the hydrophobic core HC $tgPrP_{\Delta HC}$ (Δ111-134) that show no cleavage and therefore neuropathy.

4.5 Myelination

Myelin is formed by Schwann cells in the peripheral nervous system PNS or by oligodendrocytes in the central nervous system CNS. Myelin contains 40% water and 60 % solid mass of which around 2/3 are lipids and 1/3 are proteins. The high lipid content was leading to the name "white matter" for the myelinated substance in the CNS. Ensheathing axons with myelin enhances the conduction of nerve impulses and enables saltatory conduction which makes signal propagation up to 100 times faster (Tasaki, 1939). Myelin wrapping protects the axon and glia cells play a crucial role in maintaining neuronal homeostasis. Schwann cells regulate the molecular domains of myelinated axons and rule the diameter of axons (Salzer et al., 2008). Some authors see an advantage in energy saving since action potentials in myelinated axons do not occur along the entire axon but are focused to the internodes (Wang et al., 2008). But this will not be outweighing the expenses for the generation of glia.

Remyelination occurs in the CNS and PNS after damage. Interestingly, Schwann cells and oligodendrocyte precursor cells OPCs recapitulate signaling cascades active in development during repair (Franklin and Ffrench-Constant, 2008).

4.5.1 Development of Schwann cells

Schwann cells are derived from neural crest cells which develop to Schwann cell precursors SCPs. SCPs develop in mice at E12-13 and progress to immature Schwann cells at E13-15 (Jessen and Mirsky, 2005). If an immature Schwann cell can randomly associate with a large diameter axon, it upregulates myelin signaling and will become a mature myelinating Schwann cell. Other immature Schwann cells not undergoing radial sorting develop into mature non-myelinating Schwann cells. The transcription factor Sox10 is required for glial development and it is expressed by all neural crest cells. In mice deficient of *Sox10*, SCPs are missing but neurons are initially present in normal numbers. (Britsch et al., 2001). Sox10 regulates the expression of the neuregulin1 receptor ErbB3 and therefore enables the axon to glia signaling of Nrg1. In the PNS, neuregulins are the most important regulators of Schwann cell development (Birchmeier and Nave, 2008). The most important neuregulin gene is *NRG1*. NRG1 type III is expressed on the axonal membrane and determines if an axon will be myelinated (Taveggia

et al., 2005) and it dictates the diameter of the myelin sheeth (Michailov et al., 2004). Nrg1 enables the migration of neural crest cells to the ventral location of sympathetic gangliogenesis (Britsch et al., 1998). Nrg1 regulates survival, maturation and proliferation of Schwann cell precursors (Dong et al., 1995). Cooperatively with Nrg1, expression of Notch stimulates the formation of mature Schwann cells out of SCPs and suppresses neuronal development in neural crest cells, while it enforces the glial lineage (Morrison et al., 2000). On the other hand, Bmp2 and Bmp4 are important blockers of glial differentiation from neural crest cells (Shah et al., 1996). Schwann cell precursors convert to immature Schwann cells at E13-15 in mice. Simultanously, the perineurium is formed and the nerves start to become vascularized. Immature Schwann cells are in contrast to SCPs able to maintain survival signaling in a autocrine fashion. Therefore, the molecular expression pattern changes and factors such as insulin-like growth factor 2 IGF2, platelet-derived growth factor-β PDGFB, leukemia inhibitory factor LIF and lysophosphatidic acid LPA get upregulated. Immature Schwann cells express the transcription factors Sox2, Brn2 and Oct6 and get in contact to axons in a 1:1 ratio during the process of radial sorting. If axonal contact is established, Oct6 induces expression of transcription factor Krox 20/Egr2, which is upregulated just before myelination in mature Schwann cells happens (Topilko et al., 1994).With further contact to the basal lamina, an expression pattern of mature Schwann cells is achieved and proteins such as GFAP, S-100, desert hedgehog dhh and finally the myelin proteins PMP-22, PLP and P0 are expressed.

4.5.2 G protein coupled-receptors in PNS myelination

The G protein-coupled superfamily of receptors represent the largest group of membrane receptors and they are very well known as the most druggable receptor class since the majority of pharmacological agents work via GPCRs. The role of adhesion Gpr126/Adgrg6 in PNS myelination has been identified in a genetic Zebrafish screen (Pogoda et al., 2006), see further discussion below. Interestingly, cAMP is highly elevated after Gpr126 activation (Mogha et al., 2013). As mentioned above, axonal neuregulin 1 type III is most important for Schwann cell differentiation. Nrg1 type III is cleaved extracellularly which results in the induction of prostaglandin D2 synthase PGDS. PGDS then catalyzes the generation of prostaglandin D2 PGD2 which is a ligand of Gpr44. PGD2 binds to Gpr44 on the Schwann cell membrane, Grp44 gets activated and dephosphorylates the transcription factor NFATc4, which can translocate into the nucleus and activate promyelinating signals (Kao et al., 2009; Trimarco et al., 2014). LPA1 is a GPCR present on Schwann cells. It is activated by its ligand lysophosphatidic acid LPA which is an important survival factor for Schwann cells produced by neurons (Weiner and the of Sciences, 1999). Mutations in Gpr56/Adgrg1 have been reported to cause polymicrogyria in the neocortex. Gpr56 regulates radial sorting in early Schwann cell development through RhoA signaling (Ackerman et al., 2018).

4.6 Gpr126/Adgrg6

4.6.1 Adhesion G protein-coupled receptors

Adhesion GPCRs combine the function of a GPCR with characteristics of adhesion molecules. Similar to other GPCRs, adhesion GPCRs consist of a seven-transmembrane (7TM) heptahelical domain and an intracellular domain which couples to the heterotrimeric G-proteins. A special feature of aGPCRs is the long amino-terminal extracellular domain (ECD) containing cell-cell adhesion motifs leading to the name "adhesion" GPCR. Many aGPCRs have the ability to cleave themselves into an amino-terminal (NTF) and a caboxy-terminal fragment (CTF). This cleavage occurs at the GPCR autoproteolysis inducing GAIN domain which contains the highly conserved GPCR proteolysis site GPS.

4.6.2 Adhesion GPCRs in neurological disease

Single nucleotide polymorphisms SNPs in BAI3/ADGRB3 have been identified in Schizophrenia patients (DeRosse et al., 2008). CELSR1/ADGRC1 mutations are associated with severe neural tube defects such as spina bifida (Allache et al., 2012; Lei et al., 2014; Robinson et al., 2012). SNPs in LPHN3/ADGRL3 are found in individuals with attention deficit hyperactivity disorder ADHD (Arcos-Burgos et al., 2010; Lange et al., 2012; Ribases et al., 2011). Gpr98 /ADGRV1 is involved in Usher Syndrome Type II (Weston et al., 2004). Gpr56 regulates cortical development and lamination via binding to collagen III (Luo et al., 2011).

4.6.3 Discovery and cloning of Gpr126

In 2003 Frederiksson et al. reported six novel GPCRs, Gpr123-128, found in a BLAST search in the Celera database using known long-N-termini of GPCRs as a bait (Fredriksson et al., 2003). GPR126 was identified having a GPS domain in the N-terminus and a Ser/Thr rich region. Stehlik et al. cloned GPR126 from human umbilical vein endothelial cells where it is highly expressed and they called it vascular inducible GPCR (VIGR) because its expression could be induced by treatment of human umbilical vein endothelial cells HUVEC with lipopolysaccharides LPS or thrombin (Stehlik et al., 2004).

4.6.4 GPR126 in angiogenesis

Gpr126 is highly expressed in endothelial cells as well as embryonic stem cells expressing vascular endothelial growth factor receptor 2 VEGF2 (Cui et al., 2014). Cui et al. isolated Flk1/Vegfr2-positive cells at day 4 of embryoid body formation and screened for the expression of 100 orphan GPCRs. Gpr126 mRNA showed a similar expression profile like VEGFR2. Knockdown of Gpr126 in the mouse retina resulted in inhibition of hypoxia induced angiogenesis. Defects in intersegmental vessel formation were found in zebrafish after treatment with Gpr126 specific morpholinos. GPR126 activation is leading to cAMP induced GATA2 and STAT5 expression.

4.6.5 Gpr126 in heart development

Waller-Evans et al. created targeted mutations in which the sequence encoding part of the 7TM region is deleted and a LacZ reporter gene cassette is inserted into the 7TM locus. Homozygous mice are embryonically lethal, at dpf 13,5 no viable homozygous offspring is left (Waller-Evans et al., 2010).

Dead embryos showed signs of cardiac failure such as edema, congestion and internal hemorrhage. Trabeculation of the ventricular wall is normal at dpf 10,5 and they could not identify any reduction of myocardium or trabeculation. On the other hand, embryos dissected after cardiac failure has happened, showed a thinning of the myocardial wall. Later on, Patra et al. studied heart development in Zebrafish (Patra et al., 2013). Cardiac trabeculation was inhibited at 80 hpf in Gpr126 depleted animals. When they used morpholinos targeting the NTF of GPR126 without the GPS domain, no cardiac phenotypes were observed. Mitochondria in Gpr126 depleted zebrafish remained without any abnormalities. Then they studied Riken-Gpr126$^{-/-}$ mice, which suffer from bradycardia, cardiac arrhythmia, thinner ventricular walls and lesser trabecula. Mitochondria in cardiomyocytes presented structural alterations such as complex shape, less well developed cristae and electron-dense precipitates. Gpr126$^{-/-}$ mitochondria had more lipid droplets and lesser glycogen deposits than wt mitochondria. Patra et al. conclude that the contractility phenotype of GPR126$^{-/-}$ mice is caused by defective mitochondria. A metabolic shift from fatty acid oxidation to glycolysis results in lipid accumulation. Gpr126 depleted zebrafish do not show any mitochondrial alterations, because heart morphogenesis in zebrafish relies more on glycolysis than fatty acid oxidation. Furthermore, the cardiac phenotype could be rescued by co-injection of a Gpr126-NTFdelGPS construct, indicating that Gpr126-NTF signaling is crucial for heart morphogenesis.

4.6.6 Gpr126 in inner ear development

During formation of the semicircular canals of the inner ear in zebrafish, epithelial projection outgrowth is promoted by expression of extracellular matrix ECM protein expression. The semicircular ducts fuse with the otic vesicles and form pillars. If the Gpr126 gene is disrupted, the so called “lauscher” mutants fail to fuse semicircular canals with the otic vesicle and do not downregulate ECM protein expression resulting in a swelling of the inner ear. The hypomorphic lauscher phenotype can be partially rescued by cAMP agonists indicating that Gpr126 functions via Gs signaling during inner ear development. Four Gs proteins are known in Zebrafish. Sequencing of lauscher mutant cDNA revealed two missense mutations in the fourth transmembane domain (I963N; P969L) and two nonsense mutations causing truncated receptors L463X and W804X (part of GPS motif) (Geng et al., 2013).

4.6.7 Gpr126 in disease

Kou et al. performed a genome wide association study GWAS in 1819 patients with adolescent idiopatic scoliosis AIS and identified a susceptibility locus on chromosome 6q24.1. The most significantly associated SNPs were identified in the *Gpr126* gene (Kou et al., 2013). When Gpr126 is deleted in osteochondroprogenitor cells using a Col2Cre;Gpr126fl/fl mouse model, mice develop scoliosis and pectus excavatum. Neither scoliosis nor pectus excavatum were present in the DhhCre;Gpr126fl/fl (Karner et al., 2015), which deletes Gpr126 in neuronal tissue. Therefore the AIS phenotype is not a cause of neuropathy of radicular nerves.

4.6.8 Gpr126 is crucial for radial sorting and myelination in zebrafish

Pogoda et al. published in 2006 a genetic screen, focused on disruption of myelination in zebrafish (Danio rerio)(Pogoda et al., 2006). To induce mutations in pre-meiotic germ cells, male zebrafish have been exposed to the mutagen N-nitroso-N-ethylurea (ENU). After a standard (in)-breeding scheme, homozygous mutants have been obtained in the F3 generation. F3 embryos have been screened by whole-mount in situ hybridization for myelin basic protein MBP mRNA expression. 13 mutations in 10 different genes have been identified to disrupt myelination in the posterior lateral line nerve PLLn, a big sensory and easily visible nerve in zebrafish. In the mutations st49 and st63, MBP mRNA expression was not observed in peripheral nerves but normal in the CNS. Genetic mapping assigned the mutations to Linkage group 20 (Kelly et al., 2000) containing Gpr126. Sequencing revealed a mutation in Gpr126 for both mutants st49 and st63 and a standard complementation experiment to prove a mutation in the very same gene was not necessary. The mutation in st49 is leading to a premature stop codon just in front of the GPS domain and the mutation in st63 changes a highly-conserved cysteine to a tyrosine in the 7TM domain of the receptor. To show that the phenotype was indeed caused by Gpr126, they used a morpholino blocking the splicing of Gpr126 pre-mRNA which indeed resulted in a similar phenotype (phenocopy) deficient in peripheral myelination. In situ hybridization with Gpr126 mRNA showed expression of the Gpr126 in the sensory PLLn. Quantitative PCR of PLLn could detect continuous Gpr126 expression form embryo throughout adulthood. To ask whether Gpr126 expression in neurons or Schwann cells is needed for proper myelination, they generated chimera by transplanting fluorescently labeled wildtype cells into st49 mutants. All myelinating Schwann cells had a wt genotype and some of them were ensheating Gpr126 deficient axons leading to the conclusion that Gpr126 is crucial for myelination autonomously in Schwann cells.

4.6.9 Gpr126 is crucial for myelination in mammals

To determine if Gpr126 is equally important for myelination in mammals, the Talbot lab analyzed *Gpr126* deficient mice generated by Taconic (Monk et al., 2011). In those mice, a selection cassette replaced exons 3 and 4 of the wildtype allele. Heterozygous $Gpr126^{+/-}$ mice were intercrossed and only 26 of 334 or 7.8% pups were homozygous $Gpr126^{-/-}$, which was way below the mendelian 25%. Knocking out Gpr126 was leading to increased embryonal lethality. At birth, $Gpr126^{-/-}$ pups are same size as heterozygous and wildtype littermates, but they fail to thrive, become immotile by P12 and die before weaning. Phenotypically, $Gpr126^{-/-}$ showed contractures of the joints. Sciatic nerves of $Gpr126^{-/-}$ mice were thinner and more translucent than nerves of wt mice. Transcription factor Sox10, expressed during early development in Schwann cells was identified in sciatic nerves of $Gpr126^{-/-}$ mice but they failed to express later transcription factors such as Dhh, Oct6, Egr2 or myelin basic protein MBP. Interestingly, CNS myelination of optic nerves by oligodendrocytes was not affected in $Gpr126^{-/-}$ mice. Axonal sorting of Schwann cells with axons was happening in a normal 1:1 fashion, but was severely delayed. All Schwann cells were arrested at the promyelinating stage and never generated any myelin. Furthermore, Remak bundles, in which a non-myelinating Schwann cell

ensheathes multiple axons, were not observed in *Gpr126*$^{-/-}$ mice. At postnatal day 4, *Gpr126*$^{-/-}$ mice showed significantly less axons leading to the conclusion that Gpr126 signaling is crucial for axonal maintenance.

4.7 Ligands for Gpr126

4.7.1 Laminin-211

Laminin-211 was the first reported ligand for Gpr126. The basal lamina is crucial for Schwann cell development, it mainly consists laminin, collagen IV and heparin sulfate proteoglycans HSPGs. Only laminin but not collagen IV or HSPGs is sufficient to promote myelination (Eldridge et al., 1989). The formation of the basal lamina is essential for radial sorting and myelination. Laminin-211 (formerly known as Laminin-2) is a heterotrimeric protein composed of an α-2, β-1 and γ-1 chain encoded by the genes *Lama2*, *Lamb2* and *Lamc1*. The Laminin-isoform 211 binds to β1-integrins and α-dystroglycan (Feltri and Wrabetz, 2005). Mice deficient for Laminin and β1-integrin show abnormal or absent radial sorting. And resembled the phenotype of *Gpr126*$^{-/-}$ mice. Laminins were considered to be very probable candidates for a Gpr126-ligand since adhesion GPCRs are well known for their ability to bind extracellular matrix molecules. Luo et al. already reported Collagen III as a ligand for aGpr56 (Luo et al., 2011). Interaction of β1-integrin and laminin-211 phosphorylates and activates downstream effector focal adhesion kinase FAK. p-FAK levels were not altered in Gpr126st^{47} mutants, indicating that Gpr126-NTF-signaling is bypassing FAK. In co-immunoprecipitation assays, Petersen et al. could pull down laminin-211 together with a Gpr126-NTF-hFc fusion protein in primary mouse astrocyte cultures, meningeal fibroblast cultures and P4 sciatic nerve lysates. A laminin-binding domain in Gpr126-NTF between aa 446 and 807was identified. Dorsal root ganglia DRGs cultured on laminin coatings of different concentrations showed an increased myelin basic protein expression on higher concentrations of laminin-211. *Lama2* knockdown in hypomorphic Gpr126st^{63} mutants resulted in reduced PLLn Mbp expression and Gpr126st^{63} mutants were rescued by injection of a *lama2* overexpression construct.

4.7.2 Stachel

Gpr126 has been reported to signal via G protein coupling (Mogha et al., 2013). From other adhesion GPCRs it is known that deletion of amino-terminal ectodomains can lead to increased receptor activity (Okajima et al., 2010; Paavola et al., 2011). To elucidate aGPCR activation, Liebscher et al generated amino-terminally truncated variants of Gpr126. The receptor variants were constitutively active unless a domain between the GPS cleavage site and TM1 was deleted. The tethered agonist at the very carboxy-terminus of the ectodomain was called Stachel. The authors propose a model in which ligands bind to the ectodomain of Gpr126 leading to a conformational change or simply a mechanical dislocation. Both would expose the “Stachel” sequence and activate the receptor (Liebscher et al., 2014).

4.7.3 Collagen IV

Collagen IV is a main component of the basal lamina, which drives myelination (Bunge et al., 1986), therefore it was besides of laminin a probable interacting factor with Gpr126. Paavola et al. (Paavola et al., 2014) showed that collagen IV indeed binds to Gpr126, the Cub and PTX domains mediate the interaction with collagen IV and cAMP levels in Gpr126 overexpressing Hek cells increase after collagen IV treatment. Furthermore, amino-terminally truncated Gpr126 is constitutively activated. The authors propose a model in which the NTF of Gpr126 inhibits receptor activation and collagen IV dislocates the NTF leading to receptor activation with cAMP increase.

4.8 NTF of GPR126 is sufficient for radial sorting

Zebrafish mutants gpr126st^{49} have a point mutation resulting in a premature stop codon near the GPS site. Therefore, the amino-terminal fragment NTF is intact but the entire carboxy-terminal fragment CTF is absent. Radial sorting is normal in Gpr126st^{49} leading to the conclusion that NTF is sufficient for radial sorting. Petersen et al. used TALENs to create Gpr126st^{47} mutants which have an indel resulting in a frame shift and truncated Gpr126 in the CUB domain. The gpr126st^{47} mutants missed radial sorting (Petersen et al., 2015). Transheterozygotes, containing alleles of both Gpr126st^{49} and Gpr126st^{47} mutants were significantly rescued in radial sorting.

4.9 CTF of Gpr126 activates cAMP dependent myelin gene expression

Schwann cells in Gpr126st^{49} mutants are arrested in promyelinating state. By elevation of cAMP levels through administration of forskolin, Monk et al could drive expression of myelin genes in Gpr126st^{49} mutants. Without radial sorting, there was no expression of myelin genes in Gpr126st^{47} mutants and forskolin could not promote radial sorting in gpr126st^{47} mutants. Petersen et al conclude that NTF is responsible for radial sorting and CTF raises cAMP levels resulting in expression of myelin genes *Mbp* and *P0* in promyelinating Schwann cells.

5 Scientific Aims

The cellular prion protein PrP^C became ubiquitously known for its potential capability to undergo conformational change in the context of fatal neurodegenerative diseases. However, the physiological role of this highly conserved protein is still vague. Our lab previously reported a chronic peripheral neuropathy as a common trait in four independent *Prnp*$^{-/-}$ mouse lines and showed the involvement of a non-cell autonomous function where axonal PrP^C is essential for maintenance of Schwann cells. In my thesis I studied the effect of the physiologically occurring amino-terminal flexible tail FT of PrP^C as a signaling peptide for myelin maintenance in Schwann cells. I asked if FT can bind to Schwann cells, if the interaction is based on binding to a proteinacious receptor, what class of receptors is involved and what major signaling pathways are activated by FT signaling. Finally, I aimed to identify the responsible FT receptor on Schwann cells with the goal to understand the molecular mechanism leading to chronic demyelinating neuropathy in *Prnp* deficient mice. The novel insights into FT signaling in Schwann cells could offer innovative therapeutic strategies for the treatment of neuropathies, a highly prevalent disorder.

6 Methods

6.1 Mice

Mice were bred in specified-pathogen free facilities at the University Hospital Zurich and Washington University, and housed in groups of 3-5, under a 12 h light/12 h dark cycle (from 7 am to 7 pm) at 21±1°C, with sterilized chow (Kliba No. 3431, Provimi Kliba, Kaiseraugst, Switzerland) and water *ad libitum*. Animal care and experimental protocols were in accordance with the Swiss Animal Protection Law, and approved by the Veterinary office of the Canton of Zurich (permits 123, 130/2008, 41/2012 and 90/2013). The following mice were used in the present study: C57BL/6J, $Prnp^{ZH1/ZH1}$ (Bueler et al., 1992), co-isogenic C57BL/6J $Prnp^{ZH3/ZH3}$ and $Prnp^{WT/WT}$ control mice(Nuvolone et al., 2016) and Schwann cell-specifc $Dhh^{Cre};Gpr126^{fl/fl}$ mutants. Mice of both genders were used for experiments unless specified. Archival tissues from previous studies (Bremer et al., 2010b; Nuvolone et al., 2016) were also analyzed.

6.2 Primary Schwann cell culture

Sciatic nerves from postnatal day 2-5 were dissected using microsurgical techniques. Nerves were dissociated in serum-free DMEM supplemented with 0.05% collagenase IV (Worthington) for 1h in the incubator. Sciatic nerves were mechanically dissociated using fire-polished Pasteur pipettes. Cells were filtered in a 40 µM cell strainer and washed in Schwann cell culture medium (DMEM, Pen-Strep, Glutamax, FBS 10%) by centrifugation at 300g for 10 min. Resuspended cells were plated on 3.5 cm petri dishes previously coated with poly-L-lysine 0.01% (wt/vol) and laminin (1 mg/ml). Laminin (Cat. No: L2020; from Engelbreth-Holm-Swarm murine sarcoma basement membrane) and poly-L-lysine were obtained from Sigma-Aldrich.

6.3 Purification of recombinant proteins

Full-length recombinant PrP (recPrP, residues 23-231) and globular domain (GD, residues 121-231) were purified as previously described (Hornemann et al., 2009; Lysek and Wuthrich, 2004; Zahn et al., 1997). The generation of the GST fusion FT-PrP expression vector (pGEX-KG FT-PrP) was described previously; a modified purification protocol was used (Guillot-Sestier et al., 2009). The FT-PrP expression vector was transformed into BL21 (DE3) strain of Escherichia coli (Invitrogen). Bacteria were grown in Luria-Bertani medium to an OD of 0.6, and the expression of the fusion protein was induced with 0,5mM isopropyl-1-thio-β-D-galactopyranoside (AppliChem). Cells were then grown for another 4h at 37 °C and 100 rpm shaking. Cells were pelleted at 5000g for 20 min at 4 °C (Sorvall centrifuge, DuPont). The pellet was resuspended on ice in lysis buffer (phosphate-buffered saline supplemented with complete protease inhibitors (EDTA-free, Roche), phenylmethyl sulfonyl fluoride (Sigma) and 150 µM lysozyme (Sigma) and incubated on ice for 30 min. Triton-X 100 (1%), $MgCl_2$ (10mM) and DNase I (5 µg/ml, Roche) were added, and the lysate was incubated on ice for 30 min. The

lysate was than centrifuged for 20 min at 10'000g at 4°C. Glutathione sepharose beads were washed with PBS and incubated with the cell lysate for 1h at 4°C on a rotating device. Beads were packed into a column and washed with PBS until a stable baseline was reached as monitored by absorbance at A_{280} using an ÄKTAprime (GE healthcare). The fusion protein was cleaved on the beads with 5U/ml Thrombin (GE Healthcare) for 1h at room temperature under agitation. For thrombin removal, benzamidine sepharose beads were added and incubated for 1h at 4°C on a rotating wheel. Protein preparations were analyzed by 12% NuPAGE gels followed by Coomassie- or silver-staining. To achieve a higher purity of the protein, we next applied the protein to a sulphopropyl (SP) sepharose column equilibrated with 50mM Tris-HCl buffer, pH=8.5. Elution was performed with a linear NaCl gradient ranging from 0–1000 mM. Fractions containing the protein were collected and concentrated (AMICON; MWCO 3500). The protein was then injected in 500 µl portions into a size-exclusion chromatography system (TSK-GEL G2000SW_{XL} column (Tosoh Bioscience)) and eluted with a linear gradient using PBS. Pure fractions were combined, concentrated and stored at -20°C. The purity of FT-PrP was > 95-98 % as judged by a silver-stained 12% NuPAGE gel.

6.4 Cell Culture

SW10 cells and clones derived from it were all grown in DMEM medium supplemented with 10% fetal bovine serum (FBS), penicillin-streptomycin and Glutamax (all obtained from Invitrogen). HEK293T cells and clones derived therefrom were grown in DMEM-F12 medium supplemented with 10%FCS, penicillin-streptomycin and Glutamax (all obtained from Invitrogen). Human Gpr126 (NM_020455), Gpr124, Gpr64, Gpr56, Gpr133, Gpr56 and Gpr176 expression plasmids (pCGpr126-V5, pCGpr124-V5, pCGpr65-V5, pCGpr56-V5, pCGpr133-V5, pCGpr56-V5 and pCGpr176-V5) were generated by PCR amplification of the respective cDNA followed by TOPO cloning into the pCDNA3.1/V5-His-TOPO vector. The cDNA was in frame with the V5 tag (sequence: GKPIPNPLLGLDST) at the C terminus. HEK^{GPR126}, HEK^{GPR176} cells were generated by transfecting 1µg of plasmid in one well of a subconfluent 6-well plate using 3µl Fugene (Roche) according to the manufacturer's protocol. 24h after transfection, cells were transferred to a 10cm dish and grown in selective medium containing 0.4 mg/ml G418 (Invitrogen) until emergence of resistant colonies. A limiting dilution was carried out to obtain clonal lines. Membrane expression of the transgene was assessed in the selected clones by confocal microscopy using 1:100 diluted anti-V5 antibody (Invitrogen) and the Cytofix/Cytoperm kit (Pharmingen Cat. Nr. 554714), according to manufacturer's protocol.

6.5 Cerebellar granule neuronal culture

Cerebellar granule neurons were generated from 7-8 day old $Prnp^{ZH1/ZH1}$ mice with methods described previously (Schulz et al., 1996). Cultures were plated at 350,000 cells/cm^2 in Basal Medium Eagle (BME) (Invitrogen) with 10% (v/v) FCS and maintained at 37°C in 5% CO_2.

6.6 Plasmids and Transfections

pCDNA-PrP^C was generated by cloning murine PrP^C into pCDNA3.1 vector as described previously (Dametto et al., 2015). Site-specific mutagenesis kit (Stratagene) was used to induce alanine substitutions of QPSPG and KKRPK domains in PrP^C. Primers used for generating Ala-QPSPG plasmid are: forward- GTG GAA GCC GGT ATC CCG GGG CGG CAG CCG CTG CAG GCA ACC GTT ACC C reverse: GGG TAA CGG TTG CCT GCA GCG GCT GCC GCC CCG GGA TAC CGG CTT CCA C. Primers for Ala-KKRPK are: forward- CTA TGT GGA CTG ATG TCG GCC TCT GCG CAG CGG CGC CAG CGC CTG GAG GGT GGA ACA CCG, reverse: CGG TGT TCC ACC CTC CAG GCG CTG GCG CCG CTG CGC AGA GGC CGA CAT CAG TCC ACA TAG. Transfections were performed with Lipofectamine 2000 (Invitrogen) according to manufacturer's protocol. 3µg of DNA was used per well of a 6-well plate. 24h post transfections, cells were washed using PBS, and fresh medium was added to the cells.

6.7 Immunoprecipitation

HEK293T and HEK^{GPR126} cells growing in T75 flasks at 50% density were treated with recombinant FT or GD (2µM, 20 min). Cells were washed twice in PBS and lysed in IP buffer: 1% Triton X-100 in PBS, 1x protease inhibitors (Roche) and Phospho stop (Roche) for 20 min on ice followed by centrifugation at 5000 rpm for 5 min at 4°C. BCA assays were performed to quantify the amount of protein, and 500 µg of protein was used for Immunoprecipitations. 2 µg of anti-V5 antibody were added to the cell lysate and incubated on a wheel rotator overnight at 4°C. On the following day, Protein G dynabeads (Invitrogen) were added to the samples and incubated for further 3h on the wheel at 4°C. Beads were washed three times, 5 min each using the IP buffer followed by addition of 2x sample buffer containing DTT (1mM final). Samples were heated at 95°C for 5 min, loaded on 4-12% Novex Bis-tris gels (Invitrogen), and migrated for 1.5h at 150V followed by western blotting. Immunoprecipitations were performed by adding 2 µg of POM2 antibody to 500µl of cell medium and incubating overnight on a wheel rotator at 4°C. Protein G beads were then added, and incubation on a wheel rotator at 4°C was performed again.

6.8 RNA Isolation and quantitative PCR

RNA extraction and quantitative PCR was performed as described previously (Bremer et al., 2010b). The following primers were used: EGR2 fw: 5'-AATGGCTTGGGACTGACTTG-3'; EGR2 rev: 5'-GCCAGAGAAACCTCCATT-3' CA; GAPDH fw: 5'-CCACCCCAGCAAGGAGAC-3'; GAPDH rev: 5'-GAAATTGTGAGGGAGATGCT-3'.

6.9 Zebrafish mutant strains and analysis

Adult zebrafish were maintained in the Washington University Zebrafish Consortium facility (http://zebrafishfacility.wustl.edu/) and all experiments were performed in compliance with institutional

protocols. Embryos were collected from harem matings or *in vitro* fertilization, raised at 28.5°C, and staged according to standard protocols (Kimmel et al., 1995). The *gpr126*^{st49} and *gpr126*^{st63} mutants were described previously (Monk et al., 2009; Pogoda et al., 2006).

6.10 Zebrafish peptide treatment, immunostaining, and quantification

gpr126^{st63} or *gpr126*^{st49} mutants were collected from homozygous mutant crosses and WT larvae were collected from AB* strain crosses and raised to 50 hours post fertilization (hpf). FT_{23-50} treatment of *gpr126* mutants was performed as previously described (Liebscher et al., 2014). Briefly, egg water was then replaced with either 20 µM FT_{23-50} in egg water or egg water containing an equivalent volume of DMSO. At 55 hpf, larvae were washed twice and raised in egg water to 5 days post fertilization (dpf). WT and *gpr126* larvae were fixed in 2% paraformaldehyde + 1% tricholoroacetic acid in phosphate buffered saline, and Mbp and acetylated tubulin immunostaining was performed as described previously (Lyons et al., 2005; Monk et al., 2009). Expression scoring was performed with observer blind to treatment according to the following rubric: "strong" = strong and consistent expression throughout PLLn, "some" = weak but consistent expression in PLLn, "weak" = weak and patchy expression in PLLn, "none" = no expression in PLLn. N = three independent replicate *gpr126*^{st63} assays and one *gpr126*^{st49} assay. n = 87 DMSO-treated *gpr126*^{st63} larvae, 81 Prp-FT-treated *gpr126*^{st63} larvae, n = 27 DMSO-treated *gpr126*^{st49} larvae, n = 25 Prp-FT-treated *gpr126*^{st49} larvae. Fluorescent nerve images were analyzed using the Fiji software (Schindelin et al., 2012). A rectangle region-of-interest (ROI) was drawn longitudinally over the fluorescent nerve. The longitudinal grey-scale histogram of the myelin basic protein (MBP) was normalized pixel-by-pixel to the corresponding intensity of the acetylated tubulin (AcTub). The size of the measured ROIs was kept constant across different treatment modalities.

6.11 Flow cytometry

SW10 cells were grown in P75 flasks at 50% density, rinsed with PBS, and detached from culture flasks with dissociation buffer containing EDTA (GIBCO). After detaching, cells were washed to remove residual EDTA and counted using a Neubauer chamber. Batches of 10^5 SW10 cells were transferred to FACS tubes, treated with HA-tagged recombinant peptides for 20 minutes, washed, and incubated with Alexa-488 conjugated anti-HA antibody for 30 minutes. After further washes and centrifugations, cells were resuspended in 200µl of FACS buffer (PBS +10% FBS) and analyzed with a FACS Canto II cytofluorimeter (BD Biosciences). Data were analyzed using FloJo software.

6.12 Western blot analysis

Schwann cells were lysed in cell-lysis buffer (Tris-HCl 20mM, NaCl 137mM, Triton-X-100 1%) supplemented with protease inhibitor cocktail (Roche complete mini). The lysate was homogenized by passing several times through a 26G syringe, and cleared by centrifugation at 8000g, 4°C for 2 min. in

a tabletop centrifuge (Eppendorf 5415R). Protein concentration was measured with the BCA assay (Thermo Scientific). 10 µg total protein was boiled in 4 x LDS (Invitrogen) at 95°C for 5 min. After a short centrifugation, samples were loaded on a gradient 4-12% Novex Bis-Tris Gel (Invitrogen) for electrophoresis at constant voltage of 200V. Gels were transferred to PVDF membranes with the iBlot system (Life technologies). Membranes were blocked with 5% Top-Block (Sigma) in PBS-T for 1h at room temperature. Primary antibody was incubated overnight in PBS-T with 5% Top-Block. Membranes were washed three times with PBS-T for 10 min. and incubated for 1 hour with secondary antibodies coupled to horseradish peroxidase at room temperature. After three washes with PBS-T, the membranes were developed with Crescendo chemiluminescence substrate system (Millipore). Signals were detected using a Stella 3200 imaging system (Raytest, Straubenhardt, Germany).

6.13 Antibodies

Monoclonal antibodies against PrP^C were obtained and used as described previously (Polymenidou et al., 2008). Fab3 and Fab71 antibodies were generated using the phage display technology and their epitopes were mapped with overlapping peptides. Anti AKT, p-AKT were obtained from Cell signaling and used at 1:2000 dilutions for western blotting. Anti-p75NGF receptor antibody was obtained from Abcam and used at 1:200 dilutions for immunofluorescence. Anti V5 antibody was from Invitrogen and used at a dilution of 1:500 for western blot and 2µg of the antibody was used for immunoprecipitation on 500µg of cell lysate.

6.14 Cyclic AMP measurements

In the Direct cAMP ELISA assay, cAMP levels were assessed with a colorimetric competitive immunoassay (Enzo Life Sciences). Quantitative determination of intracellular cAMP was performed in cells or tissues lysed in 0.1 M HCl to stop endogenous phosphodiesterase activity and to stabilize the released cAMP. SW10 or HEK293T cells (100’000 cells /well) were plated in 6-well plates to a ca. 50% density. Cells were treated with conditioned media or recombinant peptides (2µM, unless specified) for 20 minutes unless otherwise mentioned. Cells were lysed with 0.1M HCl lysis buffer (Direct cAMP ELISA kit, Enzo). To ensure complete detachment of cells cell scrapers were used. Lysates were homogenized with 26G needle and syringe before clearing by centrifugation at 600g for 10 min. The subsequent steps were performed according to the manufacturer’s protocol based on competition of sample cAMP with a cAMP-alkaline phosphatase conjugate. Cyclic AMP levels were calculated using a cAMP standard curve in the case of ELISA based assay. Finally, cAMP concentrations were normalized to total protein content in each sample. cAMP changes are represented as fold changes to the respective controls. For each experiment, at least three independent biological replicates were used. For normalization purposes, the median value of the respective control sample was defined as “1”. All measurements within each panel were normalized to this control value.

6.15 Generation of Schwann cell lines devoid of Gpr126

We designed two CRISPR short-guide RNA (sgRNAs) against exon 2 of Gpr126 (upper Guide CCTGTGTTCCTCTCTCAGGT and lower Guide AACAGGAACAGCAGGGCGCT). The DNA sequences corresponding to the sgRNAs were cloned into expression plasmids and transfected with EGFP-expressing Cas9-nickase plasmids. Single EGFP-expressing Schwann cells were isolated with a FACS sorter (Aria III). To determine the exact sequence of indels induced by genome editing we amplified the sgRNA-targeted locus by PCR and subcloned the fragments into blunt-TOPO vectors. Ten colonies per cell line were sequenced and showed distinct indels on each allele. A clonal subline devoid of Gpr126 was used for further studies. This cell line possessed insertions on both the alleles; a 49bp insertion at position 118 and a 5bp insertion at position 84 on each allele. Both insertions led to a frameshift and to the generation of premature stop codons leading to early translation termination.

6.16 Promoter luciferase assay

Luciferase reporter constructs were generated containing a 1.3kB sequence upstream of the transcription-starting site of Egr2. SW10 Schwann cells were transfected with Egr2 reporter construct and a renilla plasmid using lipofectamine 2000. After one day in vitro, Schwann cells were treated with recombinant full-length PrP (23-231), the globular domain of PrP (121-231) or PBS control. Luciferase activity was measured 24 hours after stimulation with Dual-Luciferase Reporter Assay System (Promega) according to the manufacturer's recommendations. Results were normalized to renilla transfection controls.

6.17 Immunocytochemistry

Glass coverslips were placed in 12-well plates (Thermo scientific) and coated with 0.01% wt/vol Poly-l-lysine solution (Sigma) overnight at room temperature. Coverslips were washed three times with ddH_2O and dried for 2h in a laminar-flow hood. Schwann cells were seeded and cultured at 50% density. Cells were treated with recombinant FT-PrP, full length recPrP or C1-PrP for 20 min., and washed with serum-free DMEM. Cells were further washed with PBS followed by fixation with 4% paraformaldehyde. Fixed cells were incubated in blocking buffer (PBS+10%FBS) for 1h. Cells were treated with various primary antibodies followed by washes and incubation with Alexa 488 and Alexa 647 tagged rabbit or mouse secondary antibodies (Life technologies). Imaging was performed by Leica SP2 confocal microscope using a 20x objective; images were processed by Image J software.

6.18 Transmission electron microscopy

Transmission electron microscopy was performed as previously described (Nuvolone et al., 2016). Briefly, mice under deep anesthesia were subjected to transcardial perfusion with PBS heparin and sciatic nerves were fixed in situ with 2.5% glutaraldehyde + 2% paraformaldehyde in 0.1 M phosphate buffer, pH 7.4 and embedded in Epon. Ultrathin sections were mounted on copper grids coated with

Formvar membrane and contrasted with uranyl acetate/lead citrate. Micrographs were acquired using a Hitachi H-7650 electron microscope (Hitachi High-Tech, Japan) operating at 80 kV. Brightness and contrast were adjusted using Photoshop. For quantification of Remak bundles and onion bulb like structures, images were captured at 1500X magnification and axon numbers and abnormal onion bulb like structures were counted manually. Quantification was performed in a blinded fashion by assigning numbers to the images and upon completion of quantification genotypes were revealed.

6.19 Recombinant peptides

HA-tagged and untagged synthetic peptides were produced by EZ Biosciences. A stock solution of 2mM was prepared by dissolving the peptides in PBS and they were used at a final concentration of 2µM unless specified. The sequences all the peptides used in this study can be found in Table 1.

7 Results

7.1 Starting a binding assay

From previous work of Juliane Bremer we learned that axonal PrP^C is essential for Schwann cell maintenance in a non-cell autonomous fashion. At the very beginning of my studies, the most obvious question was if PrP^C would directly interact with Schwann cells in a simple binding assay. A direct interaction clearly represented the easiest mechanistic explanation. Alternatively, PrP^C could have been one of many components in a multiprotein complex or the executive function could have been even more indirect through modulation of ion channels or structural alterations of the nerve-Schwann cell junction. To begin a binding assay, I had to express and purify the prion protein and some larger oligopeptides representing shorter parts of the prion protein.

7.2 Expression of recombinant N-terminal Prion potein

Full length PrP^C and the globular domain (GD, residues 121-231) were already available in our repository. The aminoterminal flexible tail of PrP^C (FT, residues 23-110) had to be expressed and purified at first. The flexible tail FT presented some specific difficulties for expression and purification. FT is a completely unstructured polypeptide containing the charge cluster 1 of charged amino acids at its N-terminus. Short unstructured peptides are known to be quickly degraded by proteases. Charged peptides can show unwanted interactions with other peptides sticking to them or they will stick to every surface and can only be eluted under harsh conditions. Our FT expression vector was generated by Guillot-Sestier (Guillot-Sestier et al., 2009) by cloning residues (23-110) of PrP into the pGEX-KG vector, which conveniently allows to express constructs with a GST-tag attached for purification. I transformed the N1-pGEX vector to BL21 E.coli cells (Invitrogen) by heat shock and cultered E. coli in buffered flasks containing Luria-Bertani medium. Once an optical density of 0.6 was reached, I induced the cells with 0,5mM isopropyl 1-thio-β-D-galactopyranoside (AppliChem).

7.3 Protein purification with GST-affinity chromatography

Then, I resuspended the pellet in lysis buffer on ice (see mateials and methods for detailed protocol).The supernatant containing the FT was then incubated with Glutathione sepharose beads. Beads were packed into a column and washed under control of A280 absorption using an Äkta prime purifier. The pGEX-KG vector provided a Thrombin recognition site in between the GST and the FT-sequence. Hence, the FT could be cleaved on column using 5U/ml Thrombin (GE Healthcare). I removed Thrombin with benzamidine sepharose. Finally, I could analyze the prurified protein by gel-electrophoresis and Coomassie staining wich resulted in a clearly visible band at 9kD (**Fig. 7.1 A**). Coomassie blue can stain peptides in the µg range and I next performed a silver staining, which could show impurities in the nanogram range (**Fig. 7.1 B).** I found some higher running bands, which could be di-, tri- or polymers of FT or represent different E. coli derived peptides. Smaller bands were most probably degraded parts of FT.

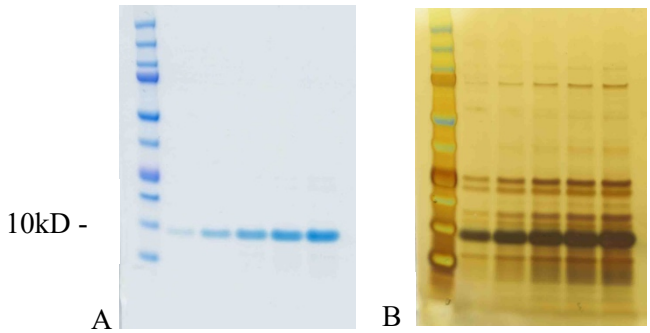

Figure 7.1 | Impurities obvious in silver gel. A Coomassie gel showing a purified 9kd protein in increasing amounts. B Silver staining of the very same gel depicts impurities in the ng range.

7.4 Cation exchange chromatography

For my binding assay and even more for the later signaling assays such as the cAMP assay I needed highly pure protein preparations. Especially heat shock proteins are abundant in E. coli and can interact in many downstream assays and applications. Therefore, I intensified my purification process by adding a cation exchange chromatography step. I hypothesized that main impurity could come from residual GST. The isoelectric point (pI) of FT can be calculated and equals 9.5, whereas the pI of GST is 6. To get rid of GST, I had to choose a pH in between 6 and 9.5, when FT was positively and GST negatively charged. The fractions were adsorbed to sulphopropyl sepharose in Tris-HCl buffer at a pH of 8.5. Elution was performed with a linear NaCl gradient and resulted in a major peak at 200mM NaCl (**Fig. 7.2**).

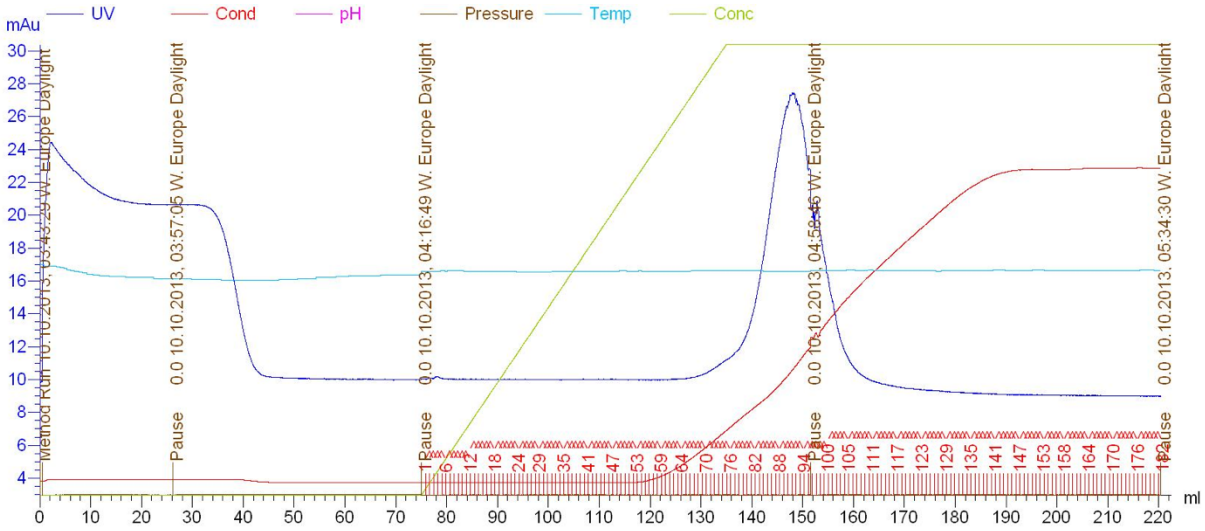

Figure 7.2 | Cation exchange chromatography. CEC using sulphopropyl sepharose in Tris-HCl buffer at a pH of 8.5. Elution with a linear 0-500mM NaCl gradient. A clear UV-peak is visible shortly after 200mM NaCl (Äkta prime).

7.5 Size exclusion chromatography

To further enhance the purity of our protein preparations, I performed size-exclusion chromatography on a high performance liquid chromatography (HPLC) TSK-GEL G2000SWXL column (Tosoh Bioscience). Size exclusion chromatography separates peptides by size and shape. The polymer beads packed in the column offer many pores where smaller peptides can hide during elution. In contrast, large peptides cannot

enter the small pores and are eluted instantaneously. By help of size exclusion chromatography I was able to get rid of a larger contaminant and still collected a nice protein peak in the fractions D9-D5 (**Fig. 7.3**).

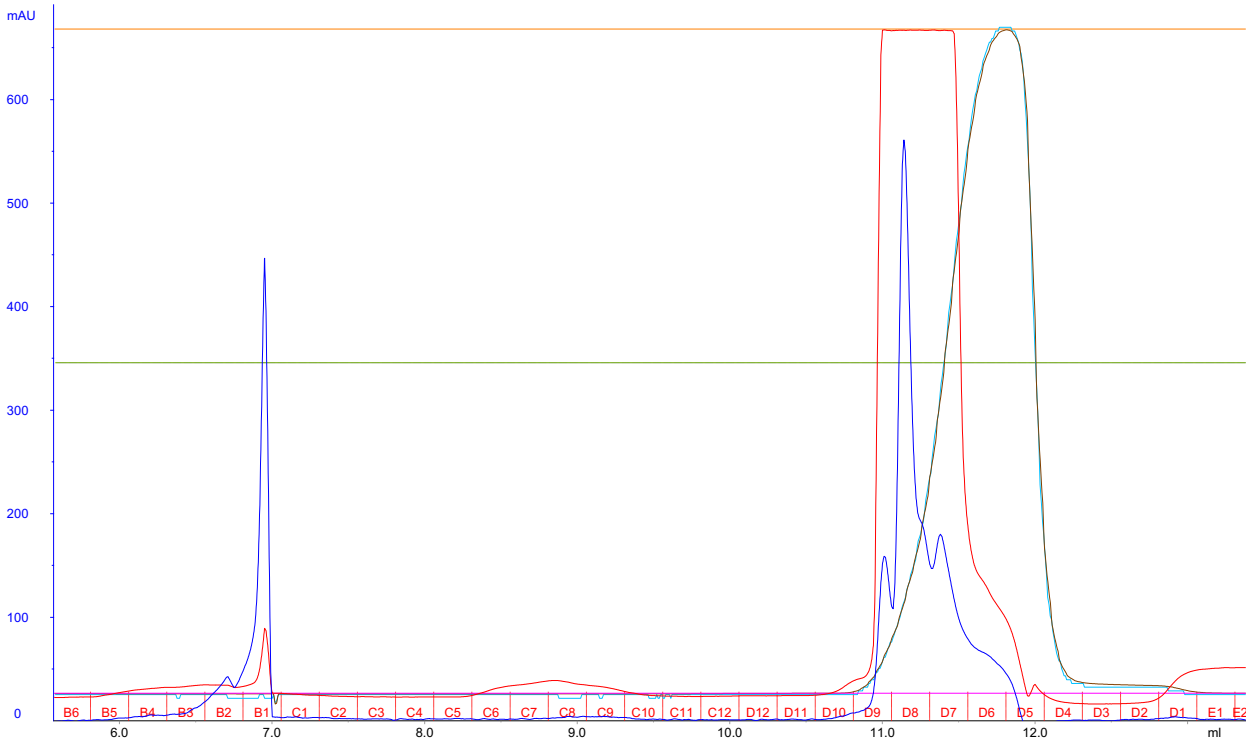

Figure 7.3 | Size exclusion chromatography. Protein absorption at 280nm showing a larger contaminant in fraction B1 and the FT-peak in fractions D9-D5.

Enhanced purification with serial ion exchange chromatography and size exclusion chromatography resulted in higher purity as seen in **(Fig. 7.4)** on a silver gel.

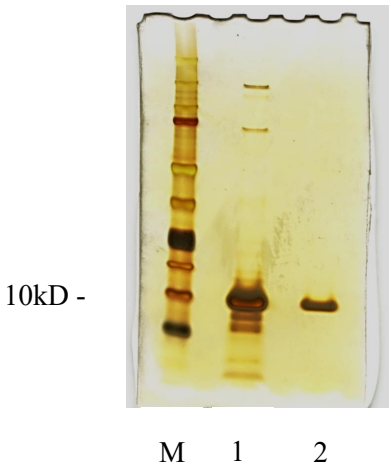

Figure 7.4 | Compraison of pre- and postpurified peptide preparation. Silver gel of FT preparation after affinity chromatography only (lane 1) and after additional ion exchange and size exclusion chromatography (lane 2). M = marker. Lane 2 shows a single band at 9kD. No other peptides appear in the ng range.

7.6 Western Blotting

I then performed a Western Blot using a POM 11 antibody recognizing the FT fragment in order to ensure that the band was the desired FT indeed (**Fig. 7.5**).

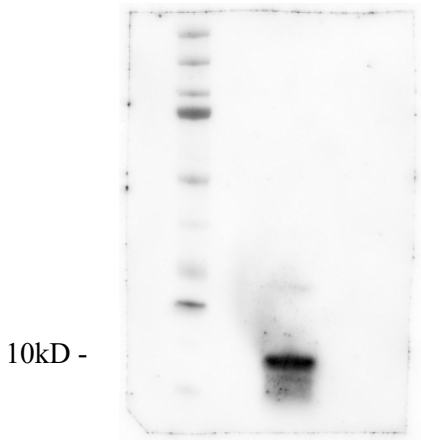

Figure 7.5 | Immunodetection of recombinant FT. Western Blot using POM 11 antibody recognizing the FT. The band at 9kD was clearly detected.

7.7 PrP^C binds to Schwann cells

At the very beginning of my thesis I started with a simple binding experiment and assessed if full-length PrP^C or fragments thereof would stick to primary Schwann cell cultures (PSC) prepared from sciatic nerves of *Prnp*$^{ZH1/ZH1}$ mice (Bueler et al., 1992). In order to avoid confounding homotypic interactions between resident and incoming PrP^C (Santuccione et al., 2005), I decided to use PSC from *Prnp* deficient mice. I exposed PSCs to bacterially expressed proteins corresponding to murine full-length PrP^C lacking its N-terminal secretory signal peptide (recPrP, residues 23-231), isolated flexible tail of PrP^C (FT, residues 23-110), or its refolded globular domain (GD, residues 121-231). Then, I treated the PSCs with POM1 and POM2 antibodies (Polymenidou et al., 2008) recognizing the GD and the FT, respectively and assessed binding by immunocytochemistry. To my surprise, both recPrP and the FT, but not the GD, were found to stain PSC, indicating an interaction of amino-terminal PrP and the Schwann cell surface (**Fig. 7.6**).

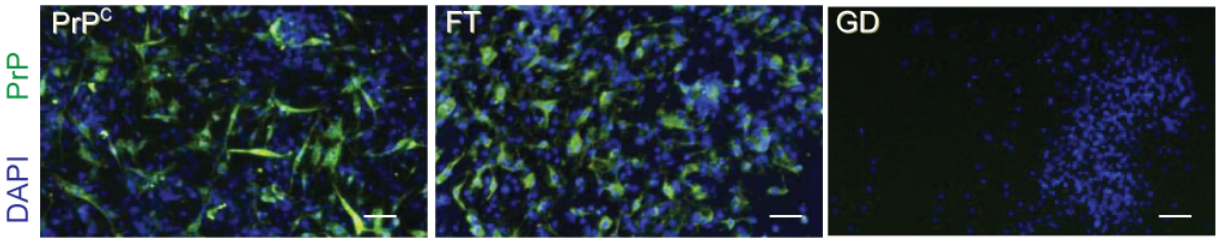

Figure 7.6 | The prion protein binds to Schwann cells. Primary Schwann cells were isolated from the sciatic nerves of *Prnp*$^{ZH1/ZH1}$ mice and grown on coverslips. Cells were exposed for 20 min to recombinant PrP^C, FT, or GD (2µM), fixed, and stained with POM2 (FT, PrP^C) or POM1 (GD). Antibodies were visualized in the green channel and nuclei were stained with DAPI (blue). PrP^C and FT, but not GD, adhered to the cells. Scale bars: 25µm

7.8 SW10 Schwann cell line

The generation of PSC is laborious and my promising first results suddenly created a need for robust and quickly growing Schwann cells. At ATCC I purchased the Schwann cell line SW10 and analyzed them for PrP expression which I could confirm to be present by Western blot (**Fig. 7.9 B**).

7.9 SW10$_{\Delta PrP}$

Again to avoid confounding interactions between resident and incoming PrP^C, I decided to ablate *Prnp* in SW10 cells using transcription activator-like effector nucleases (TALEN). Therefore, I transfected SW10 cells (Lipofectamine, Invitrogen) with the TALEN Upper Guide, the TALEN lower guide and an EGFP transfection control. The first day after transfection, I checked the efficacy by fluorescence microscopy and around 30% of cells could be transfected (**Fig. 7.7**).

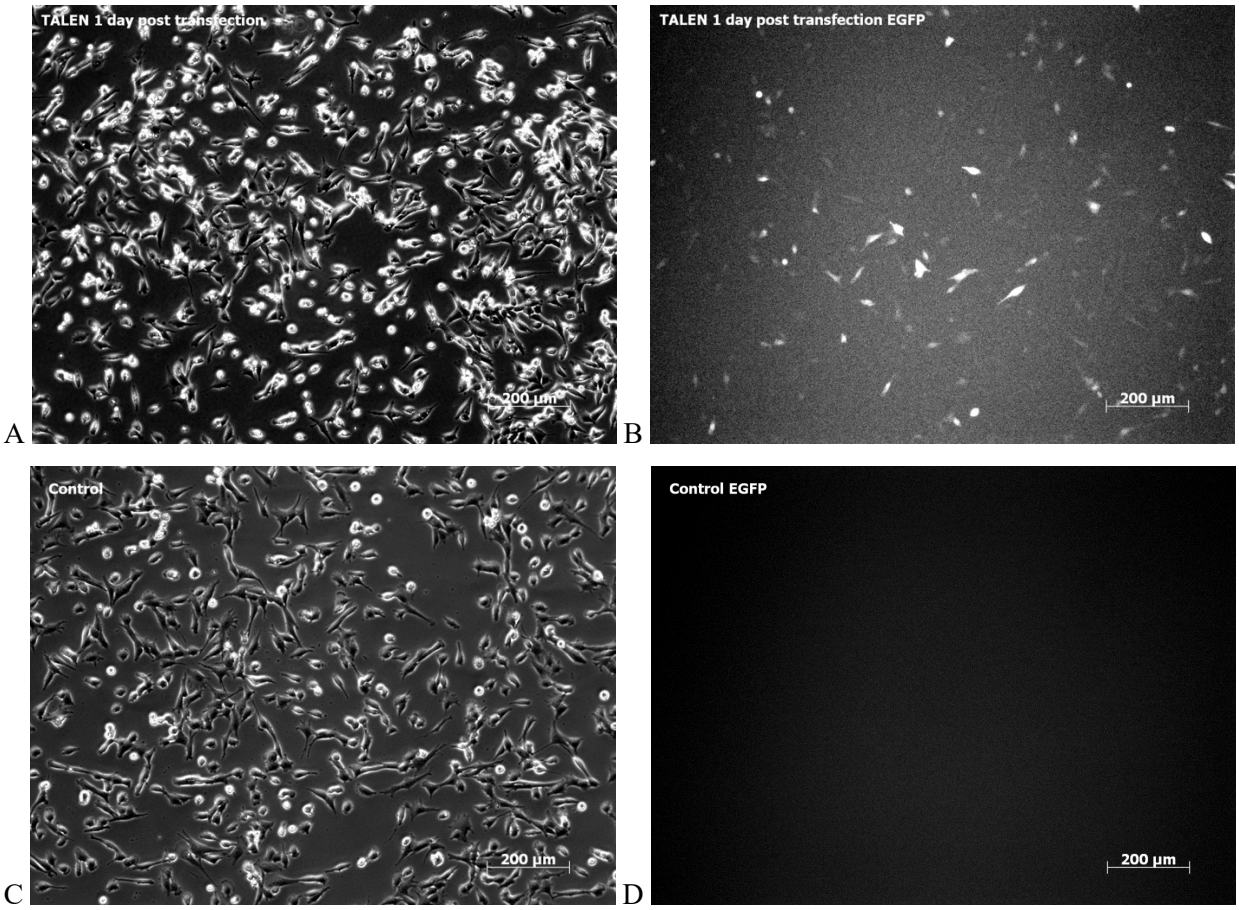

Figure 7.7 | Transfection of SW10 cells. A: Transfection with TALEN upper guide, TALEN lower guide and EGFP transfection control. **B**. Fluorescence microscopy with positively transfected cells visible (around 30%). **C**: Control SW10 treated with empty vector and Lipofectamine. **D**: Fluorescence microscopy of control without any positive cells.

In order to get clonal cell lines, I FACS-sorted positively transfected cells in 96-well plates. After 4 weeks of cell culture, I could detect cell medium discoloration in 7 wells and growth of 7 different clones was realized (**Fig. 7.8**).

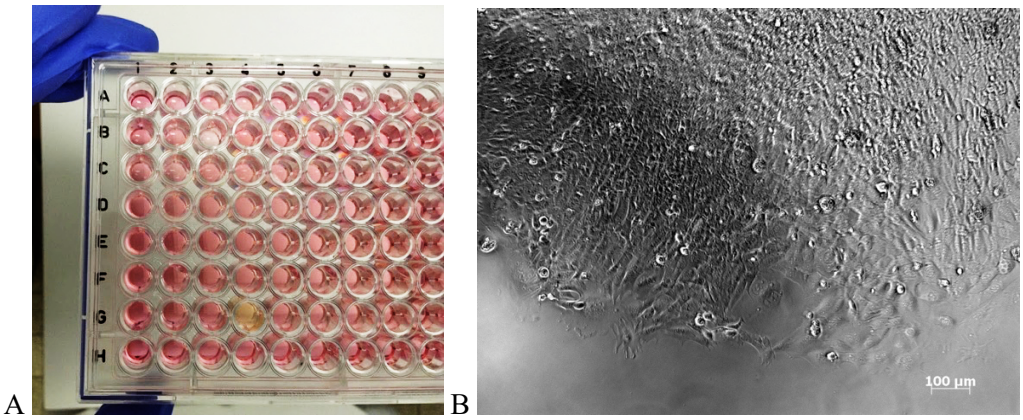

Figure 7.8 | Single cell FACS sorting. A: EGFP positive single cells were FACS-sorted in 96-well plates. Growth was detected after 4 weeks by yellow discoloration of the cell medium as seen in well 4G. **B**: Clonal cell bulk in well 4G from A.

One cell clone called SW10$_{\Delta PrP}$ contained a point mutation in the coding region of *Prnp* leading to a frameshift and a premature stop codon (**Fig. 7.9 A**) that abolishes PrP^C expression. I could prove complete ablation of PrP^C by Western Blot with POM1 antibody (**Fig. 7.9 B**).

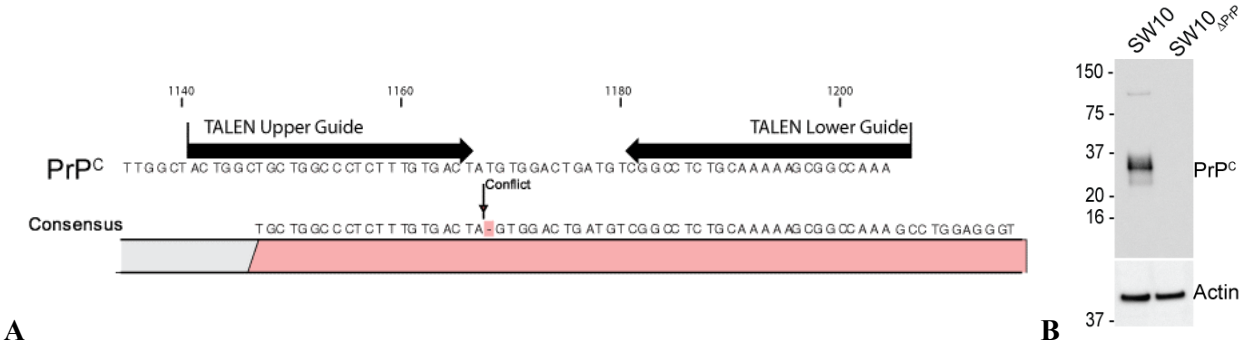

Figure 7.9. Sequencing of cell clone. A: Schematic representation of the target region for transcription activator-like endonucleases (TALEN) in the *Prnp* gene. Target guides are indicated by arrows. Gene editing resulted in a deletion leading to a frame shift in the PrP^C coding sequence (designated as conflict in the figure) and a premature stop codon identified by sequencing. **B**: Wild-type SW10 cells and a subclone isolated after treatment with TALEN (termed SW10$_{\Delta PrP}$) were probed by Western blotting using anti-PrP antibody (POM1). SW10$_{\Delta PrP}$ showed complete abrogation of PrP^C expression and was used for further experiments. Levels of actin on the same membrane were monitored to confirm equal loading of cell lysates onto the gel.

7.10 Confirmation of FT binding in SW10$_{\Delta PrP}$

To make sure that SW10$_{\Delta PrP}$ are comparable to PSC, I treated SW10$_{\Delta PrP}$ cells with recPrP, FT, or GD for 20 min, and assessed binding by immunofluorescence with POM1 and POM2 antibodies (**Fig. 7.10 + 7.11 A+B**). Confirming my previous results with PSC, recPrP and FT, but not GD, adhered to SW10$_{\Delta PrP}$ cells. Moreover, neither recPrP nor FT adhered to the PrP^{C}-ablated hippocampal cell line HpL (Kuwahara et al., 1999) (**Fig. 7.11 C**), suggesting that binding was specific to Schwann cells.

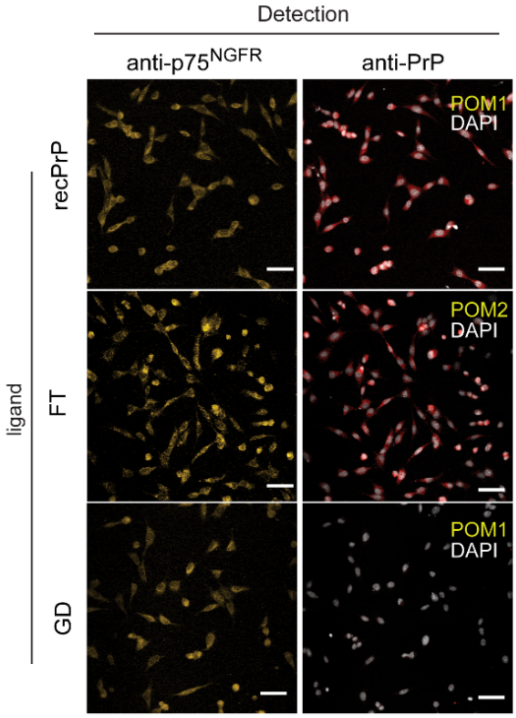

Figure 7.10 | Schwann cells selectively bind the Flexible Tail (FT) domain of PrP^{C}. *Prnp*-ablated SW10 cells (SW10$_{\Delta PrP}$) were exposed to recombinant PrP^{C}, FT, or GD ("ligand"). Binding was assessed with antibodies POM1 or POM2 (red). Grey: nuclei (DAPI). Antibodies to p75^{NGFR} were used to identify Schwann cells. PrP^{C} and FT, but not GD, adhered to Schwann cells. Scale bar: 26 µM.

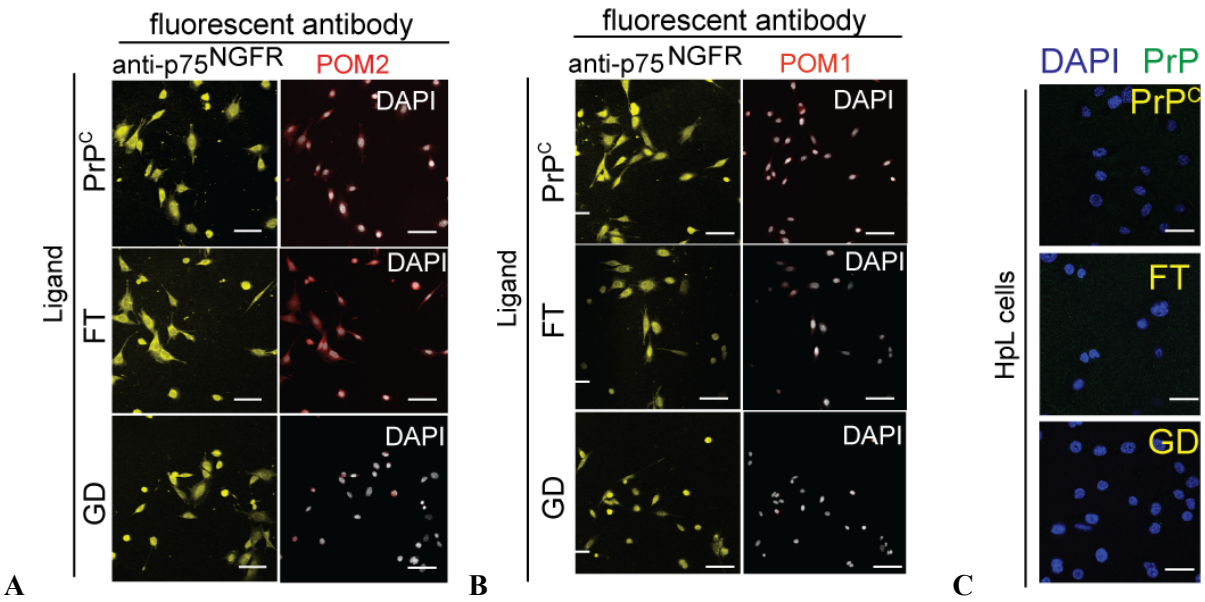

Figure 7.11 | **A-C**: SW10$_{\Delta PrP}$ cells were treated with full-length recombinant (PrP^C, residues 23-231), flexible tail (FT, 23-110), or globular domain (GD, 121-231). PrP epitopes were detected with POM2 (A) or POM1 (B) (red). Grey: DAPI. As expected, FT was detected only by POM2. Cells were also labeled with antibodies to the p75 nerve-growth factor receptor (yellow), a Schwann cell marker. PrP^C and FT, but not GD, adhered to Schwann cells. Scale bar: 26 µm. **C**: As a control, the PrP^C-deficient cell line HpL (Kuwahara et al., 1999) was treated with recombinant PrP^C, FT, and GD as in panel A. None of the recombinant proteins adhered to HpL cells. Scale bars: 20 µm.

7.11 What domain of FT is responsible for binding to Schwann cells?

I next sought to identify the minimal region within the FT responsible for binding. In this experiment I used synthetical peptides (EZ Biosciences) to make sure that no bacterial contaminants were present. I exposed SW10$_{\Delta PrP}$ cells to a series of partially overlapping hemagglutinin (HA)-tagged synthetic peptides (2 µM, 20 min) and stained them with FITC-labeled anti-HA antibody (**Fig. 7.12 A**). Then, I measured binding with fluorescence flow cytometry. FT$_{23\text{-}50}$, but neither FT$_{39\text{-}66}$ nor any of the carboxy-proximal peptides (**Table 1**), showed binding (**Fig. 7.12 B**) suggesting that residues 23-33 are essential for the interaction.

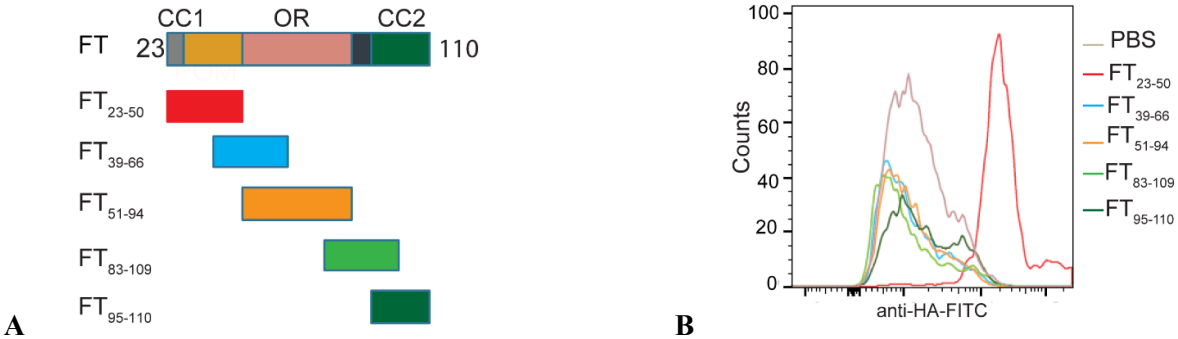

Figure 7.12 | **A**: Localization of FT-derived peptides relative to PrP^C domains. CC1 and CC2: charge clusters 1 and 2. OR: octapeptide repeats. Peptides are color-coded as in panel C. **B**: SW10ΔPrP cells were exposed to FT-derived peptides (2 µM; 20 min) carrying a carboxy-terminal hemagglutinin tag (HA). Binding was monitored by flow cytometry. Only peptide FT23-50 showed strong binding.

Name	Sequence
FT_{23-50}	KKRPKPGGWNTGGSRYPGQGSPGGNRYP
FT_{23-50}-HA	KKRPKPGGWNTGGSRYPGQGSPGGNRYPYPYDVPDYA
FT_{34-69}-HA	PGQGSPGGNRYPPQGGTWGQPKGGGWGQYPYDVPDYA
FT_{51-94}-HA	PQGGTWGQPHGGGWGQPHGGSWGQPHGGSWGQPHGGGW
FT_{83-109}-HA	PHGGGWGQGGGTHNQWNKPSKPKTNLKYPYDVPDYA
FT_{94-110}-HA	GGGTHNQWNKPSKPKTNLKHYPYDVPDYA
FT_{94-110}	GGGTHNQWNKPSKPKTNLKH
AlaQGSPG	KKRPKPGGWNTGGSRYPGAAAAAGNRYP
AlaKKRPK	AAAPAPGGWNTGGSRYPGQGSPGGNRYP
ColIV	GPRGKPGVDGYNGSRGDPGYP
ColIV-Mut	AAAGAAGVDGYNGSRGDPGYP

Table 1 | Sequence of synthetic peptides used in my study. The collagen-4 homology domain necessary for cAMP induction is highlighted in yellow.

7.12 The FT receptor is a protein

To elucidate whether the interaction partner of FT is a protein I treated SW10 cells with trypsin (2.5% w/v, 10 min) in order to degrade the extracellular domains of membrane-resident proteins. Following trypsin inactivation, I added non-trypsinized SW10 cells labeled with the cell-tracking dye Deep Red. After the addition of HA-tagged FT_{23-50} (2µM), I monitored binding by cytofluorimetry with FITC-conjugated anti-HA antibodies. 51% of non-trypsinized cells showed FT_{23-50} binding while only 5% of trypsinized cells did (**Fig. 7.13**). These results suggest the involvement of a surface protein in the interaction of the FT with Schwann cells.

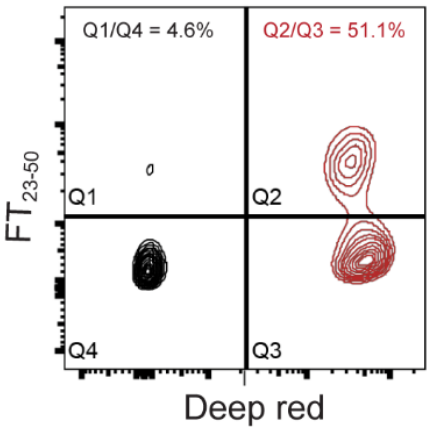

Figure 7.13 | The FT recepotor is a protein. SW10 cells trypsinized, washed, and mixed with non-trypsinized SW10 cells labeled with Deep Red cell tracker. Cells were incubated with HA-tagged peptide FT_{23-50}, and binding was visualized by flow cytometry. The Deep red signal (abscissa) was used to differentiate trypsinized from non-trypsinized cells. 51% of untreated cells, but only 5% of trypsinized cells, became decorated by FT_{23-50}-HA, indicating that FT_{23-50} reacted with trypsin-sensitive surface molecules.

7.13 The FT receptor is a non GPI-anchored protein

Because PrP^C is GPI-anchored and can undergo homotypic interactions, I wondered if the receptor might be a GPI-anchored protein. I therefore tested the binding of HA-tagged FT_{23-50} to SW10 cells treated with phosphoinositol phospholipase C (PI-PLC, 30' at 37°C), which cleaves GPI anchors. Cytofluorimetry revealed no altered binding after PI-PLC treatment, indicating that FT binding did not require GPI-

anchored surface proteins. To monitor PI-PLC effectiveness, I monitored binding of POM2 to PrP^C and found it to be greatly reduced indicating that PrP^C had been stripped from cell surfaces (**Fig. 7.14**).

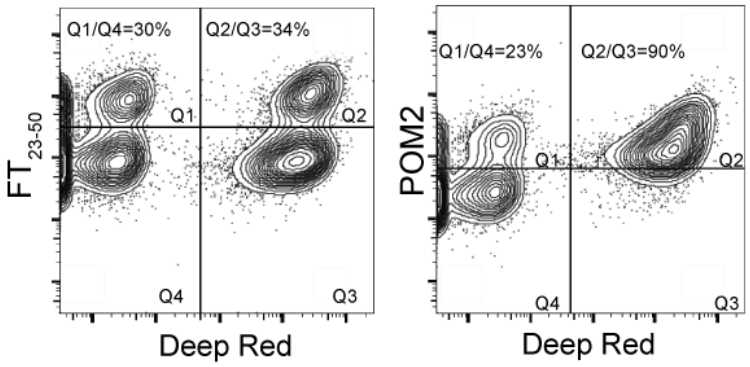

Figure 7.14. | **FT is not GPI-anchored.** SW10 cells were digested (30 min) with phosphatidylinositol phospholipase C (PI-PLC, 0.5 units), washed, and incubated with FT_{23-50}-HA along with undigested Deep-Red labeled cells (left panel). The proportion of binders in the digested (34%) and the undigested samples (30%) was similar, indicating that the FT_{23-50} receptor was neither PrP^C itself nor any other GPI-linked protein. To monitor the efficiency of PI-PLC treatment, we assessed POM2 binding to PrP^C on both treated and untreated cells (right panel). POM2 binding was significantly decreased in PI-PLC treated cells (23%) compared to untreated cells (90%).

7.14 37-kDa/67-kDa laminin receptor (LRP/LR) is not the major receptor for FT binding

The 37-kDa/67-kDa laminin receptor (LRP/LR) has been reported to interact with the cellular prion protein PrP^C (Hundt et al., 2001; Rieger et al., 1997). PrP^C can bind directly to LRP/LR with a domain including aa 144-179. Since this domain is not part of FT, it cannot be responsible for FT binding to the receptor on Schwann cells. A second binding domain including aa 53-93 was reported to be heparin sulfate dependent. First I checked if laminin treatment blocking the LRP/LR is able to abolish FT binding to the FT receptor on Schwann cells and if steric hindrance induced by binding of an anti-LRP antibody can block FT binding. Therefore, I pretreated SW10 cells with laminin or α-LRP antibody followed by FT-GST incubation. I then could detect a surface binding signal by flow cytometry using an anti-GST antibody conjugated to Alexa 488. Both laminin and α-LRP antibody were not sufficient to block binding of FT-GST to SW10 cells completely. Minor reduction in FT-GST binding was detected after LRP/LR blocking and therefore some minor binding of FT-GST to LRP/LR is possible but does not account for the entire binding of FT to Schwann cells.

7.15 Sciatic nerves from $Prnp^{-/-}$ mice have less cAMP

Next, I measured cAMP concentrations in sciatic nerve lysates mice of various ages (Bueler et al., 1992). At 4 days of age, *Prnp* ablated mice *($Prnp^{ZH1/ZH1}$)* and WT sciatic nerves showed similar cAMP levels (**Fig. 7.15 A**). At 4 weeks of age, I detected a trend towards decreased cAMP levels in $Prnp^{ZH1/ZH1}$sciatic nerves (**Fig. 7.15 B**).

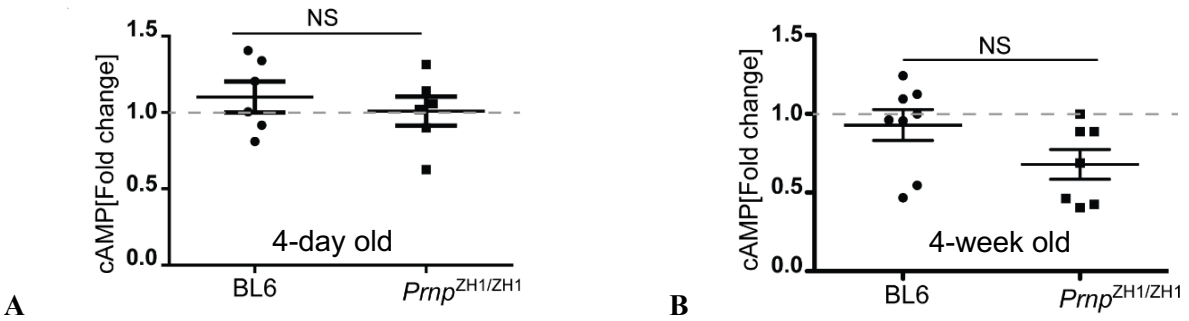

Figure 7.15 | cAMP content of Sciatic nerves from *Prnp-/-* mice compared to BL6. cAMP was measured in sciatic nerves isolated from 4-day old (**A**) or 4-week old (**B**) BL6 and $Prnp^{ZH1/ZH1}$ mice. No difference was observed in cAMP levels in 4-day old mice, whereas 4-week old $Prnp^{ZH1/ZH1}$ mice displayed a trend towards decreased cAMP levels. N.S.: non-significant. Error bars represent SEM. Unpaired Student's t-test.

At 12-16 weeks, when CDP is incipient in $Prnp^{ZH1/ZH1}$mice, myelin damage is morphologically minimal and clinically silent (Bremer et al., 2010b), $Prnp^{ZH1/ZH1}$nerves exhibited significantly lower levels of cAMP than those of wild-type BL6 mice (**Fig. 7.16 A**, p=0.0115). Strictly isogenic C57BL/6J $Prnp^{-/-}$ mice ($Prnp^{ZH3/ZH3}$) reproduced the CDP phenotype (Nuvolone et al., 2016), sciatic nerve lysates from these mice (10-16 week old) also displayed significantly lower levels of cAMP than wild-type mice (**Fig. 7.16 B**).

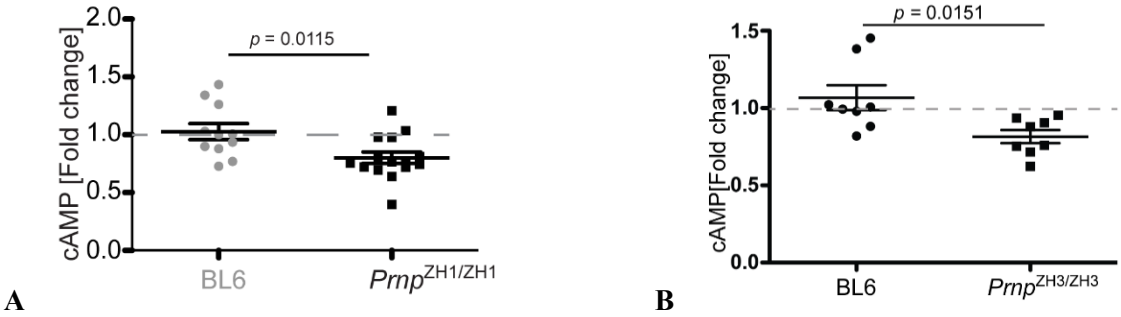

Figure 7.16 | Sciatic nerves from *Prnp-/-* mice have less cAMP compared to BL6 at 12-16 weeks. A: $Prnp^{ZH1/ZH1}$ sciatic nerves displayed significantly lower cAMP than wild-type BL6 nerves. **B**: Sciatic nerve from 10-week old $Prnp^{ZH3/ZH3}$ mice showed a significant decrease in cAMP (p= 0.0151). N.S.: non-significant. Error bars represent SEM. Unpaired Student's t-test.

7.16 Cell type specific PrP^C expression dictates cAMP content in sciatic nerves

Expression of PrP^C in neurons, but not in Schwann cells, suffices to prevent demyelination in $Prnp^{ZH1/ZH1}$ mice (Bremer et al., 2010b). Sciatic nerves from 12-16 week old *tg*NSE-PrP mice, expressing PrP^C in neurons, showed cAMP levels similar to wild-type mice, whereas *tg*MBP-PrP mice, which express PrP^C in oligodendrocytes and Schwann cells, showed significantly diminished cAMP levels in sciatic nerves (**Fig. 7.17**).

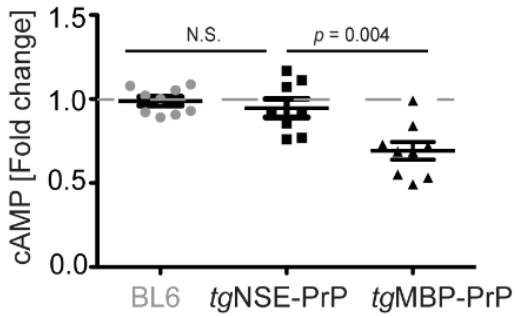

Figure 7.17 | Cell type specific PrP^C expression dictates cAMP content in sciatic nerves. Selective PrP^C expression by neurons (*tg*NSE-PrP), but not by Schwann cells (*tg*MBP-PrP) restored cAMP levels in sciatic nerves of 10-16 week-old mice. Each dot represents an individual mouse (11-15 mice/group). N.S.: non-significant. Error bars represent SEM. Unpaired Student's t-test.

7.17 Treatment of PSC and SW10 with FT induces cAMP response

I asked whether FT binding induces cAMP. PSC and SW10 cells were treated with FT (0.1-5 µM) for 20 min, and cAMP levels in cell lysates were measured. *Prnp*$^{ZH1/ZH1}$ PSC (**Fig. 7.18 A**) and SW10 cells (**Fig. 7.18 B**) reacted to FT, but not to GD, with a concentration-dependent cAMP increase. Dose-response analyses performed on PSC revealed an EC_{50} of 860 nM for FT (**Fig. 7.18. C**).

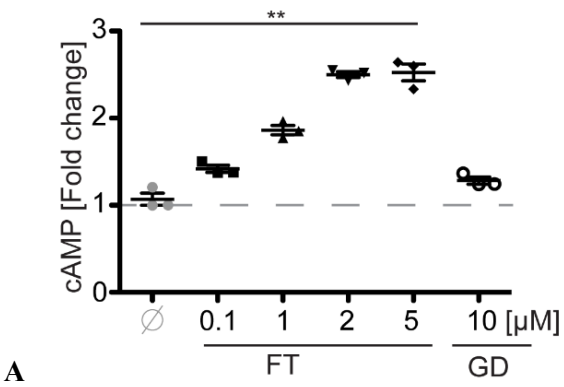

A

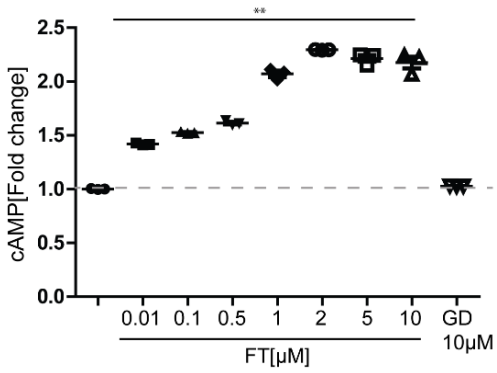

B

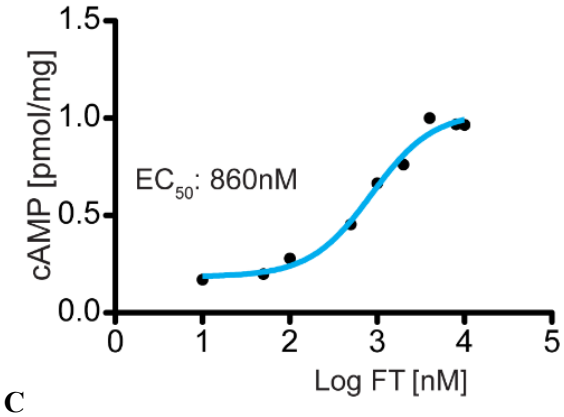

C

Figure 7.18 | FT induces cAMP. A: Primary *Prnp*$^{ZH1/ZH1}$ Schwann cells were seeded in a 6-well plates and treated (20') with increasing concentrations of recombinant FT or with 10 µM GD. Ø: untreated cells. cAMP levels were determined in cell lysates ($5x10^5$ cells/assay). Addition of FT, but not of GD, induced a concentration-dependent cAMP response in Schwann cells. Here and henceforth: *: $p<0.05$; **: $p<0.01$; ***: $p<0.001$.). **B**: SW10 cells were seeded in 6 well plates and treated (20') with recombinant FT or GD (10 µM). Addition of FT, but not of GD, resulted in a concentration-dependent intracellular cAMP increase. **C**: Primary *Prnp*$^{ZH1/ZH1}$ Schwann cells (as described in A) were treated with FT (20'), and cAMP concentrations were determined by immunoassay, and a dose-response curve was interpolated.

7.18 Transfected HEK^{PrP} cells express a soluble FT

Cytosolic cAMP spikes may result from spurious causes, including traces of bacterial contaminants, which may be difficult to identify. I transfected HEK293T cells, which express little endogenous PrP^C, with a plasmid expressing murine PrP^C or, for control, with an empty plasmid (henceforth called HEK^{PrP} and

HEK^{empty}, respectively). Immunoprecipitation of spent medium with POM2 antibody showed that PrP^{C} from HEK^{PrP} cells underwent cleavage and release of soluble FT (**Fig. 7.19 A**). The spent medium from HEK 293T cells overexpressing PrP^{C} contained ca. 37 ng FT/ml (**Fig. 7.19 B**).

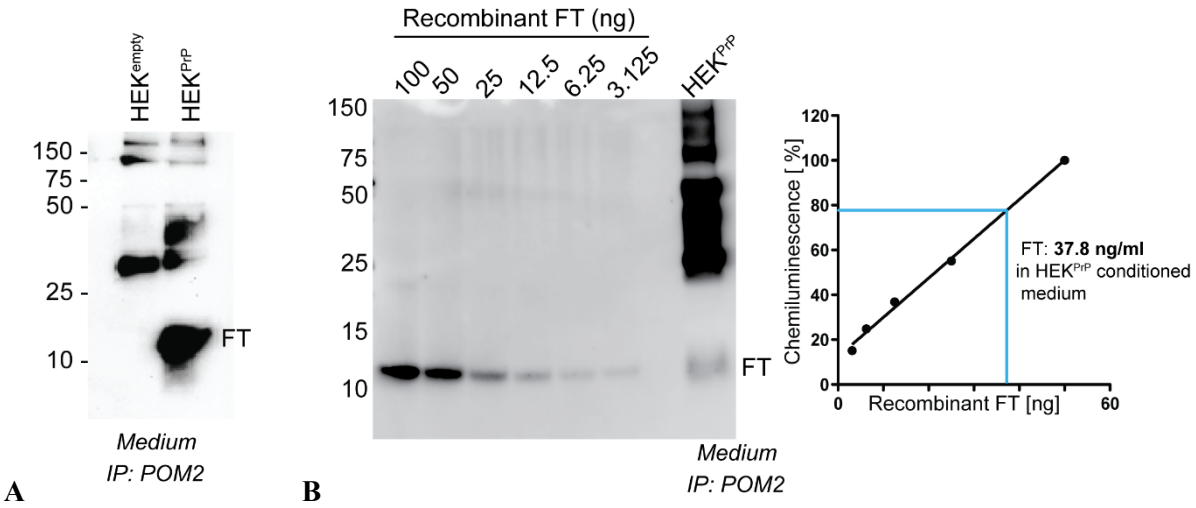

Figure 7.19 | FT is cleaved and excreted by HEK cells transfected with murine PrP^{C}. A: HEK293T cells were transfected with an empty vector (HEK^{empty}) or a plasmid expressing murine PrP^{C} (HEK^{PrP}). Cell medium was collected 48h after transfection and subjected to immunoprecipitation with monoclonal antibody POM2 (against PrP^{C}), followed by western blotting using biotinylated POM2 and streptavidin-HRP. FT was observed only in the medium from HEK^{PrP} cells. B: FT released into the conditioned medium of HEK^{PrP} was immunoprecipitated using POM2 and visualized by Western blotting with biotinylated POM2. Dilutions of recombinant FT (3.125 - 100 ng) were used for calibration, and the concentration of FT released into the medium was estimated at 37 ng/ml.

7.19 HEK^{PrP} conditioned media raises cAMP in primary Schwann cells

Exposure to conditioned medium from HEK^{PrP} cells, but not from HEK^{empty} cells, raised cAMP levels in PSC cultures generated from *Prnp*$^{ZH1/ZH1}$ mice (**Fig. 7.20 A**). These results confirm that eukaryotic PrP^{C} can lead to the spontaneous formation of FT and, in turn, to paracrine cAMP induction. Immunoprecipitation of spent medium from PSC cultures and from sciatic nerves obtained from 10 week old C57BL/6 mice did not reveal any FT, indicating that little if any FT is cleaved from PrP^{C} and released by Schwann cells (**Fig. 7.20 B-C**).

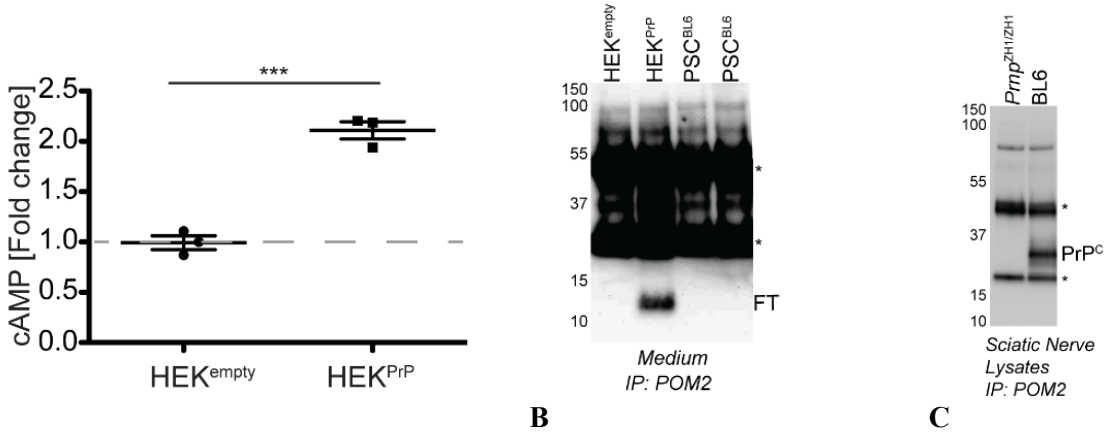

Figure 7.20 | HEKPrP conditioned media raises cAMP in primary Schwann cells. A: cAMP concentrations in primary PrnpZH1/ZH1 Schwann cell cultures exposed to medium conditioned by HEK293T cells overexpressing wild-type murine PrP^{C}

(HEKPrP, right). For control, HEK cells were transfected with a non-coding vector (HEKempty, left). FT-containing medium resulted in cAMP induction. B: Conditioned medium from primary BL6 Schwann cells cultures (PSCBL6) was subjected to immunoprecipitation with antibody POM2 (against PrP^C) followed by Western blotting with POM2. For control, we used conditioned medium from HEK cells transfected with a non-coding plasmid (HEKempty) or a with a plasmid encoding murine PrP^C (HEKPrP). FT was only detected in conditioned medium from HEKPrP cells (lane 2) but not in conditioned medium from two independent PSCBL6 cultures (lanes 3-4). Asterisks denote immunoglobulins detected by the secondary antibody. C: Sciatic nerves lysates obtained from 10 week old PrnpZH1/ZH1 and BL6 mice and subjected to immunoprecipitation with POM2 antibody followed by Western blotting with POM2. Full length PrP^C, but no FT, was detectable in the immunoprecipitates from BL6 mice.

7.20 Blocking of FT binding to Schwann cells with anti-PrP antibodies

Blocking of FT binding to Schwann cells by use of anti-FT antibodies would allow me to determine the binding domain. Therefore, I first pre-incubated FT with POM2 recognizing an epitope in the octapeptide region and POM3 recognizing an epitope close to charge cluster 2. Both pre-treatments with POM2 and POM3 enhanced binding of FT to SW10 cells and we speculate that crosslinking of FT could be the reason for this observation. POM2 which recognizes several repetitive epitopes in the OR shows the most intense signal compared to the single epitope of POM3, speaking in favor of crosslinking (**Fig. 7.21**).

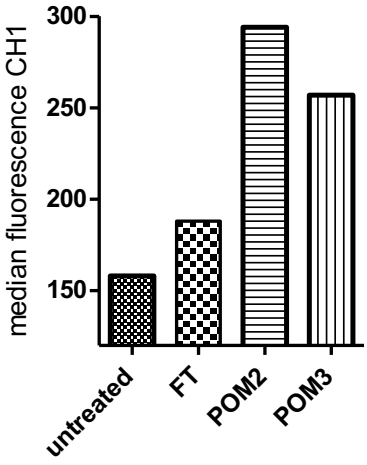

Figure 7.21 | Blocking of FT binding with anti-FT antibodies. A: Recombinant FT-GST was incubated with POM2 or POM3 antibodies before treatment of SW10 Schwann cells. Binding was detected by flow cytometry using an anti-GST antibody conjugated to Alexa488. Both POM2 and POM3 pre-incubation resulted in increased FT binding.

7.21 What part of FT induces the cAMP response?

To assess, if the FT contains motifs responsible for inducing the cAMP response, I treated $SW10_{\Delta PrP}$ cells with the same synthetic peptides previously used to assess binding to Schwann cells. Peptide FT_{23-50} induced cAMP, whereas FT_{34-69} and all carboxy proximal peptides were inactive (**Fig. 7.22**). These results suggest that residues 23-33, which contain the lysine-rich "charge cluster 1" (CC1), represent the biologically active region of the FT.

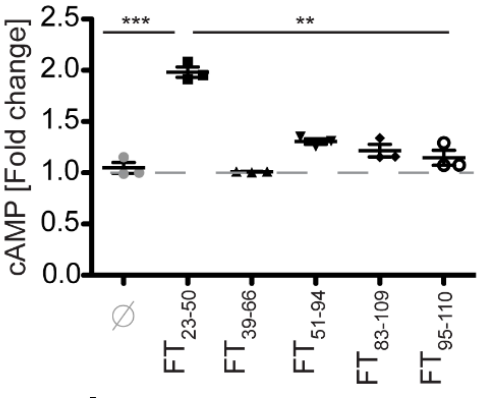

Figure 7.22 | FT23-50 induces a cAMP response. Synthetic peptides (27-44 residues) were added to SW10ΔPrP cells (2 µM each, 20 min). Only FT23-50 induced cAMP.

7.22 Selective blocking of FT23-50 with Fab fragments

To test the latter prediction, I incubated $FT_{23\text{-}50}$ with monovalent recombinant phage-derived miniantibodies recognizing the CC1 (Fab3) or the octapeptide repeats (Fab71) of PrP^C. Preincubation with Fab3, but not with Fab71, significantly quenched the ability of $FT_{23\text{-}50}$ to induce cAMP in $SW10_{\Delta PrP}$ cells (**Fig. 7.23**).

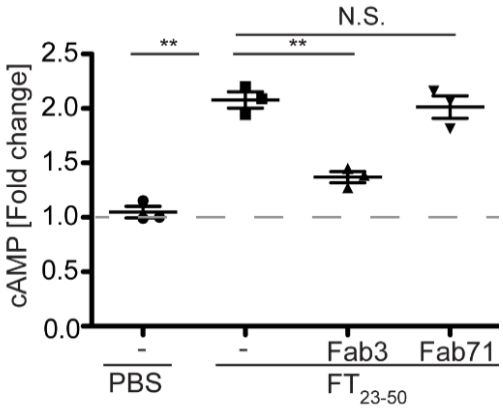

Figure 7.23 | Fab3 recognizing the CC1 can significantly lower cAMP induction by FT. FT23-50 was preincubated with a two-fold molar excess of miniantibodies Fab3 or Fab71, and added to SW10ΔPrP cells (20 min). Preincubation with Fab3, but not with Fab71, significantly quenched the FT-dependent cAMP spike. N.S.: not significant

7.23 Is the PrP^C receptor a GPCR?

Because cAMP levels are often controlled by G-protein coupled receptors (GPCR)(Hanoune and Defer, 2001), I reasoned that a GPCR may be involved in mediating the action of the FT, whose defective stimulation might trigger the CDP of PrP^C-deficient mice. In the peripheral nervous system, myelination is controlled by Gpr126, a seven-membrane spanning adhesion GPCR expressed by Schwann cells (Monk et al., 2009; Pogoda et al., 2006). Gpr126-deficient mice die during embryogenesis (Waller-Evans et al., 2010). Gpr126 undergoes constitutive cleavage resulting in the generation of N-terminal and C-terminal fragments (NTF and CTF) that remain non-covalently associated. NTF modulation of Gpr126 is thought to expose a tethered agonistic ligand (Liebscher et al., 2014). Because of these findings, Gpr126 seemed a

plausible candidate for mediating the effects of the FT. I therefore generated HEK293T cells stably overexpressing human Gpr126 or, for control, Gpr124 and Gpr176 (denoted HEK^{Gpr126}, HEK^{Gpr124}, and HEK^{Gpr176} respectively). All transfected GPCRs contained a C-terminal 14-meric V5 epitope tag (Kasof and Gomes, 2001) and were found to be expressed at the cell surface (**Fig. 7.24**).

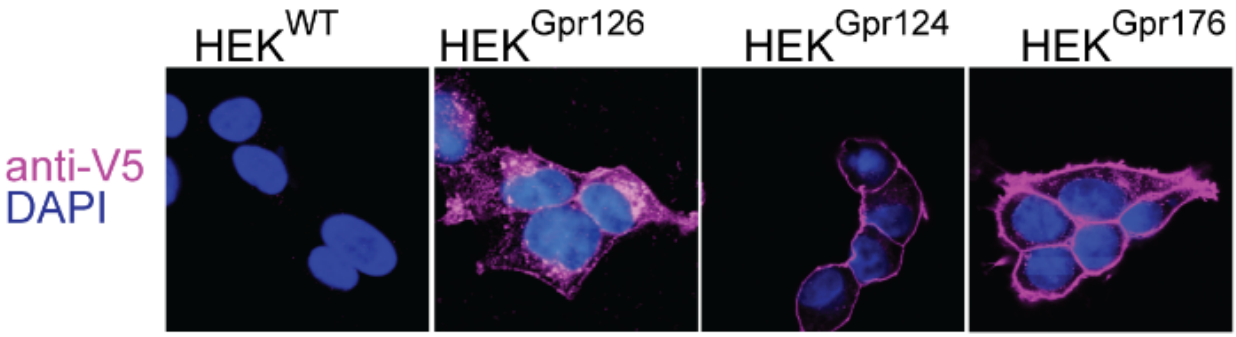

Figure 7.24 | Panel of HEK cells expressing different GPCRs. Wild type HEK293T cells (HEK^{WT}) or HEK293T cells overexpressing various GPCRs bearing V5 epitope tags (HEK^{Gpr126}, HEK^{Gpr124}, and HEK^{Gpr176}) were grown on coverslips and stained with anti V5 antibody (detecting tagged GPCRs; magenta). Nuclei were stained with DAPI (blue). Staining revealed cell surface expression of all transfected GPCRs. Scale bar: 8µm.

7.24 FT$_{23-50}$ is binding specifically to HEK^{Gpr126}

Flow cytometry with FITC-labeled anti-HA antibody revealed increased FT$_{23-50}$ binding to HEK^{Gpr126} but neither to HEK^{Gpr124} nor to HEK^{Gpr176} cells (**Fig. 7.25**).

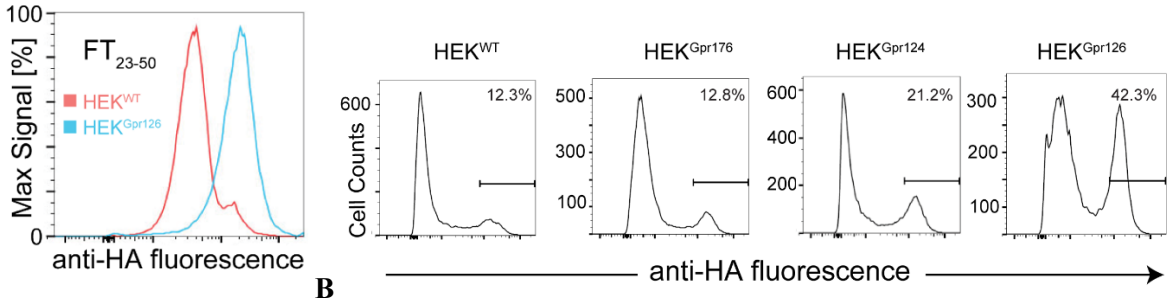

Figure 7.25 | FT$_{23-50}$ is binding to HEK^{Gpr126}. A:HA-tagged FT$_{23-50}$ peptide (2µM) was added to wild-type HEK293T (HEK^{WT}) cells or to HEK^{GPR126} cells, labeled with anti-HA antibody, and subjected to cytofluorimetry. Overexpression of Gpr126 increased the binding of FT$_{23-50}$. **B**: Binding of HA-tagged FT$_{23-50}$ to HEK^{GPR126} cells (right panel, monitored by cytofluorimetry) was conspicuously increased over that of wild-type, Gpr176, and Gpr124-overexpressing HEK293T cells.

7.25 FT$_{23-50}$ binding to HEK^{Gpr126} induces cAMP.

I next exposed HEK293T and HEK^{Gpr126} cells to FT$_{23-50}$ (20') and measured cytosolic cAMP. Even the lowest tested FT concentration (500 nM) sufficed to significantly raise cAMP levels in HEK^{Gpr126} cells but neither in HEK^{Gpr124} nor in HEK^{Gpr176} cells (**Fig. 7.26**).

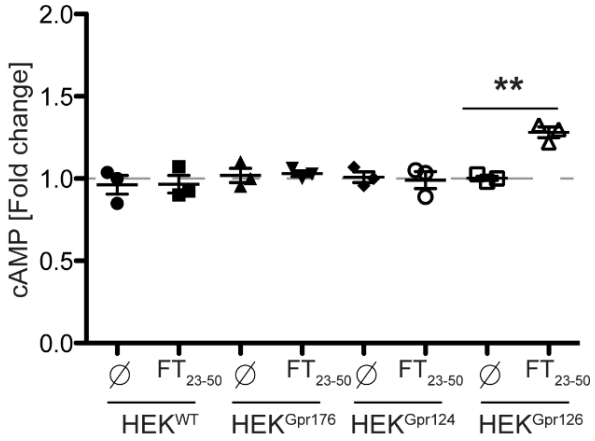

Figure 7.26 | FT_{23-50} binding to HEK^{Gpr126} induces cAMP. Intracellular cAMP in wild-type HEK293T cells and in Gpr176, Gpr124 and Gpr126 overexpressors exposed to FT_{23-50} (0.5 µM, 20 min). Only HEK^{Gpr126} cells showed a cAMP increase.

7.26 Is there a direct ligand-receptor interaction of FT with Gpr126?

Does the effect of FT on cAMP levels derive from a direct ligand-receptor interaction with Gpr126? If so, the FT should establish a physical complex with Gpr126. To detect such a complex, I treated naïve HEK293T, HEK^{Gpr124} or HEK^{Gpr126} cells with recombinant FT (2µM, 20') or, with a recombinant GD (2µM, 20'). I performed immunoprecipitations on cell lysates with anti-V5 antibodies, and probed the blots with POM2. FT was detectable only in HEK^{Gpr126} immunoprecipitates and no FT was captured by naïve HEK293T or HEK^{Gpr124} cells. Blots probed with POM1 did not reveal any GD binding in any of the cell lines. These results confirm that the FT can robustly interact with Gpr126 (**Fig. 7.27**).

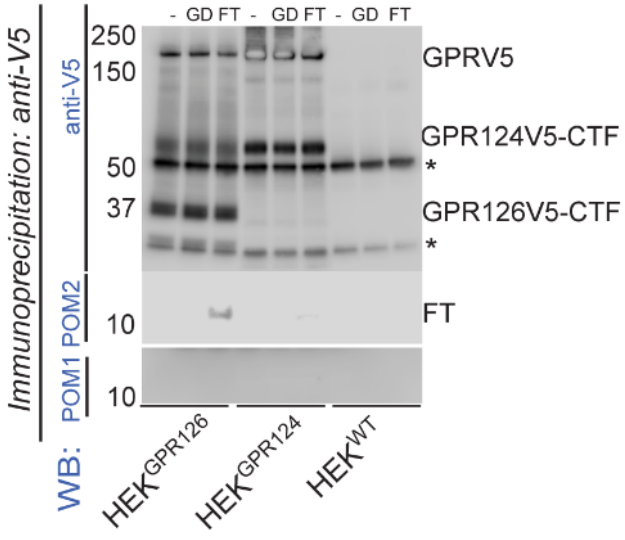

Figure 7.27 | FT co-precipitates with GPR126. HEK293T, HEK^{GPR124} and HEK^{GPR126} cells were exposed (20 min) to recombinant FT, GD (2µM), or PBS, and subjected to immunoprecipitation using the anti-V5 antibody, followed by Western blotting using POM2, anti-V5 or POM1. Anti-V5 detected both full-length Gpr126, Gpr124 (denoted as GprV5 for both proteins) and the respective C-terminal fragments (Gpr126V5-CTF, Gpr124V5-CTF). POM2 revealed a band corresponding to the FT (lane 3) that co-precipitated with GPR126. POM1 revealed no bands, indicating that GD did not bind. Lanes 1, 2 and 3: HEK^{GPR126} cells treated with PBS, GD and FT. Lanes 4, 5 and 6: HEK^{GPR124} cells treated with PBS, GD and FT. Lanes 7, 8 and 9: HEK293T cells treated with PBS, GD and FT Asterisks: immunoglobulin heavy and light chains.

7.27 A Gpr126-ablated Schwann cell line does not increase cAMP upon FT binding

To further probe the dependency of the FT-induced cAMP increase on Gpr126, I generated clonal SW10 cells devoid of endogenous Gpr126. I transfected plasmids expressing Cas9/EGFP and short-guide RNAs targeting exon 2 of Gpr126 into SW10 cells and FACS sorted the positive cells. After several weeks of

culturing, I managed to isolate a Gpr126-ablated clone designated $SW10_{\Delta Gpr126}$. When treated with $FT_{23\text{-}50}$, SW10 (but not $SW10_{\Delta Gpr126}$) cells reacted with increased cAMP levels. As a further control, I replaced all lysine residues of $FT_{23\text{-}50}$ with alanines. The modified $FT^{K\rightarrow A}_{23\text{-}50}$ peptide was ineffective in binding cells and inducing cAMP (**Fig. 7.28**).

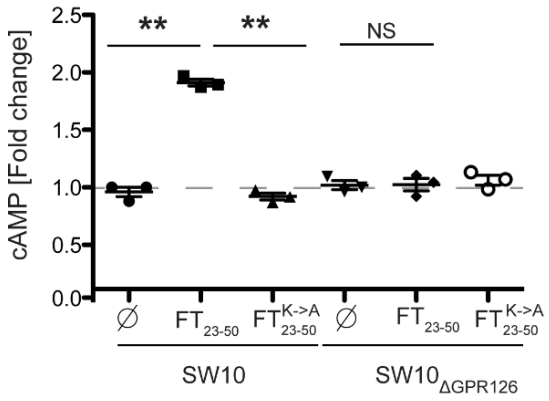

Figure 7.28 | A Gpr126-ablated Schwann cell line ($SW10_{\Delta Gpr126}$) does not increase cAMP upon FT binding. Wild-type (left) and Gpr126-ablated (right) SW10 cells were exposed to $FT_{23\text{-}50}$ (2µM, 20 min). SW10 cells, but not $SW10_{\Delta Gpr126}$ cells, respond to $FT_{23\text{-}50}$ with a cAMP spike. Moreover, SW10 cells did not respond to alanine-substituted $FT_{23\text{-}50}$ ($FT^{K\rightarrow A}_{23\text{-}50}$).

7.28 Reintroduction of GPR126 in $SW10_{\Delta Gpr126}$

I then transfected $SW10_{\Delta Gpr126}$ cells with plasmids encoding either of the human Gpr126, Gpr124, Gpr176 or Gpr56, and treated them with $FT_{23\text{-}50}$ 48 h post transfection. Only Gpr126-transfected cells showed a cAMP response (**Fig. 7.29**)

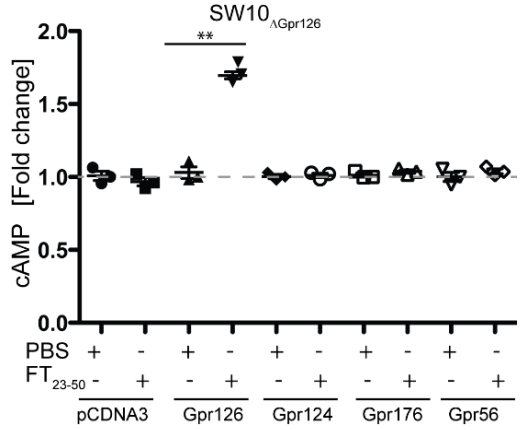

Figure 7.29 | Reintroduction of GPR126 in SW10ΔGpr126. Intracellular cAMP responses to FT treatment (2 µM, 20') in SW10 and $SW10_{\Delta Gpr126}$ cells, as well as $SW10^{huGpr126}_{\Delta Gpr126}$ cells expressing V5-tagged human Gpr126 (pCGpr126-V5). A significant increase in cAMP was observed in SW10 cells, whereas $SW10_{\Delta Gpr126}$ showed no change. In contrast, $SW10^{huGpr126}_{\Delta Gpr126}$ cells showed a significant cAMP increase, indicative of successful complementation.

The magnitude of the cAMP response in Gpr126-transfected cells was similar to that of naïve SW10 cells, suggesting that the V5 tag did not affect the function of Gpr126 (**Fig. 7.30**).

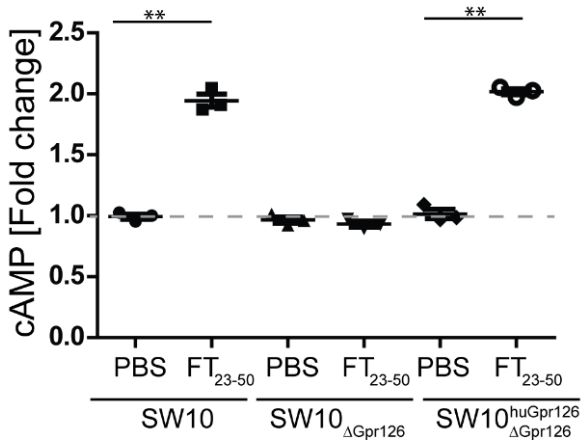

Figure 7.30 | $SW10_{\Delta Gpr126}$ cells plated at a density of 100'000 cells/well in 6-well plates were transfected with control plasmid (pCDNA3) or plasmids encoding various GPCRs (Gpr126, 124, 176, and 56) bearing C-terminal V5 tags. Only cells transfected with pCGpr126-V5 showed a cAMP response to FT_{23-50}. PBS treatment was used for control.

7.29 HEK^{PrP}-conditioned medium failed to induce cAMP in SW10$_{\Delta Gpr126}$

Next, I treated SW10 and $SW10_{\Delta Gpr126}$ cells with conditioned media from HEK^{PrP} or HEK^{empty} cells. HEK^{PrP}-conditioned medium induced cAMP in SW10 cells, but not in $SW10_{\Delta Gpr126}$ cells (**Fig. 7.31 A**). Moreover, FT adsorption was reduced in $SW10_{\Delta Gpr126}$ cells (**Fig. 7.31 B**).

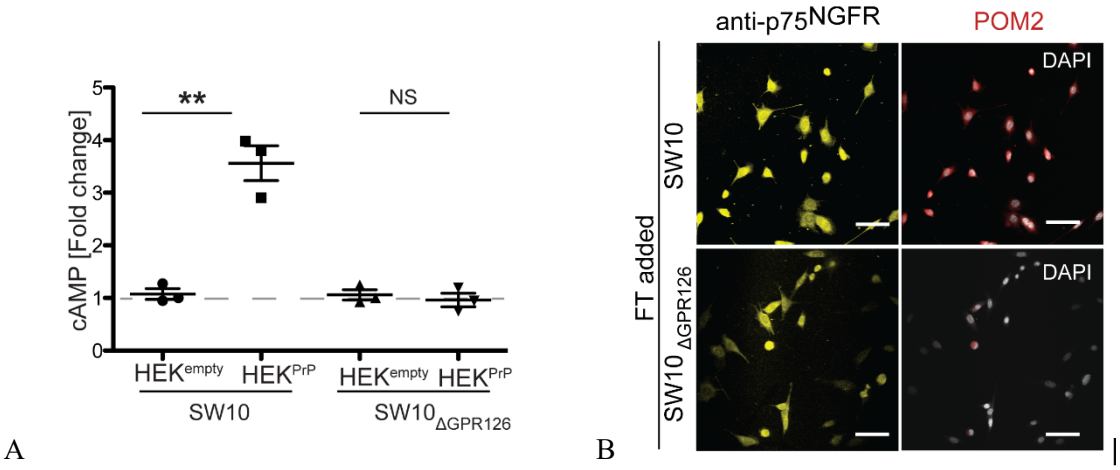

Figure 7.31 | HEKPrP-conditioned medium failed to induce cAMP in SW10ΔGpr126. A: SW10 and $SW10_{\Delta Gpr126}$ cells were incubated (20 min) with conditioned medium from HEK293T cells transiently transfected with a non-coding vector (HEK^{empty}) or with a plasmid encoding murine PrP^{C} (HEK^{PrP}). HEK^{PrP}-conditioned medium induced a robust cAMP spike in SW10, but not $SW10_{\Delta Gpr126}$ cells. **B:** SW10 and $SW10_{\Delta Gpr126}$ cells were grown on coverslips for 24h and exposed to recombinant FT (2 µM, 20 min). Cells were stained with POM2 (detecting FT; red, DAPI-stained nuclei: grey) and antibodies to $p75^{NGFR}$ (yellow). Deletion of Gpr126 largely suppressed FT binding. Scale bar: 26 µm.

7.30 Is the activity of FT specific for Gpr126?

Is the activity of FT strictly limited to Gpr126, or does it extend to additional adhesion GPCRs? To address this question, I administered FT_{23-50} (2µM, 20') to HEK^{Gpr126} cells and HEK293(H) cells that are transfected with plasmids encoding human Gpr56, Gpr64, Gpr133, or Gpr97. Once again, only Gpr126-expressing cells showed a significant cAMP response (**Fig. S3D**). The magnitude of cAMP response became limiting.

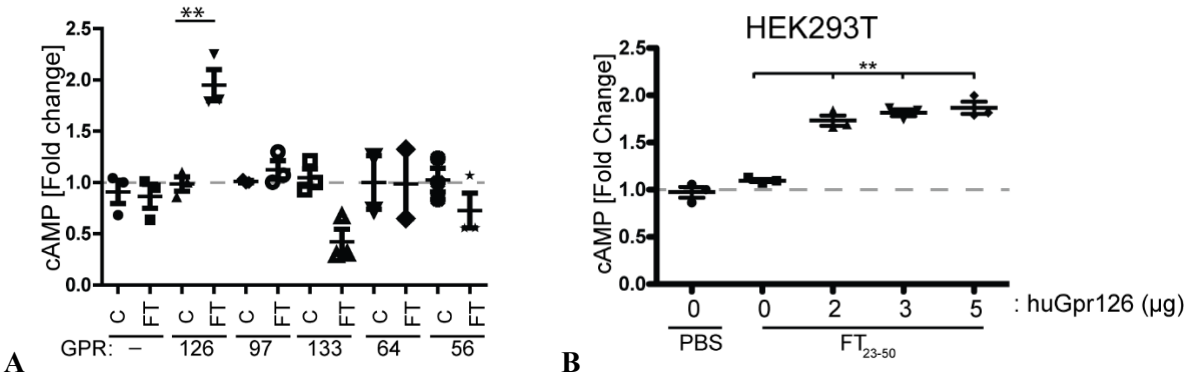

Figure 7.32 | The activity of FT is limited to Gpr126. A: HEK293(H) cell lines were transfected with plasmids expressing different adhesion GPCRs (Gpr: 97, 133, 64, 56), followed by selection of cells expressing the receptor in presence of geneticin. GPCR expressing cells and HEK^{Gpr126} cells were then treated with either FT_{23-50} or $FT_{23-50}^{K\rightarrow A}$ for control (FT and C, respectively). Only cells expressing Gpr126 responded to FT_{23-50} with a cAMP spike. Interestingly, cells expressing Gpr133 reacted with a decrease in cAMP levels. **B**: HEK293T cells were transfected with increasing amounts of human Gpr126 plasmid (2-5µg/well of a 6 well plate). 48h post transfection cells were treated with FT_{23-50} or PBS as a control. Increasing amount of Gpr126 cDNA did not result in amplification of cAMP signal.

7.31 Does FT lead to a cAMP response in the central nervous system?

I treated cerebellar granular neuronal cultures from *Prnp*$^{ZH1/ZH1}$ mice with FT_{23-50} or $FT_{23-50}^{K\rightarrow A}$. There was no induction of cAMP (**Fig. 7.33**), as might be expected from the minimal expression of Gpr126 in the brain (Zhang et al., 2014).

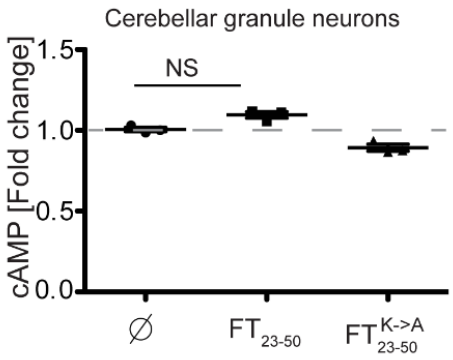

Figure 7.33 | No cAMP burst in cerebellar granular neurons after treatment with FT. Primary *Prnp*$^{ZH1/ZH1}$ cerebellar granule neuron cultures were seeded in 6-well plates at a density of $5x10^5$ cells and treated with FT_{23-50}, $FT_{23-50}^{K\rightarrow A}$, or PBS. No alterations in the levels of cAMP were noticed.

The FT is released from PrP^C by ADAM metalloproteases (Altmeppen et al., 2015). If the cAMP response to HEK^{PrP} conditioned media was caused by soluble FT, it should be reduced by inhibiting PrP^C cleavage. Indeed, after a 24-hr treatment with the metalloprotease inhibitor TAPI-2, HEK^{PrP}-conditioned medium contained significantly less FT (**Fig. 7.34 B)** and, when administered to SW10 cells, possessed a significantly reduced cAMP-inducing activity (**Fig. 7.34 A**).

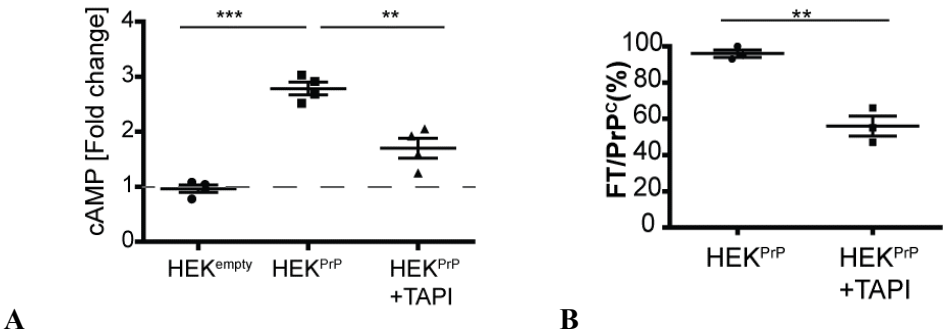

A B

Figure 7.34 | Inhibition of PrP^{C} cleavage reduces cAMP response. A: SW10 cells were exposed to conditioned medium from HEK cells that had been transfected with empty vector (HEK^{empty}) or a PrP^{C} expression vector (HEK^{PrP}). HEK^{PrP} were optionally treated with 100 µM of the TAPI-2 protease inhibitor for 24h before harvesting the medium. TAPI-2 treatment resulted in reduced cAMP induction, suggesting that impaired proteolytic cleavage of the FT from PrP^{C} resulted in decreased signaling. **B:** Quantification of FT released into the medium relative to the total amount of PrP^{C} in lysates by Western blotting. The spent medium of HEK^{PrP} cells treated with TAPI-2 contained less FT.

7.32 Sciatic nerves of Prnp$^{ZH1/ZH1}$ mice show reduced amounts of Egr2

The transcription factor Egr2 (also called Krox-20) is induced cAMP-dependently at the onset of myelination (Monuki et al., 1989; Scherer et al., 1994; Zorick et al., 1999) and controls the expression of crucial myelin genes. Conditional ablation studies have implicated Egr2 in myelin maintenance (Decker et al., 2006). Egr2 might therefore be an FT effector *in vivo*. Indeed, I found that Egr2 expression was significantly decreased in sciatic nerves of 13-week-old *Prnp*$^{ZH1/ZH1}$ mice ($p<0.05$; **Fig. 7.35**).

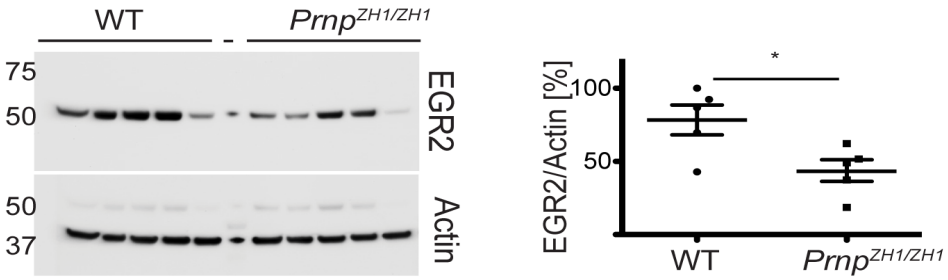

Figure 7.35 | Sciatic nerves of *Prnp$^{ZH1/ZH1}$* mice show reduced amounts of Egr2. Protein was isolated from wild-type or *Prnp*$^{ZH1/ZH1}$ sciatic nerves (13-week old female mice) and Western blots were probed for EGR2 and actin. Densitometry (right) showed reduced Egr2 in *Prnp*$^{ZH1/ZH1}$ nerves ($p=0.028$).

7.33 Luciferase reporter assay for Egr2

Moreover, I could show that recombinant FT (2 µM, 24h) can activate Egr2-dependent luciferase expression in SW10 cells (**Fig. 7.36 A**). Similarly, *Egr2* transcription was significantly upregulated in primary Schwann cells treated with recombinant FT (2 µM) for 1h (**Fig. 7.36 B**).

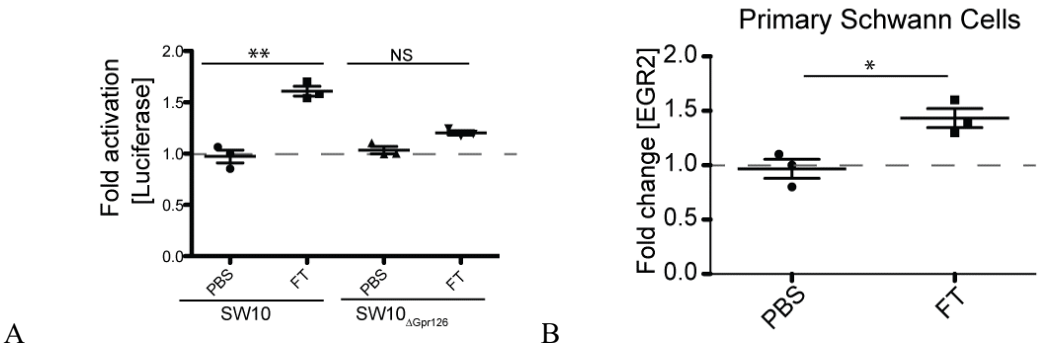

Figure 7.36 **| Luciferase reporter assay. A**: SW10 and $SW10_{\Delta Gpr126}$ cells were transfected with an Egr2-controlled firefly luciferase reporter and treated with recombinant FT (2µM) or PBS (24 hrs). Ordinate: luciferase expression normalized to a renilla luciferase control (n=3; *: $p<0.05$; t-test). Luciferase activity was observed only in SW10 cells stimulated with FT but not in $SW10_{\Delta Gpr126}$ cells. **B:** Primary Schwann cells were exposed to recombinant FT (2 µM, 1h) or PBS. Egr2 mRNA expression was measured by quantitative RT-PCR and normalized against a panel of housekeeping genes.

7.34 Akt phosphorylation assay

The PI3 kinase/Akt pathways are important in the process of proliferation, differentiation and myelination of Schwann cells (Ogata et al., 2004). I therefore measured phosphorylated Akt (p-Akt) in $SW10_{\Delta PrP}$ and $SW10_{\Delta Gpr126}$cells exposed to recombinant FT (2µM, 20 min; **Fig 7.37**). Akt phosphorylation increased rapidly starting from 5 min post treatment with FT and peaking at 10 min in $SW10_{\Delta PrP}$ cells, but not in $SW10_{\Delta Gpr126}$ cells suggesting that FT initiated signaling in Schwann cells via Gpr126.

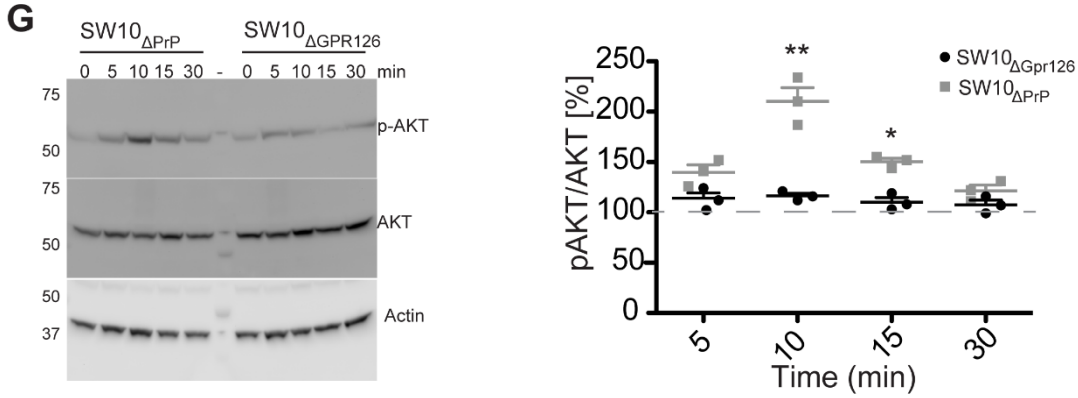

Figure 7.37 | Akt phosphorylation assay. $SW10_{\Delta PrP}$ and $SW10_{\Delta Gpr126}$ cells were grown in 6-well plates, exposed to recombinant FT (≤30 min), and analyzed by Western blotting (left). Densitometry (right) showed increased phospho-AKT/AKT ratio in $SW10_{\Delta PrP}$ cells, but not in $SW10_{\Delta Gpr126}$ cells.

7.35 Do SW10 cells still express myelin proteins?

To assess the integrity of SW10 cells and their subclones, I checked the expression of peripheral myelin genes (**Fig. 7.38**).

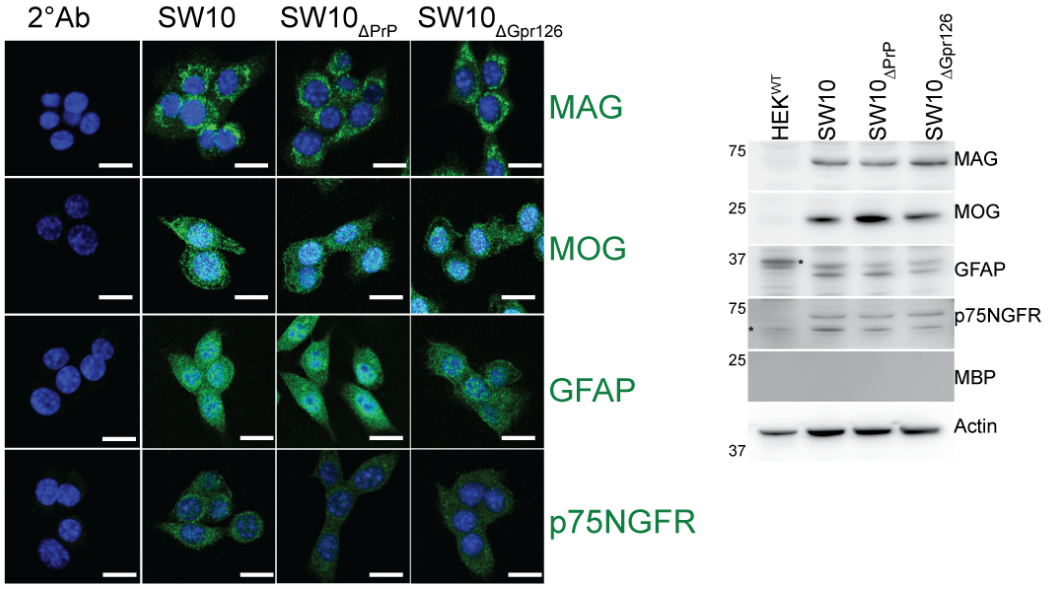

Figure 7.38 | Expression of typical Schwann cell markers in SW10 and genetically edited SW10 cell line. SW10, $SW10_{\Delta PrP}$ and $SW10_{\Delta Gpr126}$ cells were grown on coverslips and stained with antibodies against Myelin associated glycoprotein (MAG), Myelin oligodendrocyte glycoprotein (MOG), glial fibrillary acidic protein (GFAP) and p75 nerve growth factor receptor (p75NGFR) (left panel, all green; DAPI-stained nuclei: blue). Cells labeled with secondary antibody alone (2° Ab) were used as control to determine unspecific staining. Scale bars: 10µm. Expression in all cell lines was confirmed by western blotting (right panel). Lysate from HEK293T wild type cells (HEK^{WT}) was used as control. All proteins except Myelin basic protein (MBP) were expressed in SW10 cells and its derivatives.

7.36 Does FT act by the same mechanism as type-IV Collagen?

Type-IV collagen (Col4) binds Gpr126 and induces cAMP(Paavola et al., 2014), raising the question whether FT and Col4 act by the same mechanism. Sequence alignments identified two regions of similarity between the FT (KKRPKPG and QGSPG) and Col4 (GPRGKPG and QGSPG, **Fig. 7.39**).

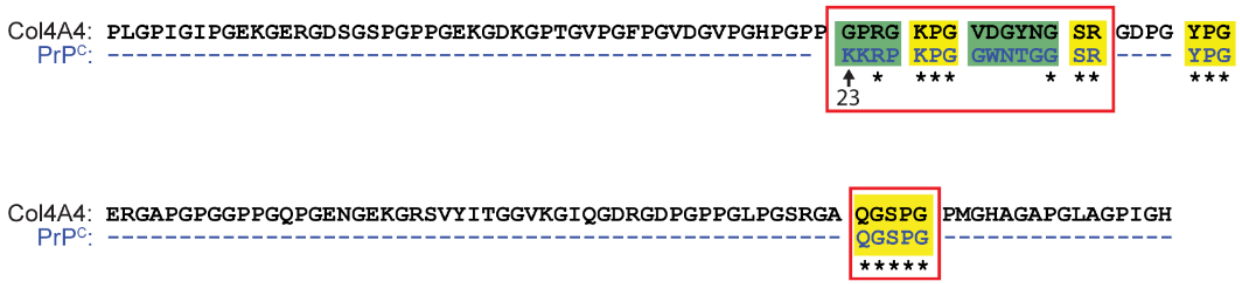

Figure 7.39 | Similarities between FT and Col4. Sequence alignment revealed two regions of similarity between the FT and Col4 (red boxes).. Yellow and green shades represent high and moderate conservation, respectively.

7.37 Which motif is crucial for signaling? KKRPK or QGSPG?

This prompted me to test the activity of $FT_{23\text{-}50}$ peptides in which the conserved cationic residues were replaced with alanines (KKRPKPG ⇨ AAAPAPG). Treatment of $SW10_{\Delta PrP}$ cells (2µM, 20') resulted in induction of cAMP by all mutant peptides except those bearing a modified KKRPK sequence (**Fig. 7.40**).

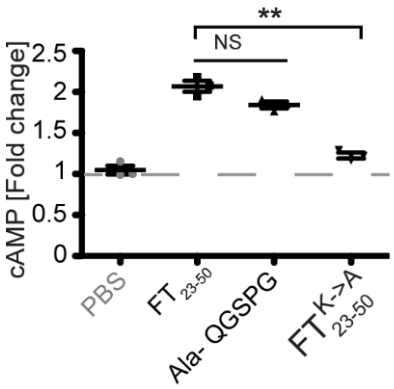

Figure 7.40 | Charge replacement in the KKRPK motif abrogates cAMP induction. $SW10_{\Delta PrP}$ cells were treated with synthetic $FT_{23\text{-}50}$ or modified version of $FT_{23\text{-}50}$ in which the KKRPK or QGSPG motifs were replaced with alanines (2µM, 20'). Alanine substitution of KKRPK (peptide $FT^{K\rightarrow A}_{23\text{-}50}$), but not of QGSPG, abrogated cAMP induction.

7.38 Charge replaced murine FT mutants expressed in HEK cells

Furthermore, I generated murine PrP^C mutants containing alanine substitutions in either one of the two conserved motifs. After transient transfection, both mutants were highly expressed by HEK293T cells **(Fig. 7.41 A**), and cleaved FT was recovered in the medium (**Fig. 7.41 B**).

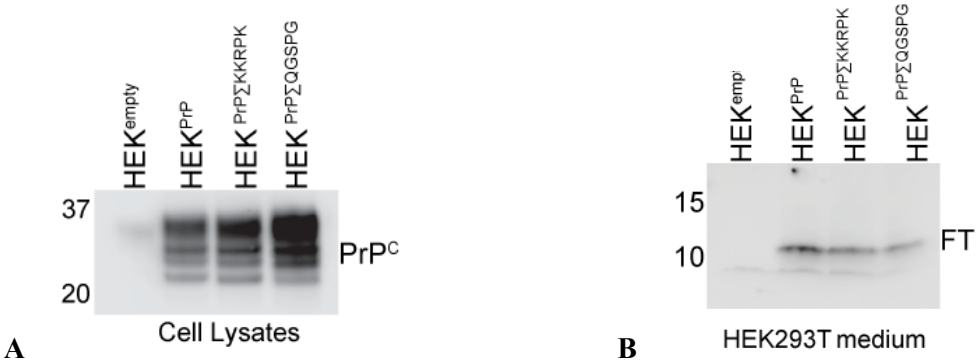

Figure 7.41 | Charge replaced murine FT mutants expressed in HEK cells. A: Western blot (developed with POM2) of HEK 293T cells transfected with expression plasmids for wild-type murine PrP^C or for PrP^C bearing lysine-to-alanine substitutions in the KKRPK and QGSPG motifs (lanes 3 and 4, respectively). The mutations did not affect the biogenesis and processing of PrP^C **B**: Western blot of the medium collected from the cells shown in panel B. FT fragments bearing the mutations were released into the medium similarly to wild-type FT.

7.39 KKRPK is the functional domain in the HEK cell assay

When applied to $SW10_{\Delta PrP}$ cells, the conditioned medium from HEK293T cells expressing PrP^C and QGSPG-mutated PrP^C ($HEK^{PrP\Sigma QGSPG}$) induced cAMP, whereas medium from cells expressing KKRPK-mutated PrP^C ($HEK^{PrP\Sigma KKRPK}$) did not (**Fig. 7.42**).

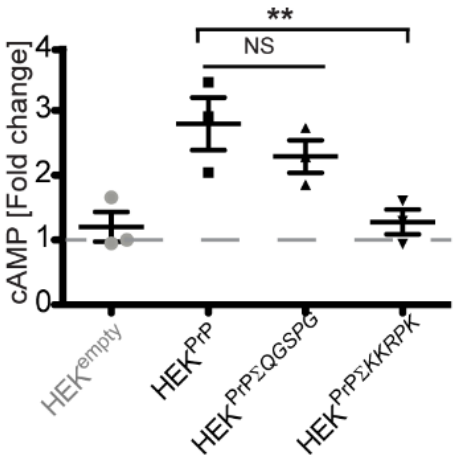

Figure 7.42. | KKRPK is the functional domain in the HEK cell assay. $SW10_{\Delta PrP}$ cells were treated with conditioned medium from HEK293T cells transfected with an empty vector (HEK^{empty}), with PrP^C (HEK^{PrP}), or with full-length PrP^C versions in which the QGSPG ($HEK^{PrP\Sigma QGSPG}$) or KKRPK ($HEK^{PrP\Sigma KKRPK}$) motifs were substituted (∑) with alanines. The charge neutralization within the KKRPK motif abrogated the cAMP induction.

7.40 Charge replacement in the GPRGKPG motif of Col4 aborgates cAMP induction

If the sequences conserved between PrP^C and Col4 mediate their biological activity, mutation of the GPRGKPG motif should abrogate the activity of Col4. I generated 21-mer peptides of Col4 bearing the native sequence or an alanine-substituted variant (AAAGAAG). The native peptide (8 µM), but not the mutated peptide, induced cAMP in $SW10_{\Delta PrP}$ cells (**Fig. 7.43**). These results suggest that Col4 and PrP^C activate Gpr126 through a similar mechanism.

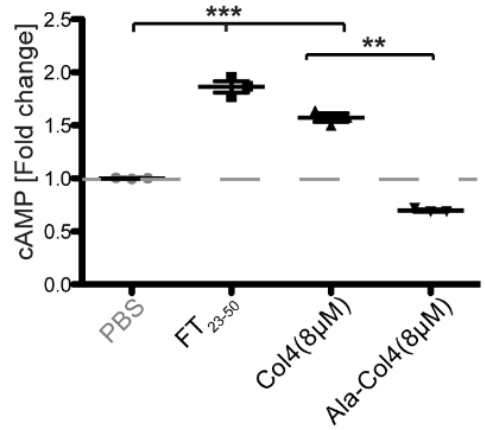

Figure 7.43 | Charge replacement in the GPRGKPG motif of Col4 aborgates cAMP induction. $SW10_{\Delta PrP}$ cells were treated with FT_{23-50} (2 µM) or a Col4-derived 21-meric synthetic peptide containing either the GPRGKPG domain or its alanine-substituted variant (AAAGAAG; both 8 µM). Both FT_{23-50} and the native Col4 peptide, but not the alanine-substituted peptide (Ala-Col4), induced cAMP.

7.41 Microstructural comparison between Prnp ablated mice and Dhh^{Cre}::$Gpr126^{fl/fl}$ mice

In zebrafish Gpr126 controls myelination but is dispensable for myelin maintenance for at least one month (Glenn and Talbot, 2013). In contrast, *Prnp* ablated mice have no obvious myelination defect but develop a late-onset peripheral neuropathy with demyelination, onion bulb formation, loss of axon-Schwann cell interactions in Remak bundles, and abnormal Schwann cell cytoplasmic protrusions (**Fig. 7.44**).

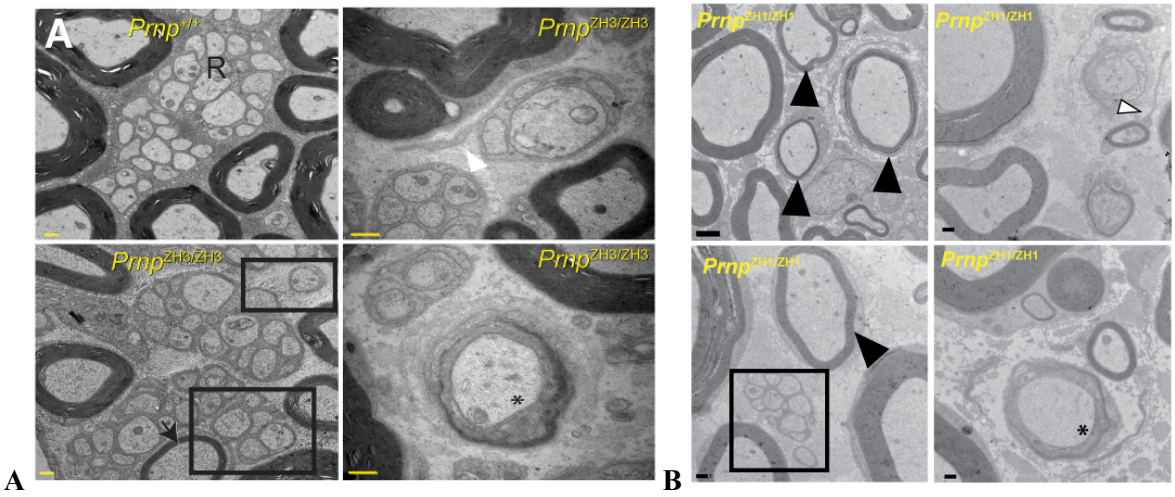

Figure 7.44 | Microstructural analysis of sciatic nerves from *Prnp* ablated mice. A: Transmission electron micrographs from 14 month old wild-type BL6 and $Prnp^{ZH3/ZH3}$ sciatic nerves (*N*=3/4 animals). Thinly myelinated axons (arrowhead), loss of axon-Schwann cell interaction (boxes), abnormal cytoplasmic Schwann cell protrusions (white arrowhead) and initial onion bulb formation (asterisk) were observed in $Prnp^{ZH3/ZH3}$ mice. Scale bars: 500 nm. **B:** Transmission electron micrographs of 14 month-old $Prnp^{ZH1/ZH1}$ sciatic nerves (ZH1). Black arrowhead: thinly myelinated axons; white arrowhead: abnormal cytoplasmic Schwann cell protrusions; boxes: loss of axon-Schwann cell interactions; asterisk: initial onion bulb formation. Scale bar: 2 µm in upper left panel; 500 nm in all other panels.

To test if Gpr126 dysfunction may cause late-onset phenotypes in mice, I examined sciatic nerves from one-year-old Dhh^{Cre}::$Gpr126^{fl/fl}$ mice. In these mice, Dhh^{Cre} drives Schwann-cell specific ablation of *Gpr126* from ~E12.5 onwards (Jaegle et al., 2003; Mogha et al., 2013). At one year of age, I noted neuropathic traits similar to those of PrP^{C}-deficient mice, including onion bulb formation, Remak bundles with reduced numbers of unmyelinated axons, and abnormal cytoplasmic Schwann cell protrusions (Bremer et al., 2010b) (**Fig. 7.45**).

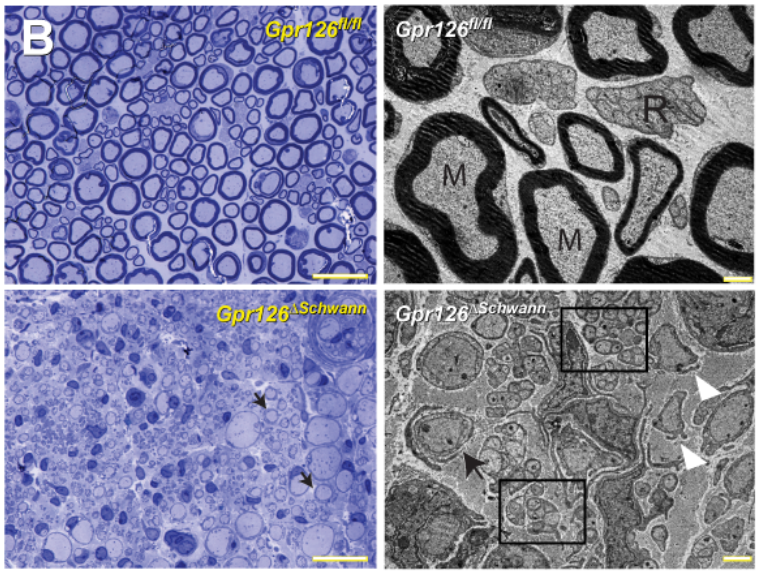

Figure 7.45 | Microstructural analysis of sciatic nerves from Dhh^{Cre}::$Gpr126^{fl/fl}$ mice. Neuropathic phenotype of one-year-old Dhh^{Cre};$Gpr126^{fl/fl}$ mutant mouse nerves. Left panels: toluidine blue-stained sections of sciatic nerves from control $Gpr126^{fl/fl}$ (phenotypically wild-type) and Dhh^{Cre}::$Gpr126^{fl/fl}$ ($Gpr126^{\Delta Schwann}$) mice. $Gpr126^{fl/fl}$ nerves were well myelinated (*N* = 3/3 animals), whereas $Gpr126^{\Delta Schwann}$ nerves exhibited myelin loss with readily apparent onion bulbs (arrowheads) (*N* = 3/3 animals). Right panels: Transmission electron micrographs from $Gpr126^{fl/fl}$ and $Gpr126^{\Delta Schwann}$ sciatic nerves. Myelinated axons ("M") and Remak bundles ("R") were found in $Gpr126^{fl/fl}$ sciatic nerves (*N* = 3/3 animals). Numerous defects were observed in $Gpr126^{\Delta Schwann}$ sciatic nerves (*N* = 3/3 animals) including onion bulbs (black arrowheads), abnormal cytoplasmic protrusions (white arrows), and loss of axon-Schwann cell interactions (boxes) similarly to $Prnp^{ZH3/ZH3}$ mice. Scale bars = 20µm (a-b), 2 µm (c-d).

7.42 Proof of principle in another species

Might the FT activate Gpr126 across species? The experiments involving zebrafish have been performed collaboration with the Monk lab in St. Louis, USA. We utilized the hypomorphic *gpr126*^{st63} zebrafish mutant, which has a point mutation in the signaling domain that reduces Gpr126 trafficking to the membrane and protein signaling (Liebscher et al., 2014; Monk et al., 2009). Myelin basic protein (MBP) expression is reduced in the posterior lateral line nerve (PLLn) of *gpr126*^{st63} zebrafish (**Fig. 7.46 A**), but can be rescued by treatment with exogenous activating small molecules and peptides (Liebscher et al., 2014; Monk et al., 2009; Petersen et al., 2015). We applied 20 uM FT_{23-50} to developing *gpr126*^{st63} zebrafish larvae 50-55h post-fertilization (hpf) and assayed MBP expression in the PLLn at 5 days post-fertilization (dpf). We found that exogenous FT_{23-50} sufficed to increase Mbp expression compared to DMSO-treated control larvae (**Fig. 7.46 B**, $p < 0.05$). To confirm that the effect of FT_{23-50} on zebrafish larvae was due to enhanced Gpr126 signaling, we also treated *gpr126*^{st49} larvae with FT_{23-50}. The *gpr126*^{st49} allele contains an early STOP codon prior to the signaling domain and encodes a truncated protein incapable of G_s signaling (Monk et al., 2009; Petersen et al., 2015). Mbp was barely detectable in both FT_{23-50} and DMSO-treated mutant *gpr126*^{st49} larvae (**Fig. 7.46 B**) indicating that FT_{23-50} functions via Gpr126 also in teleost fish.

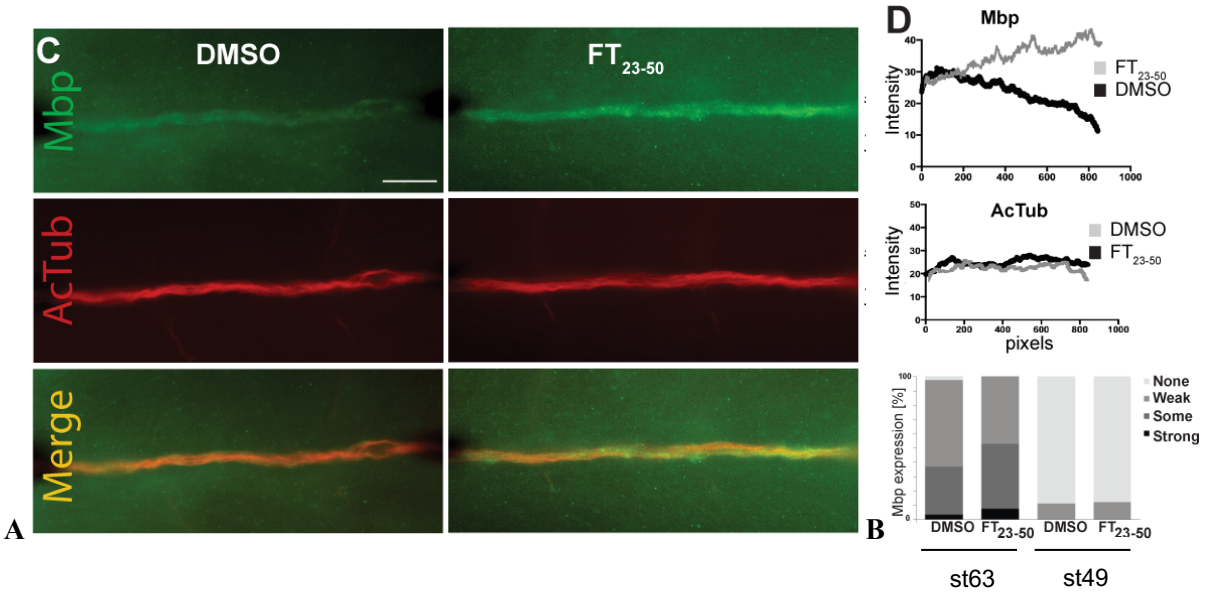

Figure 7.46 | FT rescues hypomorphic *gpr126*^{st63} zebrafish mutant. A: gpr126st63 hypomorphic mutant larvae were treated with vehicle (DMSO) or FT23-50 (20 uM) at 50-55 hours post fertilization (hpf) and immunostained at 5 days post fertilization (dpf) for myelin basic protein (Mbp, green) labeling maturing Schwann cells. AcTub: acetylated tubulin (red) labeling axons. Scale bar = 20 um. The intensity of immunofluorescence was assessed by morphometry (right graphs). FT treatment enhanced Mbp immunofluorescence without affecting AcTub. B: Mbp expression was scored in larvae treated with FT23-50 or vehicle (DMSO). FT23-50 treatment resulted in a higher proportion of rescued ("some" and "strong") MBP expression in gpr126st63 (53% vs. 34%), but not in gpr126st49 larvae ($p < 0.05$, Fisher's two-tailed exact test). N.S. = not significant. $N \geq 25$ larvae per replicate treatment.

7.43 Can FT increase cAMP levels in mouse scatic nerves and further organs by intravenous injection?

I next investigated if intravenous administration of synthetic FT_{23-50} can restore the diminished cAMP levels in sciatic nerves of *Prnp* ablated mouse lines. FT_{23-50} or $FT^{K\rightarrow A}_{23-50}$ peptide (600 µg) was administered to 10-

16 week old coisogenic C57BL/6J *Prnp*$^{ZH3/ZH3}$ and wild-type mice (N=8 per group and both groups were littermates). Animals were sacrificed 20 minutes post injection. FT_{23-50}, but not $FT^{K\rightarrow A}_{23-50}$, induced a cAMP elevation in both *Prnp*$^{ZH3/ZH3}$ and *Prnp*$^{ZH1/ZH1}$ sciatic nerves; cAMP reached levels similar to those seen in BL6 mice injected with $FT^{K\rightarrow A}_{23-50}$ (**Fig. 7.47A+B**).

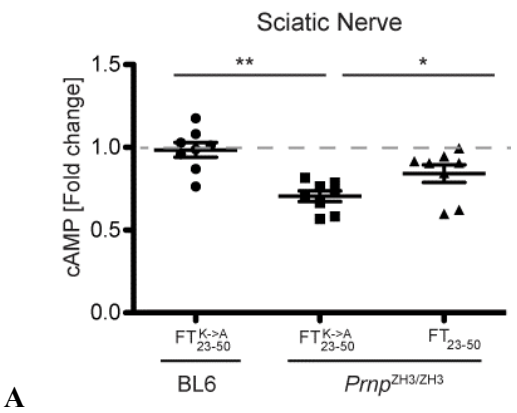
Sciatic Nerve
cAMP [Fold change]
1.5
1.0
0.5
0.0
**
*
FT K->A 23-50
FT K->A 23-50
FT 23-50
BL6
Prnp ZH3/ZH3

A

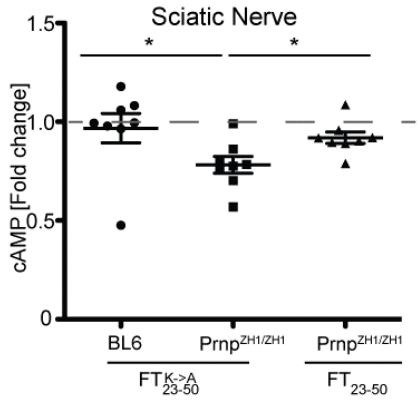
Sciatic Nerve
cAMP [Fold change]
1.5
1.0
0.5
0
*
*
BL6
Prnp ZH1/ZH1
Prnp ZH1/ZH1
FT K->A 23-50
FT 23-50

B

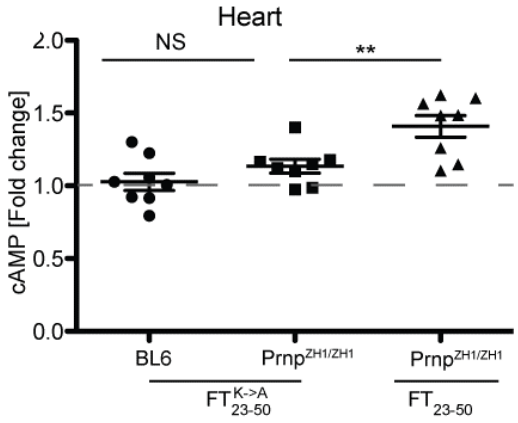
Heart
cAMP [Fold change]
2.0
1.5
1.0
0.5
0.0
NS
**
BL6
Prnp ZH1/ZH1
Prnp ZH1/ZH1
FT K->A 23-50
FT 23-50

C

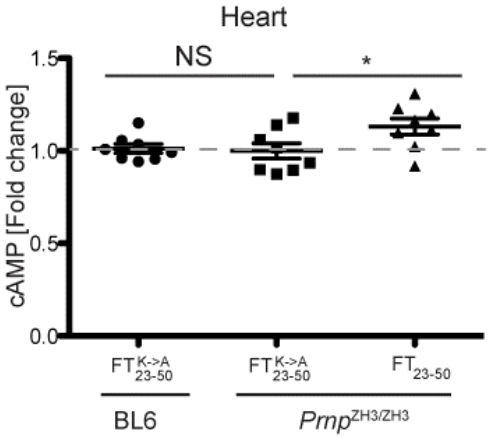
Heart
cAMP [Fold change]
1.5
1.0
0.5
0.0
NS
*
FT K->A 23-50
FT K->A 23-50
FT 23-50
BL6
Prnp ZH3/ZH3

D

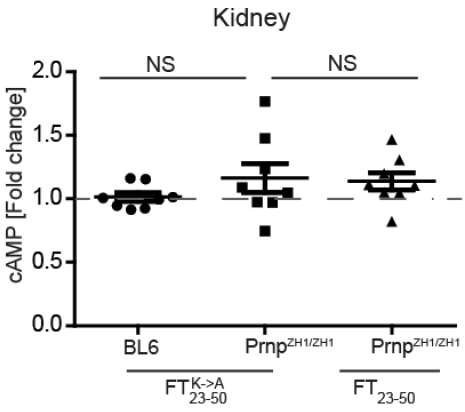
Kidney
cAMP [Fold change]
2.0
1.5
1.0
0.5
0.0
NS
NS
BL6
Prnp ZH1/ZH1
Prnp ZH1/ZH1
FT K->A 23-50
FT 23-50

E

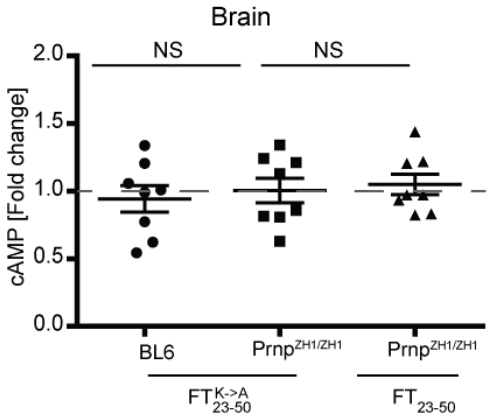
Brain
cAMP [Fold change]
2.0
1.5
1.0
0.5
0.0
NS
NS
BL6
Prnp ZH1/ZH1
Prnp ZH1/ZH1
FT K->A 23-50
FT 23-50

F

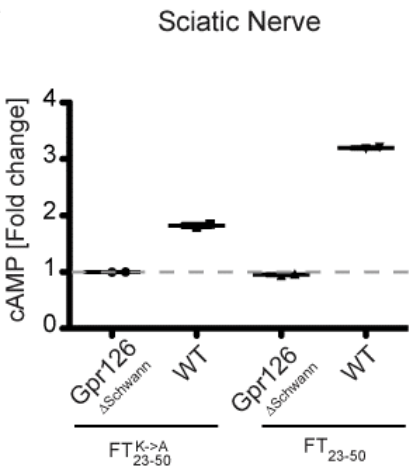
Sciatic Nerve
cAMP [Fold change]
4
3
2
1
0
Gpr126 ΔSchwann
WT
Gpr126 ΔSchwann
WT
FT K->A 23-50
FT 23-50

G

Figure 7.47 | Intrevenous FT injections in mice. A: *Prnp*$^{ZH3/ZH3}$ and BL6 mice were intravenously exposed to either $FT_{23\text{-}50}$ or its non-charged analogue $FT^{K\rightarrow A}_{23\text{-}50}$ (600 µg/animal, 20 min). *Prnp*$^{ZH3/ZH3}$ sciatic nerves showed a significant cAMP increase after injection of $FT_{23\text{-}50}$, but not of $FT^{K\rightarrow A}_{23\text{-}50}$. $FT_{23\text{-}50}$-treated *Prnp*$^{ZH3/ZH3}$ sciatic nerves reached cAMP levels similar to those of BL/6 mice injected with $FT^{K\rightarrow A}_{23\text{-}50}$. Each dot represents an individual animal. **B**: $FT_{23\text{-}50}$ or $FT^{K\rightarrow A}_{23\text{-}50}$ was intravenously administered to *Prnp*$^{ZH1/ZH1}$ and BL6 mice (600 µg/mouse, 20 min). After $FT_{23\text{-}50}$ injection, cAMP levels in *Prnp*$^{ZH1/ZH1}$ mice increased to levels approaching those of BL6 mice. Each dot represents an individual animal. **C+D:** cAMP in hearts also spiked in $FT_{23\text{-}50}$ injected *Prnp*$^{ZH1/ZH1}$mice (C) and *Prnp*$^{ZH3/ZH3}$ mice (D). **E+F:** $FT_{23\text{-}50}$ or $FT^{K\rightarrow A}_{23\text{-}50}$ was injected intravenously into 10-16-week old *Prnp*$^{ZH1/ZH1}$ or BL6 mice (600 µg/animal, 20 minutes). cAMP levels in kidneys (E) and brain (F) showed no significant changes. **G**: Control *Gpr126*$^{fl/fl}$ (WT) and *Dhh*^{Cre}*::Gpr126*$^{fl/fl}$ mutant (*Gpr126*$^{\Delta Schwann}$) mice were intravenously injected with either $FT_{23\text{-}50}$ or uncharged $FT_{23\text{-}50}$ ($FT^{K\rightarrow A}_{23\text{-}50}$) (600 µg/animal). Sciatic nerves were isolated 20 min post injection. $FT_{23\text{-}50}$ elicited a significant cAMP increase in WT mice, but not in *Gpr126*$^{\Delta Schwann}$ mice. $FT^{K\rightarrow A}_{23\text{-}50}$ injection did not alter cAMP levels (*N=2*). *: $p<0.05$; **: $p<0.01$.

$FT_{23\text{-}50}$ induced a cAMP spike also in the heart, which expresses high amounts of Gpr126 (**Fig. 7.47 C+D**), but not in kidney and brain (**Fig.7.47 E+F**), which do not express Gpr126 (Uhlen et al., 2015). I then administered intravenously $FT_{23\text{-}50}$ or $FT^{K\rightarrow A}_{23\text{-}50}$ peptide (600 µg) to *Dhh*^{Cre}*::Gpr126*$^{fl/fl}$ and control *Gpr126*$^{fl/fl}$ mice. $FT_{23\text{-}50}$ induced a robust cAMP spike in *Gpr126*$^{fl/fl}$ sciatic nerves but not in *Dhh*^{Cre}*::Gpr126*$^{fl/fl}$ nerves (**Fig. 7.47 G**).

8 DISCUSSION

8.1 Purpose of the study

At the beginning of my study, I knew from Bremer et al. that axonal prion protein plays an important role in myelin maintenance. Their meticulous work has documented a chronic demyelinating polyneuropathy CDP in four different *Prnp*$^{-/-}$ mouse strains. Nuvolone et al. generated a novel *Prnp*$^{-/-}$ mouse by use of TALEN genome editing on a strictly isogenic C57BL/6J background, the ZH3 mouse (Nuvolone et al., 2016). The ZH3 mouse was devoid of any flanking gene bias and those mice still suffer from chronic demyelinating polyneuropathy. The research aim of my study was to identify the molecular mechanism by which the cellular prion protein is signaling in myelin maintenance.

8.2 Summary of results

First, I could show that the aminoterminal fragment of PrP (aa23-50), the so called flexible tail FT, is able to directly bind to the Schwann cell membrane. Binding partner is a protein because surface digestion with trypsin abolishes binding of PrP. To what kind of Schwann cell surface protein could PrP^{C} bind? One of the most extensive groups of surface receptors are the G protein-coupled receptors, which are able to signal via Gs proteins resulting in cAMP elevation. Elevation of cAMP is well described to promote the maturation of Schwann cells from pro-myelinating to myelinating stage. In Schwann cell cultures, cAMP is artificially increased by adding forskolin, a compound raising intracellular cAMP levels. Therefore, I measured cAMP levels in sciatic nerves of *Prnp*$^{-/-}$ mice, compared to wt and I found a significant decrease of cAMP after 10 weeks of age. Next, I could show that treatment of primary Schwann cells with recombinant FT was leading to a concentration dependent cAMP increase. The calculated EC50 for FT was 860nM. Other domains of PrP^{C} were inefficient in increasing cAMP levels. Because of criticisms that recombinant proteins expressed in E. coli could contain heat shock proteins influencing cell signaling, I took either cell medium from HEK cells expressing PrP in which FT was present or synthetic peptides not expressed by bacteria. Both, HEK cell medium and synthetic peptides resulted in a dose-dependent cAMP increase in Schwann cells. Then, I blocked charge cluster 1 and the octapeptide repeats with specific monovalent phage-derived Fab fragments. Only pretreatment with the Fab fragment recognizing CC1 could block cAMP release indicating that the signaling domain of PrP^{C} in myelin maintenance is indeed part of amino acid residues 23-50. cAMP levels are often controlled by G protein-coupled receptors GPCRs. Signaling via adhesion Gpr126 has been reported to be crucial for radial sorting and myelination of the peripheral nervous system in zebrafish and mice. I therefore generated HEK293T cells over-expressing different candidate GPCRs. I could show strong binding to HEK Gpr126 cells but not to the other GPCRs tested. As a functional read-out I treated the HEK cell clones with FT23-50 and only Gpr126 expressing cells elevated their intracellular cAMP levels. To prove the physical direct interaction of FT23-50 with Gpr126, I performed immunoprecipitations. Only in cell lysates of HEK Gpr126 cells, I was able to pull down FT23-50, indicating that FT23-50 establishes a physical complex with Gpr126. As a further control I ablated Gpr126 in the Schwann cell line SW10 by use of CRISPR/Cas9 genome editing. SW10ΔGpr126 did not increase intracellular cAMP levels upon FT23-50 treatment. Then I replaced charge

cluster 1 lysine residues by uncharged alanins and the resulting modified peptide did neither bind to Schwann cells nor was it efficient in elevating cAMP levels. In order to re-introduce the receptor, I transfected SW10ΔGpr126 Schwann cells with plasmids encoding human Gpr126 and a panel of control GPCRs. Only Gpr126-transfected cells showed an elevation of cAMP upon FT23-50 treatment which was in the range of wildtype SW10 Schwann cells. Furthermore, SW10ΔGpr126 Schwann cells did not bind FT23-50 on the cell surface. At the onset of myelination, elevation of intracellular cAMP in Schwann cells activates transcription factor Egr2 (Krox-20). Egr2 is known to be the orchestrator of myelin gene expression. Egr2 in sciatic nerves from *Prnp*$^{-/-}$ mice were significantly reduced compared to wildtype controls and treatment of SW10 cells with FT23-50 significantly upregulated Egr2. The PI3 kinase/Akt pathway is important in proliferation and myelination. Therefore, I analyzed pAKT levels in a time course experiment where SW10ΔPrP and SWΔGpr126 cells were treated with FT23-50. Only in SW10ΔPrP but not in SWΔGpr126 cells pAKT peaked 10 minutes after FT23-50 addition.

Type-IV collagen (Col4) has been recently reported to be an agonistic ligand of Gpr126 and I wanted to investigate if Col4 acts by the same mechanism as FT does. Bioinformatical sequence alignment studies revealed two similarity regions between FT (KKRPKPG and QGSPG) and Col4 (GPRGKPG and QGSPG). Mutations in the QGSPG domain had no influence on cAMP release but replacement of charged amino acids both in FT's KKRPKPG and Col 4's GPRGKPG resulted in inefficient cAMP release, indicating that Col4 and PrP^{C} activate Gpr126 in a similar manner.

In Zebrafish, Gpr126 is crucial during development at the onset of myelination (Monk et al., 2009). *Prnp*$^{-/-}$ mice develop and myelinate comparable to wt controls but suffer from defective myelin maintenance (Bremer et al., 2010b). *Dhh*^{Cre}*::Gpr126*$^{fl/fl}$ mice activate expression of the Dhh gene at E12.5 leading to expression of Cre recombinase and subsequent excision of floxed Gpr126 gene. I could show that in *Dhh*^{Cre}*::Gpr126*$^{fl/fl}$ mice onion bulb formation, Remak bundles with unmyelinated axons and abnormal cytoplasmic Schwann cell protrusions are present in a similar pattern compared to changes in *Prnp*$^{-/-}$ mice.

Finally, we could show that FT is able to promote myelination across species. Hypomorphic Zebrafish larvae gpr126st63 presented enhanced MBP staining of the posterior lateral line nerve (PLLn) after FT treatment. This effect was not seen in gpr126st49 larvae which express a truncated Gpr126 incapable of Gs-signaling.

8.3 Importance of the findings

During more than two decades of prion research, many different probable functions of the prion protein have been proposed. Bremer et al. showed in their previous work that four different *Prnp* deficient mouse lines on four different genetic backgrounds (B6, 129, Balb/c and mixed) suffer from a chronic progressive polyneuropathy CDP. This finding could lately be confirmed by Nuvolone and Herrmann et al. in a new *Prnp*$^{-/-}$ mouse line ZH3 (Nuvolone et al., 2016). ZH3 mice were generated by use of TALEN genome editing on a strictly isogenic C57BL/6J background and are not affected by flanking gene bias. The CDP therefore is a very robust and a proven phenotype of the prion protein deficient mouse. In my study, I described the molecular mechanism by which axonal PrP^{C} exerts myelin maintenance. The interaction of

FT with Gpr126 leading to myelination is to my knowledge the first molecular elucidation of a phenotype caused by prion protein deficiency. So far it was known that Gpr126 has a crucial role in myelination of peripheral nerves during development (Monk et al., 2011; Petersen et al., 2015). I could show that Gpr126 is also involved in myelin maintenance. Peripheral neuropathies are very common and debilitating disorders whose prevalence is 1.66% in the general population and 6.6% among people older than 60 years (Hoffman et al., 2015). Today's treatment possibilities are extremely limited, therefore the PrP-Gpr126 interaction could offer novel therapeutic options for this spectrum of diseases.

8.4 Limitations of the study

8.4.1 PrP^C and Gpr126 knockouts are not similar

Both *Prnp*$^{-/-}$ and Gpr126$^{-/-}$ mice suffer from a disease of PNS myelin. However, there is an obvious difference between the two knockouts. *Prnp*$^{-/-}$ mice initially develop completely normal. After 8 weeks of age, first ultrastructural changes appear as digestion chambers can be found. Definite clinical signs are detected very late in life and start after an age of around 8 month. *Prnp*$^{-/-}$ mice clearly suffer from a myelin maintenance deficiency (Bremer et al., 2010b). On the other hand, Schwann cells in Gpr126$^{-/-}$ mice are arrested in promyelinating stage, crucial transcription factors such as Pou3f1, Egr2, myelin protein zero MPZ and myelin basic protein MBP are significantly reduced, non-myelinating axons in Remak bundles are not observed and radial sorting by Schwann cells is delayed. Therefore Gpr126$^{-/-}$ mice show drastic signs of developmental hypomyelination (Monk et al., 2011). This difference raises the question if Gpr126 and PrP^C really act on similar mechanisms in myelination. To circumvent the developmental stage, I analyzed *Dhh*^{Cre}*::Gpr126*$^{fl/fl}$ mice, which express Cre recombinase at E12,5 under the desert hedgehog promoter leading to a Gpr126 ko after completion of developmental myelination. Sciatic nerves of those mice show indeed ultrastructural changes comparable to *Prnp*$^{-/-}$ mice, suggesting that the two phenotypes may share mechanistic similarities. Up to a certain point, I could explain the phenotypic differences with the presence of the two described agonistic ligands type-IV collagen and laminin-211, which could compensate for missing PrP^C during development but not in long-term myelin maintenance.

8.4.2 Peripheral myelination via Gpr126 is not the only function of PrP^C

PrP^C but not Gpr126 is highly expressed in the central nervous system. Therefore, it is very probable that PrP^C exerts a diffierent function in the CNS. This other function could involve myelination via a different G protein-coupled receptor. Although Bremer et al. could not identify any CNS-myelination deficits in *Prnp*$^{-/-}$ mice.

8.4.3 Does PrP^C-Gpr126 signaling play a role in prions disease?

The prion protein has been intensively studied because it causes the severe and often fatal neurodegenerative diseases of the prion's disease spectrum. All those disorders affect the central nervous system and Grp126 is not expressed in the central nervous system as it is published in the GTEx portal (gtexportal.org). It is still possible, as mentioned above that Gpr126 is replaced in CNS by another closely related adhesion GPCR since adhesion GPCRs often share similar extracellular domains. Gpr126 is reported to be highly upregulated in Bergmann glia in the cerebellum which forms the glial scar after neuronal loss (Koirala and Corfas, 2010). Therefore, Gpr126 may play a role also in the CNS after neuronal

cell loss has already occurred. The strongest point against an implication of FT23-50 in prion disease are found in deletion studies. Mice with a truncated amino-terminus can still be infected with prions and are perfectly able to propagate them (Fischer et al., 1996).

8.5 Implications or practical applications of the study

The so far reported Gpr126 ligands, type-IV collagen (Paavola et al., 2014) and laminin-211(Petersen et al., 2015) are not easily useful for therapeutic purposes. Collagen and laminins are ubiquitously found in the body, they are sticky, sessile and because of the size prone to fast degradation. FT as a. short peptide can serve as a very useful therapeutic agent, as shown while administering systemically to hypomorphic Gpr126 mutant zebrafish. Soluble ligands may be beneficial in diseases caused by Gpr126 mutations such as idiopathic scoliosis (Kou et al., 2013). It is conceivable that certain hereditary motor-sensory neuropathies might benefit from Grp126 activation even if they are caused by defects in other myelin proteins. Also, sporadic (Esiri et al., 1997) and hereditary prion diseases (Antoine et al., 1996) frequently affect the peripheral nervous system and in some cases the neuropathy was associated with PrP^{Sc} deposition (Favereaux et al., 2004). But neuropathy is only a side symptom compared to the severe neurodegeneration in prion diseases (Neufeld et al., 1992). The treatment of polyneuropathy under these conditions is not going to change the fatal course of the disease. A systematic screen of mutations in the *PRNP* gene among 108 patients suffering from hereditary motor and sensory neuropathies did not identify a single mutation (Koop et al., 2005) leading to the conclusion, that *PRNP* mutations play a minor role in otherwise highly prevalent neuropathies. On the other hand, enhanced PrP-Gpr126 signaling might drive myelination in the presence of other myelin disorders.

8.6 Further research to be done

Although Gpr126 is not expressed in the central nervous system (CNS), certain mutants of PrP^{C} cause myelin pathology in vivo (Radovanovic et al., 2005). This observation raises the question whether inappropriate activation of GPCRs may play a role in driving the pathogenesis of prion diseases within the CNS. Close relatives of Gpr126 expressed in the CNS with similar extracellular motifs should be screened for interaction with PrP^{C}. Furthermore, the course of prion infection in Gpr126 deficient mice should be studied. Amino-terminally truncated mice Δ23-50 should be analyzed for presence of chronic demyelinating neuropathy as a proof of principle. Today, it is not yet known or published to what specific domain of Gpr126 FT is binding. The process of Gpr126 activation by PrP^{C} is of great importance for the understanding of adhesion GPCR function. Does FT bind to one of the amino-terminally exposed cell adhesion motifs? Does this lead to a dislocation of the long extracellular aminoterminus which exposes a Stachel-like autoactivating domain? Out of a therapeutic interest, a small compound comprising aa 23-50 of PrP^{C} could serve as a potent pro-myelinating agent, useful to drive myelination in diverse demyelinating disorders such as neuropathies, inflammatory or paraneoplastic demyelination or in idiopathic scoliosis. Preclinical studies using FT as a therapeutic compound are missing so far.

9 ACKNOWLEDGEMENTS

First of all, I'd like to thank **Adriano Aguzzi** for his enormous motivation and constant scientific input during successful times and even much more for his unbroken support in darker hours. His lab is a rare place in academy, where no restrictions in any kind could hinder scientific achievements.

Without **Asvin K.K. Lakkaraju** there would be no paper. His enormous work allowed us to finish the project after I have left for clinical work in neurosurgery. His efforts were beyond comparison. He's an amazing teacher in science and a wonderful friend.

During my application for the MD-PhD grant, I enjoyed great support by **Juliane Bremer**. **Tracy O'Connor** was a fantastic first postdoc and I miss her dark humor every day. The publication was a big team approach achieved by **Kristina Airich**, **Cédric Doucerain**, **Rajlakshmi Marpakwar**, **Pamela Bakirci**, **Assunta Senatore**, **Arnaud Monnard**, **Carmen Schiavi** and **Mario Nuvolone**.

Many thanks for the best transatlantic collaboration go to **Kelly Monk** and **Amit Mogha** from Washington University School of Medicine, St. Louis for their work with zebrafish and Gpr126 deficient mice.

Recombinant protein expression and purification was supported by **Simone Hornemann**, **Cinzia, Tiberi** and **Rita Moos**. I was extremely grateful for the continuous help from **Petra Schwarz**, you are terrific!

I would like to thank the Swiss National Science Foundation for funding this work with a MD-PhD grant and the University of Zurich for extending the financial support with a career development award (Forschungskredit).

We had great support from Novartis Institutes for Biomedical research NIBR in Basel and it was a great pleasure to work with **Bianka Grosshans** and **Frédéric Bassilana**.

10 Curriculum vitae

Alexander Friedrich Küffer
Dr. med. Dr. med. dent.
geboren am 02. Juni 1982 in Biel/Bienne
Heimatort: Ins, Kanton Bern, Schweiz

Ausbildung

2010-2015	PhD-Studium, Institut für Neuropathologie, Universitätsspital Zürich
2011	Promotion zum Dr. med. dent.
2010	Staatsexamen Zahnmedizin
2007-2010	Universität Bern, Studium der Zahnmedizin.
2007	Staatsexamen Humanmedizin und Promotion zum Dr. med. US-Staatsexamen ECFMG, certificate 0-716-716-6, Los Angeles USA
2001-2007	Universität Bern, Studium der Humanmedizin
1995-2001	Deutsches Gymnasium Biel, Auszeichnung für den besten Maturitätsabschluss 2001. Maturaarbeit 2001 mit Auszeichnung.

Berufliche Tätigkeiten

2015-	Assistenzarzt Klinik für Neurochirurgie, Universitätsspital Zürich, Prof. Dr. med. L. Regli
2010-2015	Assistenzarzt Neuropathologie, Teilzeit 20% (kumulativ 1 Jahr), Universitätsspital Zürich, Prof. Dr. med. A. Aguzzi.
2007-2010	Assistenzarzt Chirurgie, Teilzeit 30% (kumulativ 1 Jahr), Universitäres Notfallzentrum, Inselspital Bern, Prof. Dr. med. H. Zimmermann.
2009	Advanced Trauma Life Support ATLS-Kurs, Hôpitaux Universitaires de Genève HUG, Dr. D. Vettorel.

Publikationen

- Küffer, A. et al. The prion protein is an agonistic ligand of the G protein-coupled receptor Adgrg6. Nature (2016).
- Deubelbeiss, A. N. et al. Imported human rabies in Switzerland, 2012: a diagnostic conundrum. Journal of clinical virology : the official publication of the Pan American Society for Clinical Virology (2013).
- Hunziker, E. B., Enggist, L., Küffer, A., Buser, D. & Liu, Y. Osseointegration: the slow delivery of BMP-2 enhances osteoinductivity. Bone (2012).
- Scheidegger, O., Küffer, A. F., Kamm, C. P. & Rösler, K. M. Reproducibility of sensory nerve

conduction studies of the sural nerve using ultrasound-guided needle positioning. Muscle Nerve (2011).

- Liu, Y., Enggist, L., Küffer, A. F., Buser, D. & Hunziker, E. B. The influence of BMP-2 and its mode of delivery on the osteoconductivity of implant surfaces during the early phase of osseointegration. Biomaterials (2007).

Grants

2013-2014	Forschungskredit Candoc, Projekt- und Personenförderung, Universität Zürich, (CHF 55‘200).
2010-2013	MD-PhD Stipendium des Schweizerischen Nationalfonds (CHF 180‘000).
2006	Best Presentation Award, Swiss Bone and Mineral Society (SBMS), Annual Meeting 2006, (CHF 300).

Schweizer Armee

Seit 2012	Major, Fliegerarzt der Luftwaffe, Stab LT Verbände 3

11 References

Ackerman, S., Aguzzi, A., Feltri, M.L., Piao, X., and of, M.-K.R. (2018). GPR56/ADGRG1 regulates development and maintenance of peripheral myelin. Journal of ….

Aguzzi, A., Baumann, F., and Bremer, J. (2008). The Prion's Elusive Reason for Being. Annu Rev Neurosci 31, 439-477.

Aguzzi, A., and Hardt, W.-D. (2003). Dangerous Liaisons between a Microbe and the Prion Protein. The Journal of Experimental Medicine 198, 1-4.

Allache, R., Marco, P., Merello, E., Capra, V., and Kibar, Z. (2012). Role of the planar cell polarity gene CELSR1 in neural tube defects and caudal agenesis. Birth Defects Research Part A: Clinical and Molecular Teratology 94, 176-181.

Altmeppen, H.C., Prox, J., Krasemann, S., Puig, B., Kruszewski, K., Dohler, F., Bernreuther, C., Hoxha, A., Linsenmeier, L., Sikorska, B., et al. (2015). The sheddase ADAM10 is a potent modulator of prion disease. Elife 4.

Antoine, J.C., Laplanche, J.L., Mosnier, J.F., Beaudry, P., Chatelain, J., and Michel, D. (1996). Demyelinating peripheral neuropathy with Creutzfeldt-Jakob disease and mutation at codon 200 of the prion protein gene. Neurology 46, 1123-1127.

Arcos-Burgos, M., Jain, M., Acosta, M.T., Shively, S., Stanescu, H., Wallis, D., Domené, S., Vélez, J.I., Karkera, J.D., Balog, J., et al. (2010). A common variant of the latrophilin 3 gene, LPHN3, confers susceptibility to ADHD and predicts effectiveness of stimulant medication. Mol Psychiatry 15, 1053.

Ballerini, C., Gourdain, P., Bachy, V., Blanchard, N., Levavasseur, E., Grégoire, S., Fontes, P., Aucouturier, P., Hivroz, C., and Carnaud, C. (2006). Functional implication of cellular prion protein in antigen-driven interactions between T cells and dendritic cells. Journal of immunology (Baltimore, Md : 1950) 176, 7254-7262.

Beck, J.A., Mead, S., Campbell, T.A., Dickinson, A., Wientjens, D.P., Croes, E.A., Van Duijn, C.M., and Collinge, J. (2001). Two-octapeptide repeat deletion of prion protein associated with rapidly progressive dementia. Neurology 57, 354-356.

Bendheim, P.E., Brown, H.R., Rudelli, R.D., Scala, L.J., Goller, N.L., Wen, G.Y., Kascsak, R.J., Cashman, N.R., and Bolton, D.C. (1992). Nearly ubiquitous tissue distribution of the scrapie agent precursor protein. Neurology 42, 149-156.

Benvegnù, S., Roncaglia, P., Agostini, F., Casalone, C., Corona, C., Gustincich, S., and Legname, G. (2011). Developmental influence of the cellular prion protein on the gene expression profile in mouse hippocampus. Physiol Genomics 43, 711-725.

Beraldo, F.H., Arantes, C.P., Santos, T.G., Machado, C.F., Roffe, M., Hajj, G.N., Lee, K.S., Magalhães, A.C., Caetano, F.A., Mancini, G.L., et al. (2010). Metabotropic glutamate receptors transduce signals for neurite outgrowth after binding of the prion protein to laminin γ1 chain. The FASEB Journal 25, 265-279.

Bernardi, L., Cupidi, C., Frangipane, F., Anfossi, M., Gallo, M., Conidi, M.E., Vasso, F., Colao, R., Puccio, G., Curcio, S.A., et al. (2014). Novel N-terminal domain mutation in prion protein detected in 2 patients diagnosed with frontotemporal lobar degeneration syndrome. Neurobiol Aging 35, 800196224-800196211.

Birchmeier, C., and Nave, K.-A.A. (2008). Neuregulin-1, a key axonal signal that drives Schwann cell growth and differentiation. Glia 56, 1491-1497.

Bremer, J., Baumann, F., Tiberi, C., Wessig, C., Fischer, H., Schwarz, P., Steele, A.D., Toyka, K.V., Nave, K.-A., Weis, J., et al. (2010a). Axonal prion protein is required for peripheral myelin maintenance. Nat Neurosci 13, 310.

Bremer, J., Baumann, F., Tiberi, C., Wessig, C., Fischer, H., Schwarz, P., Steele, A.D., Toyka, K.V., Nave, K.A., Weis, J., et al. (2010b). Axonal prion protein is required for peripheral myelin maintenance. Nat Neurosci 13, 310-318.

Britsch, S., Goerich, D.E., Riethmacher, D., Peirano, R.I., Rossner, M., Nave, K.-A., Birchmeier, C., and Wegner, M. (2001). The transcription factor Sox10 is a key regulator of peripheral glial development. Genes Dev 15, 66-78.

Britsch, S., Li, L., Kirchhoff, S., and …, T.-F. (1998). The ErbB2 and ErbB3 receptors and their ligand, neuregulin-1, are essential for development of the sympathetic nervous system. Genes & ….

Brown, D.R., Qin, K., Herms, J.W., Madlung, A., Manson, J., Strome, R., Fraser, P.E., Kruck, T., von Bohlen, A., Schulz-Schaeffer, W., et al. (1997). The cellular prion protein binds copper in vivo. Nature 390, 684-687.

Bueler, H., Aguzzi, A., Sailer, A., Greiner, R.A., Autenried, P., Aguet, M., and Weissmann, C. (1993). Mice devoid of PrP are resistant to scrapie. Cell 73, 1339-1347.

Bueler, H., Fischer, M., Lang, Y., Bluethmann, H., Lipp, H.P., DeArmond, S.J., Prusiner, S.B., Aguet, M., and Weissmann, C. (1992). Normal development and behaviour of mice lacking the neuronal cell-surface PrP protein. Nature 356, 577-582.

Bunge, R.P., Bunge, M.B., and Eldridge, C.F. (1986). Linkage Between Axonal Ensheathment and Basal Lamina Production by Schwann Cells. Annu Rev Neurosci 9, 305-328.

Chadi, S., Young, R., Guillou, S., Tilly, G., Bitton, F., Martin-Magniette, M.-L., Soubigou-Taconnat, L., Balzergue, S., Vilotte, M., Peyre, C., et al. (2010). Brain transcriptional stability upon prion protein-encoding gene invalidation in zygotic or adult mouse. BMC Genomics 11, 448.

Chen, S.G., Teplow, D.B., Parchi, P., Teller, J.K., Gambetti, P., and Autilio-Gambetti, L. (1995). Truncated forms of the human prion protein in normal brain and in prion diseases. J Biol Chem 270, 19173-19180.

Coitinho, A.S., Roesler, R., Martins, V.R., Brentani, R.R., and Izquierdo, I. (2003). Cellular prion protein ablation impairs behavior as a function of age. Neuroreport 14, 1375-1379.

Colling, S.B., Khana, M., Collinge, J., and Jefferys, J.G. (1997). Mossy fibre reorganization in the hippocampus of prion protein null mice. Brain Res 755, 28-35.

Collinge, J., Whittington, M.A., Sidle, K.C., Smith, C.J., Palmer, M.S., Clarke, A.R., and Jefferys, J.G. (1994). Prion protein is necessary for normal synaptic function. Nature 370, 295-297.

Criado, J.R., Sanchez-Alavez, M., Conti, B., Giacchino, J.L., Wills, D.N., Henriksen, S.J., Race, R., Manson, J.C., Chesebro, B., and Oldstone, M.B. (2005). Mice devoid of prion protein have cognitive deficits that are rescued by reconstitution of PrP in neurons. Neurobiol Dis 19, 255-265.

Cui, H., Wang, Y., Huang, H., Yu, W., Bai, M., Zhang, L., Bryan, B.A., Wang, Y., Luo, J., Li, D., et al. (2014). GPR126 protein regulates developmental and pathological angiogenesis through modulation of VEGFR2 receptor signaling. J Biol Chem 289, 34871-34885.

Dametto, P., Lakkaraju, A.K., Bridel, C., Villiger, L., O'Connor, T., Herrmann, U.S., Pelczar, P., Rulicke, T., McHugh, D., Adili, A., et al. (2015). Neurodegeneration and unfolded-protein response in mice expressing a membrane-tethered flexible tail of PrP. PLoS One 10, e0117412.

de Almeida, C.J.G., Chiarini, L.B., da Silva, J., e Silva, P.M.R., Martins, M., and Linden, R. (2005). The cellular prion protein modulates phagocytosis and inflammatory response. J Leukoc Biol 77, 238-246.

Decker, L., Desmarquet-Trin-Dinh, C., Taillebourg, E., Ghislain, J., Vallat, J.M., and Charnay, P. (2006). Peripheral myelin maintenance is a dynamic process requiring constant Krox20 expression. J Neurosci 26, 9771-9779.

DeRosse, P., Lencz, T., Burdick, K.E., Siris, S.G., Kane, J.M., and Malhotra, A.K. (2008). The Genetics of Symptom-Based Phenotypes: Toward a Molecular Classification of Schizophrenia. Schizophr Bull 34, 1047-1053.

Dong, Z., Brennan, A., Liu, N., Yarden, Y., and Neuron, L.-G. (1995). Neu differentiation factor is a neuron-glia signal and regulates survival, proliferation, and maturation of rat Schwann cell precursors. Neuron.

Eldridge, C.F., Bunge, M.B., and Bunge, R.P. (1989). Differentiation of axon-related Schwann cells in vitro: II. Control of myelin formation by basal lamina. The Journal of neuroscience : the official journal of the Society for Neuroscience 9, 625-638.

Esiri, M.M., Wilcock, G.K., and Morris, J.H. (1997). Neuropathological assessment of the lesions of significance in vascular dementia. J Neurol Neurosurg Psychiatry 63, 749-753.

Evans, E.G.B., Pushie, M.J., Markham, K.A., Lee, H.-W., and Millhauser, G.L. (2016). Interaction between the Prion Protein's Copper-Bound Octarepeat Domain and a Charged C-terminal Pocket Suggests a Mechanism for N-terminal Regulation. Structure (London, England : 1993) 24, 1057-1067.

Favereaux, A., Perret-Liaudet, A., and Vital, A. (2004). Extraneural pathologic prion protein. N Engl J Med 350, 732-733; author reply 732-733.

Feltri, M., and Wrabetz, L. (2005). Laminins and their receptors in Schwann cells and hereditary neuropathies. Journal of the Peripheral Nervous System 10, 128-143.

Fischer, M., Rulicke, T., Raeber, A., Sailer, A., Moser, M., Oesch, B., Brandner, S., Aguzzi, A., and Weissmann, C. (1996). Prion protein (PrP) with amino-proximal deletions restoring susceptibility of PrP knockout mice to scrapie. The EMBO journal 15, 1255-1264.

Flechsig, E., Shmerling, D., Hegyi, I., Raeber, A.J., Fischer, M., Cozzio, A., von Mering, C., Aguzzi, A., and Weissmann, C. (2000). Prion protein devoid of the octapeptide repeat region restores susceptibility to scrapie in PrP knockout mice. Neuron 27, 399-408.

Fontes, P., Alvarez-Martinez, M.-T., Gross, A., Carnaud, C., Köhler, S., and Liautard, J.-P. (2005). Absence of Evidence for the Participation of the Macrophage Cellular Prion Protein in Infection with Brucella suis. Infect Immun 73, 6229-6236.

Franklin, R.J., and Ffrench-Constant, C. (2008). Remyelination in the CNS: from biology to therapy. Nature reviews Neuroscience 9, 839-855.

Fredriksson, R., Höglund, P.J.J., Gloriam, D.E., Lagerström, M.C., and Schiöth, H.B. (2003). Seven evolutionarily conserved human rhodopsin G protein-coupled receptors lacking close relatives. FEBS Lett 554, 381-388.

Geng, F.-S., Abbas, L., Baxendale, S., Holdsworth, C.J., Swanson, G.A., Slanchev, K., Hammerschmidt, M., Topczewski, J., and Whitfield, T.T. (2013). Semicircular canal morphogenesis in the zebrafish inner ear requires the function of gpr126 (lauscher), an adhesion class G protein-coupled receptor gene. Development 140, 4362-4374.

Glenn, T.D., and Talbot, W.S. (2013). Signals regulating myelination in peripheral nerves and the Schwann cell response to injury. Curr Opin Neurobiol 23, 1041-1048.

Goldfarb, L.G., Brown, P., McCombie, W.R., Goldgaber, D., Swergold, G.D., Wills, P.R., Cervenakova, L., Baron, H., Gibbs, C.J., and Gajdusek, D.C. (1991). Transmissible familial Creutzfeldt-Jakob disease

associated with five, seven, and eight extra octapeptide coding repeats in the PRNP gene. Proc Natl Acad Sci U S A 88, 10926-10930.

Goniotaki, D., Lakkaraju, A.K.K., Shrivastava, A.N., Bakirci, P., Sorce, S., Senatore, A., Marpakwar, R., Hornemann, S., Gasparini, F., Triller, A., et al. (2017). Inhibition of group-I metabotropic glutamate receptors protects against prion toxicity. PLoS Pathog 13, e1006733.

Guillot-Sestier, M.V., Sunyach, C., Druon, C., Scarzello, S., and Checler, F. (2009). The alpha-secretase-derived N-terminal product of cellular prion, N1, displays neuroprotective function in vitro and in vivo. J Biol Chem 284, 35973-35986.

Hanoune, J., and Defer, N. (2001). Regulation and role of adenylyl cyclase isoforms. Annu Rev Pharmacol Toxicol 41, 145-174.

Harris, D.A., Huber, M.T., van Dijken, P., Shyng, S.L., Chait, B.T., and Wang, R. (1993). Processing of a cellular prion protein: identification of N- and C-terminal cleavage sites. Biochemistry 32, 1009-1016.

Herms, J., Tings, T., Gall, S., Madlung, A., Giese, A., Siebert, H., Schurmann, P., Windl, O., Brose, N., and Kretzschmar, H. (1999). Evidence of presynaptic location and function of the prion protein. J Neurosci 19, 8866-8875.

Herms, J.W., Kretzchmar, H.A., Titz, S., and Keller, B.U. (1995). Patch-clamp analysis of synaptic transmission to cerebellar purkinje cells of prion protein knockout mice. Eur J Neurosci 7, 2508-2512.

Herms, J.W., Tings, T., Dunker, S., and Kretzschmar, H.A. (2001). Prion Protein Affects Ca2+-Activated K+ Currents in Cerebellar Purkinje Cells. Neurobiol Dis 8, 324-330.

Hoffman, E.M., Staff, N.P., Robb, J.M., St Sauver, J.L., Dyck, P.J., and Klein, C.J. (2015). Impairments and comorbidities of polyneuropathy revealed by population-based analyses. Neurology 84, 1644-1651.

Hornemann, S., Christen, B., von Schroetter, C., Perez, D.R., and Wuthrich, K. (2009). Prion protein library of recombinant constructs for structural biology. FEBS J 276, 2359-2367.

Hu, N.W., Nicoll, A.J., Zhang, D., and Nature …, M.-A.J. (2014). mGlu5 receptors and cellular prion protein mediate amyloid-β-facilitated synaptic long-term depression in vivo. Nature ….

Huber, R., Deboer, T., and Tobler, I. (1999). Prion protein: a role in sleep regulation? J Sleep Res 8 Suppl 1, 30-36.

Hundt, C., Peyrin, J.M., Haik, S., Gauczynski, S., Leucht, C., Rieger, R., Riley, M.L., Deslys, J.P., Dormont, D., Lasmezas, C.I., et al. (2001). Identification of interaction domains of the prion protein with its 37-kDa/67-kDa laminin receptor. The EMBO journal 20, 5876-5886.

Hutter, G., Heppner, F.L., and Aguzzi, A. (2003). No superoxide dismutase activity of cellular prion protein in vivo. Biol Chem 384, 1279-1285.

Iwasaki, Y., Mori, K., Ito, M., Nokura, K., Tatsumi, S., Mimuro, M., Kitamoto, T., and Yoshida, M. (2014). Gerstmann-Sträussler-Scheinker disease with P102L prion protein gene mutation presenting with rapidly progressive clinical course. Clinical Neuropathology 33, 344-353.

Jaegle, M., Ghazvini, M., Mandemakers, W., Piirsoo, M., Driegen, S., Levavasseur, F., Raghoenath, S., Grosveld, F., and Meijer, D. (2003). The POU proteins Brn-2 and Oct-6 share important functions in Schwann cell development. Genes Dev 17, 1380-1391.

Jeffrey, M., Halliday, W.G., Bell, J., Johnston, A.R., MacLeod, N.K., Ingham, C., Sayers, A.R., Brown, D.A., and Fraser, J.R. (2000). Synapse loss associated with abnormal PrP precedes neuronal degeneration in the scrapie-infected murine hippocampus. Neuropathol Appl Neurobiol 26, 41-54.

Jessen, K.R., and Mirsky, R. (2005). The origin and development of glial cells in peripheral nerves. Nat Rev Neurosci 6, 671-682.

Kao, S.C., Wu, H., Xie, J., Chang, C.P., and …, R.-J.A. (2009). Calcineurin/NFAT signaling is required for neuregulin-regulated Schwann cell differentiation. ….

Karner, C.M., Long, F., Solnica-Krezel, L., Monk, K.R., and Gray, R.S. (2015). Gpr126/Adgrg6 deletion in cartilage models idiopathic scoliosis and pectus excavatum in mice. Hum Mol Genet 24, 4365-4373.

Kasof, G.M., and Gomes, B.C. (2001). Livin, a novel inhibitor of apoptosis protein family member. J Biol Chem 276, 3238-3246.

Kelly, P.D., Chu, F., Woods, I.G., Ngo-Hazelett, P., Cardozo, T., Huang, H., Kimm, F., Liao, L., Yan, Y.-L., Zhou, Y., et al. (2000). Genetic Linkage Mapping of Zebrafish Genes and ESTs. Genome Res 10, 558-567.

Kimmel, C.B., Ballard, W.W., Kimmel, S.R., Ullmann, B., and Schilling, T.F. (1995). Stages of embryonic development of the zebrafish. Dev Dyn 203, 253-310.

Klamt, F., Dal-Pizzol, F., Conte da Frota, M.L., Jr., Walz, R., Andrades, M.E., da Silva, E.G., Brentani, R.R., Izquierdo, I., and Fonseca Moreira, J.C. (2001). Imbalance of antioxidant defense in mice lacking cellular prion protein. Free Radic Biol Med 30, 1137-1144.

Koirala, S., and Corfas, G. (2010). Identification of novel glial genes by single-cell transcriptional profiling of Bergmann glial cells from mouse cerebellum. PloS one 5, e9198.

Koop, O., Timmerman, V., de Jonghe, P., Ringelstein, B., Young, P., and Kuhlenbaumer, G. (2005). Absence of mutations in the prion-protein gene in a large cohort of HMSN patients. Neuromuscul Disord 15, 549-551.

Kou, I., Takahashi, Y., Johnson, T.A., Takahashi, A., Guo, L., Dai, J., Qiu, X., Sharma, S., Takimoto, A., Ogura, Y., et al. (2013). Genetic variants in GPR126 are associated with adolescent idiopathic scoliosis. Nat Genet 45, 676-679.

Kuwahara, C., Takeuchi, A.M., Nishimura, T., Haraguchi, K., Kubosaki, A., Matsumoto, Y., Saeki, K., Matsumoto, Y., Yokoyama, T., Itohara, S., et al. (1999). Prions prevent neuronal cell-line death. Nature 400, 225-226.

Lange, M., Norton, W., Coolen, M., Chaminade, M., Merker, S., Proft, F., Schmitt, A., Vernier, P., Lesch, K.P., and Bally-Cuif, L. (2012). The ADHD-linked gene Lphn3.1 controls locomotor activity and impulsivity in zebrafish. Mol Psychiatry 17, 855.

Lei, Y., Zhu, H., Yang, W., Ross, E.M., Shaw, G.M., and Finnell, R.H. (2014). Identification of Novel CELSR1 Mutations in Spina Bifida. PLoS ONE 9.

Lewis, V., Johanssen, V.A., Crouch, P.J., Klug, G.M., Hooper, N.M., and Collins, S.J. (2016). Prion protein "gamma-cleavage": characterizing a novel endoproteolytic processing event. Cellular and molecular life sciences : CMLS 73, 667-683.

Liebscher, I., Schon, J., Petersen, S.C., Fischer, L., Auerbach, N., Demberg, L.M., Mogha, A., Coster, M., Simon, K.U., Rothemund, S., et al. (2014). A tethered agonist within the ectodomain activates the adhesion G protein-coupled receptors GPR126 and GPR133. Cell Rep 9, 2018-2026.

Lipp, H.P., Stagliar-Bozicevic, M., Fischer, M., and Wolfer, D.P. (1998). A 2-year longitudinal study of swimming navigation in mice devoid of the prion protein: no evidence for neurological anomalies or spatial learning impairments. Behav Brain Res 95, 47-54.

Lledo, P.M., Tremblay, P., DeArmond, S.J., Prusiner, S.B., and Nicoll, R.A. (1996). Mice deficient for prion protein exhibit normal neuronal excitability and synaptic transmission in the hippocampus. Proc Natl Acad Sci U S A 93, 2403-2407.

Lobão-Soares, B., Bianchin, M., Linhares, M., Carqueja, C., Tasca, C., Souza, M., Marques, W., Brentani, R., Martins, V.R., Sakamoto, A.C., et al. (2005). Normal brain mitochondrial respiration in adult mice lacking cellular prion protein. Neurosci Lett 375, 203-206.

Luo, R., Jeong, S.-J., Jin, Z., Strokes, N., Li, S., and Piao, X. (2011). G protein-coupled receptor 56 and collagen III, a receptor-ligand pair, regulates cortical development and lamination. Proceedings of the National Academy of Sciences 108, 12925-12930.

Lyons, D.A., Pogoda, H.M., Voas, M.G., Woods, I.G., Diamond, B., Nix, R., Arana, N., Jacobs, J., and Talbot, W.S. (2005). erbb3 and erbb2 are essential for schwann cell migration and myelination in zebrafish. Curr Biol 15, 513-524.

Lysek, D.A., and Wuthrich, K. (2004). Prion protein interaction with the C-terminal SH3 domain of Grb2 studied using NMR and optical spectroscopy. Biochemistry 43, 10393-10399.

Mange, A., Beranger, F., Peoc'h, K., Onodera, T., Frobert, Y., and Lehmann, S. (2004). Alpha- and beta-cleavages of the amino-terminus of the cellular prion protein. Biology of the cell / under the auspices of the European Cell Biology Organization 96, 125-132.

Manson, J.C., Hope, J., Clarke, A.R., Johnston, A., Black, C., and MacLeod, N. (1995). PrP gene dosage and long term potentiation. Neurodegeneration : a journal for neurodegenerative disorders, neuroprotection, and neuroregeneration 4, 113-114.

Mansour, S.L., Thomas, K.R., and Capecchi, M.R. (1988). Disruption of the proto-oncogene int-2 in mouse embryo-derived stem cells: a general strategy for targeting mutations to non-selectable genes. Nature 336, 348-352.

Michailov, G.V., Sereda, M.W., Brinkmann, B.G., Fischer, T.M., Haug, B., Birchmeier, C., Role, L., Lai, C., Schwab, M.H., and Nave, K.-A.A. (2004). Axonal neuregulin-1 regulates myelin sheath thickness. Science (New York, NY) 304, 700-703.

Miele, G., Jeffrey, M., Turnbull, D., Manson, J., and Clinton, M. (2002). Ablation of Cellular Prion Protein Expression Affects Mitochondrial Numbers and Morphology. Biochem Biophys Res Commun 291, 372-377.

Minikel, E.V., Vallabh, S.M., Lek, M., Estrada, K., Samocha, K.E., Sathirapongsasuti, J.F., McLean, C.Y., Tung, J.Y., Yu, L.P., Gambetti, P., et al. (2016). Quantifying prion disease penetrance using large population control cohorts. Science translational medicine 8.

Mogha, A., Benesh, A.E., Patra, C., Engel, F.B., Schoneberg, T., Liebscher, I., and Monk, K.R. (2013). Gpr126 functions in Schwann cells to control differentiation and myelination via G-protein activation. J Neurosci 33, 17976-17985.

Monk, K.R., Naylor, S.G., Glenn, T.D., Mercurio, S., Perlin, J.R., Dominguez, C., Moens, C.B., and Talbot, W.S. (2009). A G protein-coupled receptor is essential for Schwann cells to initiate myelination. Science 325, 1402-1405.

Monk, K.R., Oshima, K., Jörs, S., Heller, S., and Talbot, W.S. (2011). Gpr126 is essential for peripheral nerve development and myelination in mammals. Development (Cambridge, England) 138, 2673-2680.

Monuki, E.S., Weinmaster, G., Kuhn, R., and Lemke, G. (1989). SCIP: a glial POU domain gene regulated by cyclic AMP. Neuron 3, 783-793.

Moore, R.C., Lee, I.Y., Silverman, G.L., Harrison, P.M., Strome, R., Heinrich, C., Karunaratne, A., Pasternak, S.H., Chishti, M.A., Liang, Y., et al. (1999). Ataxia in prion protein (PrP)-deficient mice is associated with upregulation of the novel PrP-like protein doppel. J Mol Biol 292, 797-817.

Morrison, S.J., Perez, S.E., Qiao, Z., Verdi, J.M., and Cell, H.-C. (2000). Transient Notch activation initiates an irreversible switch from neurogenesis to gliogenesis by neural crest stem cells. Cell.

Muramoto, T., DeArmond, S.J., Scott, M., Telling, G.C., Cohen, F.E., and Prusiner, S.B. (1997). Heritable disorder resembling neuronal storage disease in mice expressing prion protein with deletion of an alpha-helix. Nat Med 3, 750-755.

Naslavsky, N., Stein, R., Yanai, A., Friedlander, G., and Taraboulos, A. (1997). Characterization of Detergent-insoluble Complexes Containing the Cellular Prion Protein and Its Scrapie Isoform. J Biol Chem 272, 6324-6331.

Neufeld, M.Y., Josiphov, J., and Korczyn, A.D. (1992). Demyelinating peripheral neuropathy in Creutzfeldt-Jakob disease. Muscle Nerve 15, 1234-1239.

Nuvolone, M., Hermann, M., Sorce, S., Russo, G., Tiberi, C., Schwarz, P., Minikel, E., Sanoudou, D., Pelczar, P., and Aguzzi, A. (2016). Strictly co-isogenic C57BL/6J-Prnp-/- mice: A rigorous resource for prion science. J Exp Med 213, 313-327.

Nuvolone, M., Kana, V., Hutter, G., Sakata, D., Mortin-Toth, S.M., Russo, G., Danska, J.S., and Aguzzi, A. (2013). SIRPalpha polymorphisms, but not the prion protein, control phagocytosis of apoptotic cells. J Exp Med 210, 2539-2552.

Ogata, T., Iijima, S., Hoshikawa, S., Miura, T., Yamamoto, S., Oda, H., Nakamura, K., and Tanaka, S. (2004). Opposing extracellular signal-regulated kinase and Akt pathways control Schwann cell myelination. J Neurosci 24, 6724-6732.

Okajima, D., Kudo, G., and Yokota, H. (2010). Brain-specific angiogenesis inhibitor 2 (BAI2) may be activated by proteolytic processing. J Recept Signal Transduct Res 30, 143-153.

Oldoni, E., Fumagalli, G.G., Serpente, M., Fenoglio, C., Scarioni, M., Arighi, A., Bruno, G., Talarico, G., Confaloni, A., Piscopo, P., et al. (2016). PRNP P39L Variant is a Rare Cause of Frontotemporal Dementia in Italian Population. J Alzheimers Dis 50, 353-357.

Oliveira-Martins, J.B., Yusa, S.-i., Calella, A., Bridel, C., Baumann, F., Dametto, P., and Aguzzi, A. (2010). Unexpected Tolerance of α-Cleavage of the Prion Protein to Sequence Variations. PLoS ONE 5.

Paavola, K.J., Sidik, H., Zuchero, J.B., Eckart, M., and Talbot, W.S. (2014). Type IV collagen is an activating ligand for the adhesion G protein-coupled receptor GPR126. Sci Signal 7, ra76.

Paavola, K.J., Stephenson, J.R., Ritter, S.L., Alter, S.P., and Hall, R.A. (2011). The N terminus of the adhesion G protein-coupled receptor GPR56 controls receptor signaling activity. J Biol Chem 286, 28914-28921.

Patra, C., van Amerongen, M.J., Ghosh, S., Ricciardi, F., Sajjad, A., Novoyatleva, T., Mogha, A., Monk, K.R., Muhlfeld, C., and Engel, F.B. (2013). Organ-specific function of adhesion G protein-coupled receptor GPR126 is domain-dependent. Proc Natl Acad Sci U S A 110, 16898-16903.

Petersen, S.C., Luo, R., Liebscher, I., Giera, S., Jeong, S.J., Mogha, A., Ghidinelli, M., Feltri, M.L., Schoneberg, T., Piao, X., et al. (2015). The Adhesion GPCR GPR126 Has Distinct, Domain-Dependent Functions in Schwann Cell Development Mediated by Interaction with Laminin-211. Neuron 85, 755-769.

Pogoda, H.M., Sternheim, N., Lyons, D.A., Diamond, B., Hawkins, T.A., Woods, I.G., Bhatt, D.H., Franzini-Armstrong, C., Dominguez, C., Arana, N., et al. (2006). A genetic screen identifies genes essential for development of myelinated axons in zebrafish. Dev Biol 298, 118-131.

Polymenidou, M., Moos, R., Scott, M., Sigurdson, C., Shi, Y.Z., Yajima, B., Hafner-Bratkovic, I., Jerala, R., Hornemann, S., Wuthrich, K., et al. (2008). The POM monoclonals: a comprehensive set of antibodies to non-overlapping prion protein epitopes. PLoS One 3, e3872.

Prusiner, S.B. (1982). Novel proteinaceous infectious particles cause scrapie. Science 216, 136-144.

Radovanovic, I., Braun, N., Giger, O.T., Mertz, K., Miele, G., Prinz, M., Navarro, B., and Aguzzi, A. (2005). Truncated prion protein and Doppel are myelinotoxic in the absence of oligodendrocytic PrPC. J Neurosci 25, 4879-4888.

Rangel, A., Burgaya, F., Gavín, R., Soriano, E., Aguzzi, A., and del Río, J.A. (2007). Enhanced susceptibility of Prnp-deficient mice to kainate-induced seizures, neuronal apoptosis, and death: Role of AMPA/kainate receptors. J Neurosci Res 85, 2741-2755.

Ribases, M., Ramos-Quiroga, J.A., Sanchez-Mora, C., Bosch, R., Richarte, V., Palomar, G., Gastaminza, X., Bielsa, A., Arcos-Burgos, M., Muenke, M., et al. (2011). Contribution of LPHN3 to the genetic susceptibility to ADHD in adulthood: a replication study. Genes Brain Behav 10, 149-157.

Richt, J.A., Kasinathan, P., Hamir, A.N., Castilla, J., Sathiyaseelan, T., Vargas, F., Sathiyaseelan, J., Wu, H., Matsushita, H., Koster, J., et al. (2007). Production of cattle lacking prion protein. Nat Biotechnol 25, 132-138.

Rieger, R., Edenhofer, F., Lasmezas, C.I., and Weiss, S. (1997). The human 37-kDa laminin receptor precursor interacts with the prion protein in eukaryotic cells. Nat Med 3, 1383-1388.

Riek, R., Hornemann, S., Wider, G., Billeter, M., Glockshuber, R., and Wuthrich, K. (1996). NMR structure of the mouse prion protein domain PrP(121-231). Nature 382, 180-182.

Robinson, A., Escuin, S., Doudney, K., Vekemans, M., Stevenson, R.E., Greene, N., Copp, A.J., and Stanier, P. (2012). Mutations in the planar cell polarity genes CELSR1 and SCRIB are associated with the severe neural tube defect craniorachischisis. Hum Mutat 33, 440-447.

Sailer, A., Bueler, H., Fischer, M., Aguzzi, A., and Weissmann, C. (1994). No propagation of prions in mice devoid of PrP. Cell 77, 967-968.

Sakaguchi, S., Katamine, S., Nishida, N., Moriuchi, R., Shigematsu, K., Sugimoto, T., Nakatani, A., Kataoka, Y., Houtani, T., Shirabe, S., et al. (1996). Loss of cerebellar Purkinje cells in aged mice homozygous for a disrupted PrP gene. Nature 380, 528-531.

Salzer, J.L., Brophy, P.J., and Peles, E. (2008). Molecular domains of myelinated axons in the peripheral nervous system. Glia 56, 1532-1540.

Santuccione, A., Sytnyk, V., Leshchyns'ka, I., and Schachner, M. (2005). Prion protein recruits its neuronal receptor NCAM to lipid rafts to activate p59fyn and to enhance neurite outgrowth. J Cell Biol 169, 341-354.

Scherer, S.S., Wang, D.Y., Kuhn, R., Lemke, G., Wrabetz, L., and Kamholz, J. (1994). Axons regulate Schwann cell expression of the POU transcription factor SCIP. J Neurosci 14, 1930-1942.

Schindelin, J., Arganda-Carreras, I., Frise, E., Kaynig, V., Longair, M., Pietzsch, T., Preibisch, S., Rueden, C., Saalfeld, S., Schmid, B., et al. (2012). Fiji: an open-source platform for biological-image analysis. Nat Methods 9, 676-682.

Schulz, J.B., Weller, M., and Klockgether, T. (1996). Potassium deprivation-induced apoptosis of cerebellar granule neurons: a sequential requirement for new mRNA and protein synthesis, ICE-like protease activity, and reactive oxygen species. J Neurosci 16, 4696-4706.

Shah, N.M., Groves, A.K., and Cell, A.-D.J. (1996). Alternative neural crest cell fates are instructively promoted by TGFβ superfamily members. Cell.

Shmerling, D., Hegyi, I., Fischer, M., Blattler, T., Brandner, S., Gotz, J., Rulicke, T., Flechsig, E., Cozzio, A., von Mering, C., et al. (1998). Expression of amino-terminally truncated PrP in the mouse leading to ataxia and specific cerebellar lesions. Cell 93, 203-214.

Šišková, Z., Reynolds, R.A., O'Connor, V., and Perry, V.H. (2013). Brain region specific pre-synaptic and post-synaptic degeneration are early components of neuropathology in prion disease. PloS one 8.

Sonati, T., Reimann, R.R., Falsig, J., Baral, P.K., O'Connor, T., Hornemann, S., Yaganoglu, S., Li, B., Herrmann, U.S., Wieland, B., et al. (2013). The toxicity of antiprion antibodies is mediated by the flexible tail of the prion protein. Nature 501, 102-106.

Stehlik, C., Kroismayr, R., Dorfleutner, A., Binder, B.R., and Lipp, J. (2004). VIGR--a novel inducible adhesion family G-protein coupled receptor in endothelial cells. FEBS Lett 569, 149-155.
Stöckel, J., Safar, J., Wallace, A.C., Cohen, F.E., and Prusiner, S.B. (1998). Prion protein selectively binds copper(II) ions. Biochemistry 37, 7185-7193.

Tasaki, I. (1939). The electro-saltatory transmission of the nerve impulse and the effect of narcosis upon the nerve fiber. American Journal of Physiology-Legacy Content.

Taveggia, C., Zanazzi, G., Petrylak, A., Yano, H., Rosenbluth, J., Einheber, S., Xu, X., Esper, R.M., Loeb, J.A., Shrager, P., et al. (2005). Neuregulin-1 type III determines the ensheathment fate of axons. Neuron 47, 681-694.

Thackray, A.M., and Bujdoso, R. (2002). PrPc Expression Influences the Establishment of Herpes Simplex Virus Type 1 Latency. J Virol 76, 2498-2509.

Tobler, I., Gaus, S.E., Deboer, T., Achermann, P., Fischer, M., Rülicke, T., Moser, M., Oesch, B., McBride, P.A., and Manson, J.C. (1996). Altered circadian activity rhythms and sleep in mice devoid of prion protein. Nature 380, 639-642.

Topilko, P., Schneider-Maunoury, S., Levi, G., Baron-Van Evercooren, A., Chennoufi, A.B.Y., Seitanidou, T., Babinet, C., and Charnay, P. (1994). Krox-20 controls myelination in the peripheral nervous system. Nature 371, 796-799.

Trimarco, A., Forese, M.G., Alfieri, V., and Nature …, L.-A. (2014). Prostaglandin D2 synthase/GPR44: a signaling axis in PNS myelination. Nature ….

Uhlen, M., Fagerberg, L., Hallstrom, B.M., Lindskog, C., Oksvold, P., Mardinoglu, A., Sivertsson, A., Kampf, C., Sjostedt, E., Asplund, A., et al. (2015). Proteomics. Tissue-based map of the human proteome. Science 347, 1260419.

Um, J.W., Kaufman, A.C., Kostylev, M., Heiss, J.K., Stagi, M., Takahashi, H., Kerrisk, M.E., Vortmeyer, A., Wisniewski, T., Koleske, A.J., et al. (2013). Metabotropic glutamate receptor 5 is a coreceptor for Alzheimer abeta oligomer bound to cellular prion protein. Neuron 79, 887-902.

Um, J.W., and Strittmatter, S.M. (2013). Amyloid-beta induced signaling by cellular prion protein and Fyn kinase in Alzheimer disease. Prion 7, 37-41.

Varela-Nallar, L., Toledo, E.M., Larrondo, L.F., Cabral, A.L., Martins, V.R., and Inestrosa, N.C. (2006). Induction of cellular prion protein gene expression by copper in neurons. American journal of physiology Cell physiology 290, 81.

Viles, J.H., Cohen, F.E., Prusiner, S.B., Goodin, D.B., Wright, P.E., and Dyson, J.H. (1999). Copper binding to the prion protein: Structural implications of four identical cooperative binding sites. Proceedings of the National Academy of Sciences 96, 2042-2047.

Waggoner, D.J., Drisaldi, B., Bartnikas, T.B., Casareno, R.B., Prohaska, J.R., Gitlin, J.D., and Harris, D.A. (2000). Brain Copper Content and Cuproenzyme Activity Do Not Vary with Prion Protein Expression Level. J Biol Chem 275, 7455-7458.

Waller-Evans, H., Promel, S., Langenhan, T., Dixon, J., Zahn, D., Colledge, W.H., Doran, J., Carlton, M.B., Davies, B., Aparicio, S.A., et al. (2010). The orphan adhesion-GPCR GPR126 is required for embryonic development in the mouse. PLoS One 5, e14047.

Walz, R., Amaral, O.B., Rockenbach, I.C., Roesler, R., Izquierdo, I., Cavalheiro, E.A., Martins, V.R., and Brentani, R.R. (1999). Increased Sensitivity to Seizures in Mice Lacking Cellular Prion Protein. Epilepsia 40, 1679-1682.

Wang, S.S., Shultz, J.R., Burish, M.J., Harrison, K.H., Hof, P.R., Towns, L.C., Wagers, M.W., and Wyatt, K.D. (2008). Functional trade-offs in white matter axonal scaling. The Journal of neuroscience : the official journal of the Society for Neuroscience 28, 4047-4056.

Watarai, M., Kim, S., Erdenebaatar, J., Makino, S.-i., Horiuchi, M., Shirahata, T., Sakaguchi, S., and Katamine, S. (2003). Cellular Prion Protein Promotes Brucella Infection into Macrophages. The Journal of Experimental Medicine 198, 5-17.

Watt, N.T., Taylor, D.R., Kerrigan, T.L., Griffiths, H.H., Rushworth, J.V., Whitehouse, I.J., and Hooper, N.M. (2012). Prion protein facilitates uptake of zinc into neuronal cells. Nature Communications 3, 1134.

Weiner, J.A., and the of Sciences, C.-J. (1999). Schwann cell survival mediated by the signaling phospholipid lysophosphatidic acid. … of the National Academy of Sciences.

Westergard, L., Turnbaugh, J.A., and Harris, D.A. (2011). A naturally occurring C-terminal fragment of the prion protein (PrP) delays disease and acts as a dominant-negative inhibitor of PrPSc formation. J Biol Chem 286, 44234-44242.

Weston, M.D., Luijendijk, M.W.J., Humphrey, K.D., Möller, C., and Kimberling, W.J. (2004). Mutations in the VLGR1 Gene Implicate G-Protein Signaling in the Pathogenesis of Usher Syndrome Type II. The American Journal of Human Genetics 74, 357-366.

Whittington, M.A., Sidle, K.C., Gowland, I., Meads, J., Hill, A.F., Palmer, M.S., Jefferys, J.G., and Collinge, J. (1995). Rescue of neurophysiological phenotype seen in PrP null mice by transgene encoding human prion protein. Nat Genet 9, 197-201.

Yamazaki, M., Oyanagi, K., Mori, O., Kitamura, S., Ohyama, M., Terashi, A., Kitamoto, T., and Katayama, Y. (1999). Variant Gerstmann-Straussler syndrome with the P105L prion gene mutation: an unusual case with nigral degeneration and widespread neurofibrillary tangles. Acta Neuropathol 98, 506-511.

Yu, G., Chen, J., Yu, H., Liu, S., Chen, J., Xu, X., Sha, H., Zhang, X., Wu, G., Xu, S., et al. (2006). Functional disruption of the prion protein gene in cloned goats. J Gen Virol 87, 1019-1027.

Zahn, R., von Schroetter, C., and Wuthrich, K. (1997). Human prion proteins expressed in Escherichia coli and purified by high-affinity column refolding. FEBS Lett 417, 400-404.

Zhang, W., Jiao, B., Xiao, T., Pan, C., Liu, X., Zhou, L., Tang, B., and Shen, L. (2016). Mutational analysis of PRNP in Alzheimer's disease and frontotemporal dementia in China. Sci Rep 6, 38435.

Zhang, Y., Chen, K., Sloan, S.A., Bennett, M.L., Scholze, A.R., O'Keeffe, S., Phatnani, H.P., Guarnieri, P., Caneda, C., Ruderisch, N., et al. (2014). An RNA-sequencing transcriptome and splicing database of glia, neurons, and vascular cells of the cerebral cortex. J Neurosci 34, 11929-11947.

Zorick, T.S., Syroid, D.E., Brown, A., Gridley, T., and Lemke, G. (1999). Krox-20 controls SCIP expression, cell cycle exit and susceptibility to apoptosis in developing myelinating Schwann cells. Development 126, 1397-1406.